

MASTER

The Rydberg-based Implementation of Perfect State Transfer for the Variational Quantum Eigensolver Algorithm under Noise and Decoherence Effects

Postema, Jasper J.

Award date:
2021

[Link to publication](#)

Disclaimer

This document contains a student thesis (bachelor's or master's), as authored by a student at Eindhoven University of Technology. Student theses are made available in the TU/e repository upon obtaining the required degree. The grade received is not published on the document as presented in the repository. The required complexity or quality of research of student theses may vary by program, and the required minimum study period may vary in duration.

General rights

Copyright and moral rights for the publications made accessible in the public portal are retained by the authors and/or other copyright owners and it is a condition of accessing publications that users recognise and abide by the legal requirements associated with these rights.

- Users may download and print one copy of any publication from the public portal for the purpose of private study or research.
- You may not further distribute the material or use it for any profit-making activity or commercial gain

EINDHOVEN UNIVERSITY OF TECHNOLOGY

DEPARTMENT APPLIED PHYSICS
PLASMA PHYSICS AND RADIATION TECHNOLOGY
COHERENCE AND QUANTUM TECHNOLOGY

The Rydberg-based Implementation of Perfect State Transfer for the Variational Quantum Eigensolver Algorithm under Noise and Decoherence Effects

Master's Thesis

SUPERVISOR:	S.J.J.M.F. KOKKELMANS
SECONDARY SUPERVISOR:	G.P. GROENEVELD
AUTHOR:	J.J. POSTEMA
	0940055

Geleen, The Netherlands, June 16, 2021

Abstract

Without access to full quantum error correction, other kinds of measures have to be invoked to mitigate error propagation in quantum computers, in order to build the bridge between few-qubit noisy quantum computers, and full fault-tolerant quantum processors employing $\gtrsim 10^5$ qubits and a full-fledged quantum error correction code. This intermediate era, called the Noisy Intermediate-Scale Quantum (NISQ) era, poses some demanding hurdles regarding how noise is sufficiently mitigated on a quantum computer.

Hybrid quantum computers, adopting both quantum computing and classical computing, are expected to be at the center of the NISQ era. The Variational Quantum Eigensolver (VQE) algorithm has proven to be an excellent choice for the benchmarking the performance of a hybrid quantum computer, establishing a strong foundation to build up from. With the addition of post-measurement error mitigation techniques that do not require additional overhead qubit resources, VQE can perform certain quantum chemistry calculations within chemical accuracy, the universal agreed upon measure of accuracy in chemistry, up to 8 qubits.

Quantum simulators based on encoding qubit states in the state manifold of trapped ultracold Rydberg atoms are explored. Their strong long range interactions, high degree of control and their high fidelities (99%+) make them powerful candidates for the realisation of a quantum computer. They are shown to span the universal set of quantum gates, when controlled by laser pulses, and they allow for many other gate operations to be performed directly without a decomposition in this universal basis. Because of their long range interactions, they are also favourable candidates for the implementation of multi-qubit entanglement operations.

The viability of perfect state transfer (PST) as a robust mechanism to transfer quantum states with unit fidelity is also investigated. It is shown that a system of Rydberg-dressed qubits interacting through resonant dipolar interactions are able to facilitate PST, and exact solutions for the underlying conditions are calculated for $N = 2, 3$ and 4 qubits.

Contents

List of Acronyms	5
1 Introduction	6
2 Hartree-Fock through VQE	9
2.1 The VQE algorithm	9
2.1.1 Introduction to quantum chemistry	9
2.1.2 The canonical approach to Hartree-Fock	9
2.1.3 The variational principle	11
2.1.4 Hessian optimisation	12
2.2 The quantum circuit	13
2.2.1 Initialisation	13
2.2.2 The Givens rotation sequence	14
2.2.3 Energy estimation	15
2.2.4 Sampling the 1-RDM terms	16
2.3 Neural networks	18
3 Coherent and decoherent noise	20
3.1 Noise on a QPU	20
3.2 Fidelity in quantum computing	20
3.2.1 Mixed states and the density operator	20
3.2.2 Quantum fidelity	21
3.2.3 The fidelity witness	21
3.3 Quantification of high-fidelity propagation	22
3.3.1 Clifford gates	22
3.3.2 Concurrence and n -tangles	22
3.4 Coherent noise channels	23
3.5 Decoherent noise channels	24
3.5.1 Decoherent noise	24
3.5.2 Qubit relaxation and dephasing	24
3.5.3 Depolarisation channel	24
3.6 The Lindbladian	25
3.6.1 The von Neumann equation	25
3.6.2 The Born-Markov master equation	25
3.6.3 The Lindblad equation	26
4 Error mitigation and quantification techniques	28
4.1 Introduction to partial QEC	28
4.2 Post-circuit error mitigation for VQE	28
4.2.1 Post-selection	28
4.2.2 McWeeny purification	29
4.2.3 Countering gate/propagation imperfections	30
4.3 Richardson's deferred approach to the limit	31
4.3.1 Richardson extrapolation	31
4.3.2 The original proposal	31
4.3.3 Application to VQE	33
5 Rydberg quantum circuits	35
5.1 Physics of Rydberg atoms	35
5.1.1 Introduction	35
5.1.2 Laser excitation	35
5.2 Rydberg interactions	37
5.2.1 Dipolar interactions	37
5.2.2 Van der Waals interactions	37
5.2.3 The Rydberg blockade effect	38

5.3	Quantum gate implementation	40
5.3.1	Rydberg-based QPUs	40
5.3.2	Choice of qubits	40
5.3.3	Single-qubit gates	41
5.3.4	Two-qubit gates	41
5.3.5	Multi-qubit gates	42
6	Multi-qubit entanglement through perfect state transfer	44
6.1	PST in the single excitation manifold Γ_1	44
6.1.1	Introduction to PST	44
6.1.2	Hilbert space decomposition analysis	45
6.1.3	The symmetry matching condition	46
6.1.4	The inverse eigenvalue problem	47
6.2	PST in higher order excitation manifolds	48
6.2.1	Independent fermion dynamics	48
6.2.2	Graph vertex wedge product \wedge	49
6.2.3	Qubit wedge product \wedge	50
6.2.4	Local unitary corrections	50
6.3	Examples of PST-facilitating Hamiltonians	51
6.3.1	The Krawtchouk chain	51
6.3.2	XY -Hamiltonian with magnetic field	52
6.4	Residual NNN couplings	52
6.5	Erroneous PST dynamics	53
6.5.1	Uniform coupling perturbations	53
6.5.2	Pulse time uncertainty	54
6.5.3	Excitation relaxation	54
6.5.4	$XX + YY$ system-bath interactions	55
7	Engineering PST for Rydberg QPUs	57
7.1	Natural Rydberg $XX + YY$ interactions	57
7.1.1	Dipole-dipole flip-flop interactions	57
7.1.2	Adiabatic elimination of van der Waals couplings	58
7.2	Rydberg-dressing for PST	60
7.2.1	Rydberg-dressed atoms	60
7.2.2	Choice of qubit manifold	61
7.2.3	Van Vleck perturbation theory	62
7.2.4	Position-dependent coupling	64
7.3	Alternative Rydberg-dressed systems	64
7.3.1	Two-photon gr -qubit system	64
7.3.2	Fourth order photon process system	65
8	Simulations for PST in small qubit registers	67
8.1	$N = 2$ qubit register	67
8.2	$N = 3$ qubit register	68
8.3	$N = 4$ qubit register	68
8.4	Beyond $N \geq 5$ qubits	69
9	Conclusion and discussion	71
	References	81
	Appendix A: Addition of angular momentum	82
	Appendix B: PST under Bose Hamiltonian dynamics	83
	Appendix C: Graph theory and quantum walks	84

Appendix D: Eigenvalues of the $N = 3$ XY-Hamiltonian	85
Appendix E: Eigenvalues of the $N = 4$ XY-Hamiltonian	87

List of Acronyms

AH	Augmented Hessian
AI	Artificial Intelligence
BCH	Baker-Campbell-Hausdorff
CC	Coupled Cluster
CPTP	Completely Positive Trace Preserving
CPU	Central Processing Unit
ESR	Eigenvalue Spacing Requirement
FCI	Full Configuration Interaction
HF	Hartree-Fock
GHZ	Greenberger–Horne–Zeilinger
IEP	Inverse Eigenvalue Problem
IT	Ion Trap
NNN	Next Nearest Neighbours
PEP	Pauli Exclusion Principle
PGST	Pretty Good State Transfer
PST	Perfect State Transfer
RDA	Richardson’s Deferred Approach (to the limit)
RDM	Reduced Density Matrix
SC	Super Conducting
SMS	Spectrum of Minimal Spread
SO(N)	Special Orthogonal group of order N
SPSA	Simultaneous Perturbation Stochastic Approximation
STO-nG	Slater-Type Orbital of Gaußian type and order n
SU(N)	Special Unitary group of order N
QAOA	Quantum Approximate Optimization Algorithm
QC	Quantum Computing
QEC	Quantum Error Correction
QNN	Quantum Neural Network
QPU	Quantum Processing Unit
VQE	Variational Quantum Eigensolver
WCF	Worst Case Fidelity

1 Introduction

Up until recently, Moore’s law has been able to predict the growth of the number of transistors that fit in an integrated circuit to great accuracy [1]. This process of continuously scaling down transistors is about to hit its physical limits, however, as the size of such a transistor approaches the wavelength of the electrons inside. The number of bits stored inside a circuit therefore has a limit. A computer whose elementary components are made of quantum objects and their interactions, is able to effectively evade this problem. Such computers, referred to as quantum computers, and envisioned by Richard Feynman [2], are expected to become of vital importance in many scientific areas in the future. The most optimistic view is that eventually, quantum computers that employ millions of qubits in a robust fashion, will completely outperform classical computers in many areas such as the simulation of the time evolution of quantum systems [3][4], or finding the energy eigenstates of a certain quantum system, but will also be able to solve more fine-tuned problems like the factorisation of large numbers into its prime constituents, such as Shor’s algorithm, or the efficient search of an entry in a long list, such as Grover’s algorithm [5][6].

Though, in the present, most quantum computing experiments are performed on small simulators. Modern quantum computing calculations employ $\lesssim 12$ qubits to perform benchmarking experiments, so that their performance can be compared to their classical counterparts [7][8][9][10]. Such benchmarks make a trade-off between the complexity of the quantum model that is to be studied, and the computational complexity. The inherent noise sensitive nature of quantum computers is a great challenge to tackle, and despite many efforts to mitigate these errors, both theoretical and experimental, this erroneous behaviour still renders most calculations inaccurate with respect to established measures such as chemical accuracy. In the future, however, it is expected that a full Quantum Error Correction (QEC) code is available that will make quantum computing with a high number of gates and qubits feasible, possibly employing on the order of millions of qubits and gate operations [11].

The intermediate time period between few-qubit quantum computing and a fully fault-tolerant one is coined the Noisy Intermediate-Scale Quantum (NISQ) era, popularised by John Preskill [12]. In the early stages of this era, quantum computers employing $\lesssim 100$ qubits will outperform classical computers at certain tasks, while for bigger system sizes, the errors that emerge during calculations can not be mitigated to give reliable results yet [13]. Yet, quantum advantage will break down at certain noise scales due to the sensitivity of quantum systems to decoherence effects. In later stages of the NISQ era, it may even be possible to push the qubit register size to $\sim 10^5$ qubits [14]. In figure 1.3, an overview is given of the qubit number line that links each relevant quantum computing (QC) era to the approximate number of qubits that is expected to be employed, thus also serving as a chronological order.

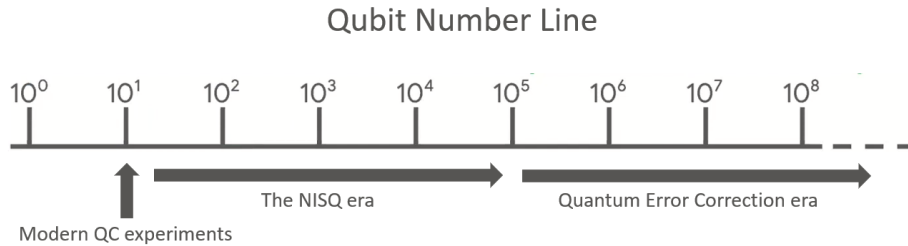


Figure 1.1: A logarithmically scaled qubit number line, indicating what qubit number regimes belong to which quantum computing era [14].

NISQ era technology serves as a bridge to cross the virtual gap between the quantum computational era of today and the future where full fault-tolerant quantum computing is expected to be available. It is theorised that the first demonstrations of practical algorithms that provide a significant computational supremacy over classical computers, will be calculations of fermionic problems on a hybrid quantum computer. Such a computer separates an algorithm into a part that is efficiently calculated on a classical computer, and a calculation that is efficiently performed on a quantum computer. This way, the computational burden of an algorithm can be efficiently distributed, giving an advantage. The quantum processing unit (QPU) endows the hybrid quantum computer with a quantum advantage that originates from the specific properties of the research problem.

Showcasing the computational superiority of a hybrid quantum computer over a classical computer is done by running variational quantum algorithms such as the Variational Quantum Eigensolver (VQE) or Quantum Approximate Optimisation Algorithms (QAOA), few of the key cornerstones that belong to the NISQ era [15][16][17]. The former of the both, VQE, is a rich algorithm that employs the variational principle in quantum mechanics by forming an ansatz of a wavefunction, encoded in qubits, and then minimising its corresponding eigenenergy with respect to some system Hamiltonian. For this, Hartree-Fock (HF) theory is chosen, avoiding more computationally taxing theories such as Coupled Cluster (CC) or Full Configuration Interaction (FCI) theory, while still providing an excellent framework in which quantum chemistry can be understood and tested [18]. If the state of a quantum system is rigorously mapped onto qubits, and its Hamiltonian or dynamics mapped to a series of unitary quantum gates, then performing the VQE algorithm corresponds to finding the ground state eigenenergy of that system, as well as its associated wavefunction[19][20]. A lot of useful information can be extracted from this, such as chemical reaction rates [21]. The quantum phase space search that is efficient on a QPU, and the classical optimisation that is efficiently performed on a classical computer, directly feed into each other, clearly demonstrating the hybrid nature of the VQE algorithm. This principle is shown in figure 1.2.

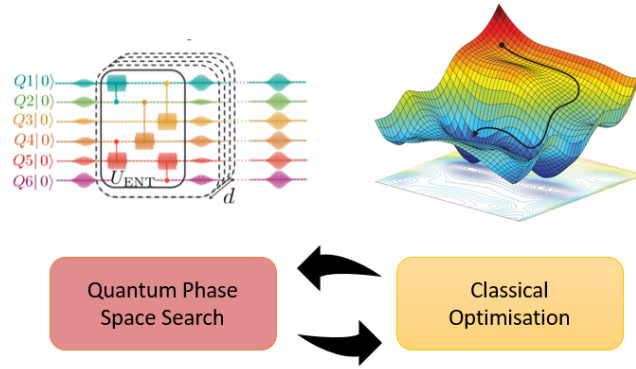


Figure 1.2: A representation of the quantum phase space search and the classical optimisation algorithm forming a feedback loop, showing the hybrid nature of the VQE algorithm [22][23].

This thesis focus on ultra-cold Rydberg atoms trapped in a lattice, which provide an excellent way of implementing a quantum circuit. Not only are they, through laser interactions, able to directly simulate condensed matter systems such as the quantum Ising model and lattices on which particles are trapped with $SU(N)$ degree of freedoms, serving as an analog quantum simulator [24], but they also span the set of universal quantum operators, so that any quantum circuit can be decomposed by implementation of precise Rydberg controls [25]. Additionally, on average, they have high initialisation and read-out fidelities, and coherence times on par with other quantum computer types such as those based on superconducting (SC) qubits or ion traps (IT) [26][27][28]. For certain qubit implementations, the fidelities and coherence times actually far exceed even those of said SC or IT qubits [29][30].

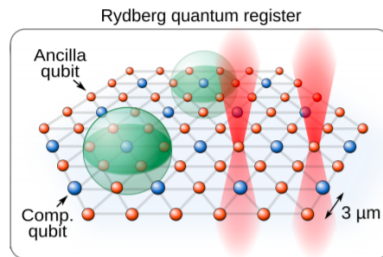


Figure 1.3: Ultracold Rydberg atoms can be loaded onto a 2D array, carrying qubit states in their state manifold. All qubit interactions can be experimentally controlled, and their role (ancilla/computational qubit) can be assigned a priori [25].

Instead of using single-qubit and two-qubit quantum gates only, it is compelling to also look at multi-qubit entanglement operations that could provide a speed-up of the convergence of the VQE algorithm. Because of the long range interactions between Rydberg atoms, generating long range entanglement and state transfer is a natural option for Rydberg-based QPUs. One specific example is perfect state transfer (PST), that allows the transfer of a quantum state along a one-dimensional qubit chain with unit fidelity. Such dynamics are allowed under very specific conditions, such as those provided by the Krawtchouk chain Hamiltonian. Engineering this Hamiltonian could provide unique insights in the transportation of quantum states, such as multi-qubit entanglement, entanglement distribution, or the transportation of states between different QPUs [31][32]. It could also boost the rate of convergence of the VQE algorithm [33], for which certain simulations have already provided clues [34].

In section 2, the theory of the VQE algorithm is explained. Many variations of the implementation of the algorithm exist, but the formalism that has been used in the recent largest quantum chemical experiment up to date by the Google AI group is taken [9]. Section 3 introduces the concept of errors in the context of quantum computing, and several quantities are discussed that can be used to quantify error propagation and the preservation of a pure qubit state and entanglement. Several types of error mitigation are then introduced in section 4, and their relation to the VQE algorithm is emphasised. In section 5, the physics of ultracold Rydberg atoms trapped in an optical lattice is presented, and how these atoms can be used to realise qubits and quantum gates. Then, in section 6, the theory behind PST is elaborated on. From basic principles, requirements are constructed that are needed for PST to take place along a 1D qubit chain. The results of several simple simulations of PST along small sized qubit chains is given in section 7, as well as the chain length specific conditions that have to be met. Section 8 presents an overview of this thesis. Several conclusions are drawn about the viability of VQE and PST on a Rydberg-based platform, and a future outlook is presented.

2 Hartree-Fock through VQE

2.1 The VQE algorithm

2.1.1 Introduction to quantum chemistry

Hartree-Fock theory is a mean-field theory, used in quantum chemistry, that provides a framework to find the stationary ground state wavefunction and its associated eigenenergy [35][36][37]. Central to Hartree-Fock theory are molecular energy problems, such as finding the lowest eigenstate of a molecular Hamiltonian, given in Hartree units by

$$\mathcal{H} = -\sum_A \frac{\nabla_A^2}{2m_A} - \sum_i \frac{\nabla_i^2}{2} - \sum_A \sum_i \frac{Z_A}{|\vec{r}_i - \vec{R}_A|} + \frac{1}{2} \sum_{A \neq B} \frac{Z_A Z_B}{|\vec{R}_A - \vec{R}_B|} + \frac{1}{2} \sum_{i \neq j} \frac{1}{|\vec{r}_i - \vec{r}_j|}. \quad (2.1)$$

Here, capital letters denote nuclei and lowercase letters denote electrons. m_A is the mass of nucleus A , Z_A is the charge of nucleus A , \vec{R}_A is the position vector of nucleus A and \vec{r}_i is the position vector of electron i . Hartree-Fock employs the Born-Oppenheimer approximation, which assumes that the nuclei are stationary and that the wavefunction Ψ of the molecule is separable:

$$\Psi = \Psi_{elec} \Psi_{nucl}, \quad (2.2)$$

such that Ψ_{elec} is the electronic wavefunction for a fixed nuclear configuration with wavefunction Ψ_{nucl} [38]. As nuclei are heavier than electrons, the kinetic energy of the former can be neglected. Additionally, the nuclei-nuclei repulsions are captivated into a single repulsion operator V_{nn} . The resulting Hamiltonian, still in first quantisation, can be rewritten in the second quantisation formalism. This second quantised molecular Hamiltonian is given by

$$\mathcal{H} = \sum_{ij} h_{ij} a_i^\dagger a_j + \sum_{pqrs} V_{pqrs} a_p^\dagger a_q^\dagger a_r a_s + V_{nn}. \quad (2.3)$$

As per usual, the operators a_x^\dagger and a_x are creation and annihilation operators of fermionic modes, filling and emptying spin-orbital x respectively. A filled orbital is referred to as occupied, while an empty orbital is referred to as virtual. These operators satisfy the usual fermionic anti-commutation relationships

$$\{a_i, a_j\} = \{a_i^\dagger, a_j^\dagger\} = 0, \quad (2.4)$$

$$\{a_i, a_j^\dagger\} = \delta_{ij}. \quad (2.5)$$

The terms $[\mathbf{h}]_{ij} = h_{ij}$ and $[\mathbf{V}]_{pqrs} = V_{pqrs}$ are called the one-electron integrals and two-electron integrals respectively. The former describe the electrons' kinetic energy and their potential energy in the potential landscape induced by the atomic nuclei. The latter describe the electron-electron repulsion energies. These integrals are given by

$$h_{ij} = \int \chi_i^*(\vec{r}) \left(-\frac{\nabla^2}{2} - \sum_A \frac{Z_A}{|\vec{r} - \vec{R}_A|} \right) \chi_j(\vec{r}) d\vec{r}, \quad (2.6)$$

and

$$V_{pqrs} = \frac{1}{2} \iint \frac{\chi_p^*(\vec{r}_1) \chi_q^*(\vec{r}_2) \chi_s(\vec{r}_2) \chi_r(\vec{r}_1)}{|\vec{r}_1 - \vec{r}_2|} d\vec{r}_1 d\vec{r}_2, \quad (2.7)$$

where the spin-orbitals χ are found by diagonalising the one-body integrals $[\mathbf{h}]_{ij}$, described in some basis. Usually an STO-nG basis is taken, as their Gaussian forms alleviate some of the taxing computations. The most common bases are STO-3G, STO-3G* and STO-6G [39][40].

2.1.2 The canonical approach to Hartree-Fock

One of the main pillars of Hartree-Fock theory is finding a solution to the time-independent Schrödinger equation by enforcing an anti-symmetrised product state as an ansatz, as is required by fermionic rules. Because of the nature of the mean field theory, this puts equal weight to every electron, each of which

feels only the mean potential induced by all other electrons. Let $\{\varphi_i\}$ be a set of orthogonal spatial wavefunctions and let $\{\chi_i\}$ be a set of mixed spatial one-electron wavefunctions, formed from linear superpositions of the old wavefunctions:

$$\chi_i = \sum_j c_{ij} \varphi_j. \quad (2.8)$$

Then, a state ansatz would be a Slater determinant type wavefunction formed from the anti-symmetrisation of the new mixed wavefunctions. Thus, the wavefunction $|\psi(r_1, \dots, r_n)\rangle$ that is to be variationally optimised, is given by

$$|\psi(r_1, \dots, r_n)\rangle = \frac{1}{\sqrt{n!}} A_n (\chi_1(r_1) \cdots \chi_n(r_n)), \quad (2.9)$$

where $A_n(\cdot)$ is the complete anti-symmetriser of dimension n . It is given by its tensor definition over a discrete set of functions $f_k(x)$:

$$A_n(f_1(x_1) \cdots f_n(x_n)) \stackrel{\text{def}}{=} \epsilon^{i_1, \dots, i_n} f_1(x_{i_1}) \cdots f_n(x_{i_n}), \quad (2.10)$$

where ϵ^{\dots} is the totally anti-symmetric permutation tensor, $i_1 \leq i_2 \leq \dots \leq i_n \in \{1, 2, \dots, n\}$, and where Einstein summation over the indices i_k is implied. Collapsing this state onto the position bra vector reveals its more familiar form

$$\langle r | \psi \rangle = \langle r | \prod_{i=1}^n a_i^\dagger | 0 \rangle = \frac{1}{\sqrt{n!}} \det \begin{pmatrix} \chi_1(r_1) & \cdots & \chi_1(r_n) \\ \vdots & \ddots & \vdots \\ \chi_n(r_1) & \cdots & \chi_n(r_n) \end{pmatrix}. \quad (2.11)$$

The representation of this antisymmetrised wavefunction as a determinant over the new basis functions gives this wavefunction the name 'Slater determinant'. For the VQE algorithm, it is beneficial to work with such Slater determinant type wavefunctions. In the context of scaling up hybrid algorithms in preparation of the NISQ era, this offers simplifications to highlight the benchmark performance. Advantages include:

1. For N qubits, the number of samples for energy estimation drops from $\mathcal{O}(N^4)$ to $\mathcal{O}(N^2)$.
2. Circuits can be concatenated into one circuit without changing the number of quantum gates.
3. The 1-RDM correlation functions $\langle a_i^\dagger a_i \rangle$ for a Slater-type wavefunction, defined later in section 2.2.3, can be purified.
4. The gradient of the energy with respect to the variational parameter is directly accessible from the 1-RDM.

Suppose that N spatial molecular orbital functions $\varphi_p(r)$ are uniquely encoded in N qubit states. Then a quantum circuit can implement an orbital basis rotation according to (2.8) as follows:

$$\tilde{\varphi}_p(r) = \sum_{q=1}^N [e^\kappa]_{pq} \varphi_q(r). \quad (2.12)$$

Here, κ is an $N \times N$ anti-Hermitian matrix that encodes the information about this basis rotation. Anti-Hermiticity ensures that the rotation is unitary so that a quantum circuit can simulate this. To be more precise, the circuit has to implement an $SO(N)$ -type rotation among the core orbitals rather than an $SU(N)$ -type, but since $SU(N) \supset SO(N)$, this can be achieved nonetheless.

This basis rotation can be encoded by the exponentiation of free fermion dynamics, as a result of work delivered by David Thouless [41]. For an initial state $|\eta\rangle$, the Slater determinant will then be given by

$$|\psi(\kappa)\rangle = \exp \left(\sum_{pq} \kappa_{pq} a_p^\dagger a_q \right) |\eta\rangle. \quad (2.13)$$

In order to illustrate why one-body fermionic operators generate a unitary operator that prepares this Slater determinant, it must be noted that these operators form a closed Lie algebra with Lie bracket relationships

$$[a_p^\dagger a_q, a_r^\dagger a_s] = \delta_{qr} a_p^\dagger a_s - \delta_{ps} a_r^\dagger a_q. \quad (2.14)$$

This is the adjoint representation of elements of the algebra κ . Its commutator with creation and annihilation operators is given by

$$[\kappa, a_p^\dagger] = a_q^\dagger \kappa_{pq}, \quad [\kappa, a_p] = a_q \kappa_{pq}^*. \quad (2.15)$$

These operators transform under this basis rotation to

$$e^K a_p^\dagger e^{-K} = \sum_q a_q^\dagger [e^\kappa]_{qp}, \quad e^K a_p e^{-K} = \sum_q a_q [e^\kappa]_{qp}^*, \quad (2.16)$$

according to the Baker-Campbell-Hausdorff (BCH) formula. Here, e^K is a representation of e^κ . Any rotation in the new basis can be rewritten as a similarity transform of operators in the old basis, such that any wavefunction $|\psi\rangle \stackrel{\text{def}}{=} \prod_{i=1}^n a_i^\dagger |0\rangle$ can be linked to a new wavefunction $|\phi(\kappa)\rangle$ according to

$$|\phi(\kappa)\rangle = e^K a_1^\dagger e^{-K} e^K a_2^\dagger e^{-K} \dots e^K a_n^\dagger e^{-K} |0\rangle = e^K |\psi\rangle, \quad (2.17)$$

where the identity $e^{-K} e^K = \mathbb{I}$ and the invariance of the vacuum state under basis rotations $e^{-K} |0\rangle = |0\rangle$ were used. This concludes the proof that a Slater determinant can be generated by implementing e^K as a series of quantum gates in the quantum circuit \mathcal{Q} , with an initial computational basis state.

Unlike qubit operators, fermionic operators do not commute in general. Therefore one would expect that the implementation of the unitary $U_\kappa = \exp\left(\sum_{pq} \kappa_{pq} a_p^\dagger a_q\right)$ can only be achieved by methods such as Trotterisation. This is not necessary, however, and it is possible to map this operator to a set of two-qubit operators, the amount of which is determined solely by the system size and number of electrons [42].

2.1.3 The variational principle

The variational principle of quantum mechanics suggests that one can find the ground state energy E_{gs} of a Hamiltonian \mathcal{H} by guessing a wavefunction that depends on a set of variational parameters, then finding for which parameter values this energy is globally minimised by some optimisation method. A usual formulation is analogous to the minimisation of a cost function, in this case the ground state energy. For any normalised wavefunction $|\Psi\rangle$, the variational principle states that

$$\langle \mathcal{H} \rangle_{|\Psi\rangle} = \langle \Psi | \mathcal{H} | \Psi \rangle \geq E_{gs}. \quad (2.18)$$

The set of parameters that parameterise the quantum circuit \mathcal{Q} can be updated through a classical feedback loop. Many such algorithms exist, such as the simultaneous perturbation stochastic approximation (SPSA) algorithm that has been employed by IBM for their largest quantum chemistry experiment up to date [22]. In the next section, a more robust algorithm called Hessian optimisation is presented that does not depend on a randomly generated walk through parameter space.

Another formulation of the variational principle is that the energy of a state is stationary with respect to first order perturbations in that wavefunction:

$$\langle \delta\psi | \mathcal{H} | \psi \rangle = 0. \quad (2.19)$$

Here, $\langle \delta\psi |$ is a first order change in the wavefunction $\langle \psi |$ [9][43]. Given the complete set of orbital functions, of which the ones used for the product wavefunction are labelled by $\{i\}$ and the ones unused by $\{a\}$, this change is expressed as

$$\langle \delta\psi | = \langle \psi | a_i^\dagger a_a \zeta, \quad (2.20)$$

where ζ is the first order change to an orbital χ_i . This changes (2.19) into the condition

$$\langle \psi | a_i^\dagger a_a \mathcal{H} | \psi \rangle = 0. \quad (2.21)$$

Every term in (2.19) can be evaluated by Wick's theorem given that the state $|\psi\rangle$ is a product state [44]. In Hartree-Fock theory, this equation naturally leads to a self-consistent field theory.

2.1.4 Hessian optimisation

The stationarity condition of the variational principle states that small disturbances in the wavefunction $\tilde{\Psi}$ should not lead to a change in energy to lowest order in the disturbance parameter. Following work by W. Kutzelnigg [45], this can be reformulated so that the equality

$$\delta\tilde{E} = \langle \tilde{\Psi} | \mathcal{H} | \tilde{\Psi} \rangle = 0 \quad (2.22)$$

holds with respect to a unitary basis rotation $U = e^R$, where R is an anti-Hermitian generator. Using the BCH formula, this stationarity condition can be rewritten in the following way: a variation in the energy \tilde{E} is given by

$$\tilde{E}' = \tilde{E} + \langle \tilde{\Psi} | [\mathcal{H}, R] | \tilde{\Psi} \rangle + \frac{1}{2} \langle \tilde{\Psi} | [[\mathcal{H}, R], R] | \tilde{\Psi} \rangle + \dots, \quad (2.23)$$

where stationarity is implied by the vanishing of the first order correction:

$$\langle \tilde{\Psi} | [\mathcal{H}, R] | \tilde{\Psi} \rangle = 0 \quad \forall R = -R^\dagger. \quad (2.24)$$

Suppose that a quantum circuit prepares a wavefunction Φ that does not satisfy (2.24) for some fixed generator R , such that

$$A_R \stackrel{\text{def}}{=} \langle \Phi | [\mathcal{H}, R] | \Phi \rangle \neq 0. \quad (2.25)$$

The wavefunction Φ can then be updated, keeping R fixed, by the following transformation

$$\Xi = e^{-f_R R} \Phi, \quad (2.26)$$

for an associated scalar f_R . The energy evaluation for this new wavefunction can be found to second order according to the BCH expansion

$$E_\Xi = \langle \Xi | \mathcal{H} | \Xi \rangle = \langle \Phi | e^{f_R R} \mathcal{H} e^{-f_R R} | \Phi \rangle = \langle \Phi | \left(\mathcal{H} + f_R [\mathcal{H}, R] + \frac{1}{2} f_R^2 [[\mathcal{H}, R], R] + \dots \right) | \Phi \rangle. \quad (2.27)$$

By stationarity, the derivative of the energy with respect to this update parameter f_R should vanish to first order. This is very similar to the Newton-Raphson optimisation process. Thus,

$$\frac{dE_\Xi}{df_R} = \langle \Phi | ([\mathcal{H}, R] + f_R [[\mathcal{H}, R], R] + \dots) | \Phi \rangle = 0. \quad (2.28)$$

If one defines a new quantity,

$$B_R \stackrel{\text{def}}{=} \langle \Phi | [[\mathcal{H}, R], R] | \Phi \rangle, \quad (2.29)$$

then the solution of (2.28) is

$$f_R = -\frac{A_R}{B_R}, \quad (2.30)$$

which does not vanish, leaving the transformation (2.26) non-trivial, unless the right stationary ground state wavefunction has been found.

It is easier, however, to consider updating the components of the generator R itself individually, because this directly correlates to particular changes in the κ -matrix, which eventually determines the gate rotations that have to be tuned experimentally. Let the generator $R^{(0)} \stackrel{\text{def}}{=} \sum_{pq} R_{pq}^{(0)} a_p^\dagger a_q$ be the starting point of the Hessian optimisation. Then for every iteration step k , every entry to this generator is updated by adding a multiplicative factor of f_{pq} . Let the gradient at step k be given by

$$g_{pq}^{(k)} = \left. \frac{\partial E}{\partial R_{pq}} \right|_{R^{(k)}}, \quad (2.31)$$

and let the Hessian matrix at step k be given by

$$H_{pqrs}^{(k)} = \left. \frac{\partial^2 E}{\partial R_{pq} \partial R_{rs}} \right|_{R^{(k)}}. \quad (2.32)$$

From equation (2.27), the gradient and Hessian can be rewritten in terms of quantities that depend on the sampled terms that comprise the 1-RDM. Then, they can be written as

$$g_{pq}^{(k)} = \langle \Phi | [\mathcal{H}, a_p^\dagger a_q] | \Phi \rangle \quad (2.33)$$

and

$$H_{pqrs}^{(k)} = \langle \Phi | [[\mathcal{H}, a_p^\dagger a_q], a_r^\dagger a_s] | \Phi \rangle. \quad (2.34)$$

The augmented Hessian equation, also known as the AH equation or the augmented Hessian Newton-Raphson method, gives the solution for these update parameters [46][47]. It is given by the matrix equation

$$\begin{pmatrix} 0 & \mathbf{g}^{(k)\top} \\ \mathbf{g}^{(k)} & \mathbf{H}^{(k)} \end{pmatrix} \begin{pmatrix} 1 \\ f_{pq} \end{pmatrix} = \epsilon \begin{pmatrix} 1 \\ f_{pq} \end{pmatrix}. \quad (2.35)$$

The wavefunction update is regularised by imposing a maximum update constraint, characterised by a small parameter γ . If the update parameters f_{pq} are smaller than γ , they remain the same, but if they are greater than γ , their influence will be decreased so that the solution convergence is controlled. The true update is then given by

$$f_{pq, \text{true}} = \begin{cases} f_{pq} & \text{if } f_{pq} \leq \gamma \\ \frac{\gamma}{\max f_{pq}} f_{pq} & \text{if } f_{pq} > \gamma \end{cases}. \quad (2.36)$$

2.2 The quantum circuit

2.2.1 Initialisation

The quantum circuit that has been used for this experiment is different from ones that have been used before. Let N be the number of spatial orbital basis functions. Then this circuit uses N qubits to encode these orbitals. First, the molecular Hamiltonian (2.3), without the electron-electron interactions, is diagonalised. The influence of these interactions on the eigenenergy of the ground state re-enter the Hartree-Fock calculations through the \mathbf{V} terms in the energy estimation of the molecular Hamiltonian. The eigenfunctions of this new diagonal Hamiltonian are the spatial orbitals that are uniquely mapped to qubits. Typically, the orbitals are ordered by their energy eigenvalues, from lowest to highest. Then, each qubit state will represent the occupancy number of the orbital that it represents, seen in figure 2.1. The state $|0\rangle$ therefore represents an empty orbital, also called a virtual orbital, while the $|1\rangle$ state denotes a filled orbital.

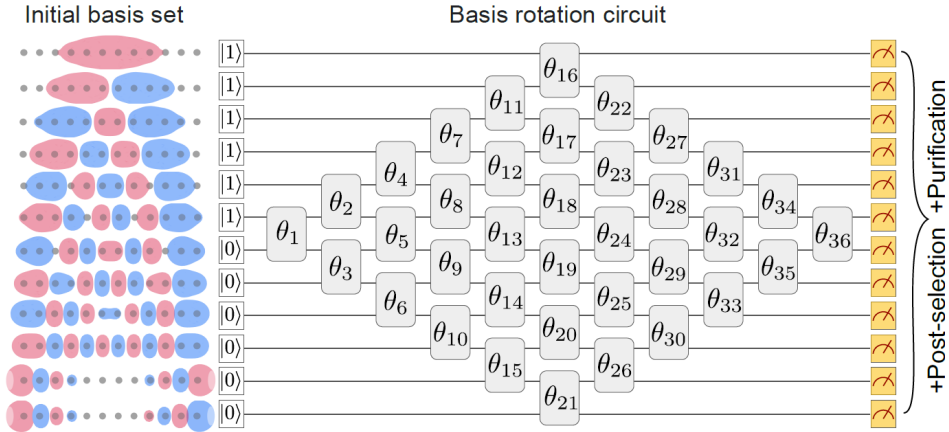


Figure 2.1: The quantum circuit that mixes the orbital states, for the artificial molecule H_{12} . Variational parameters control these mixing angles, and are variationally optimised to prepare the ground state Slater determinant [9].

If the molecule contains 2η electrons, then the first η qubit states will be initialised to be equal to $|1\rangle$. The remaining $N - \eta$ qubit states will be initialised as $|0\rangle$. The reason why only half of all electrons need

to be simulated is because HF theory is an effective mean field theory that does not refer to spin. It can therefore be assumed that all electrons form singlet configurations in the new orbital states. Every pair of spin-orbitals that share the same spatial orbitals can therefore be described by just a single qubit. If the state of one electron is known, then the state of the other with which it shares a singlet state can be deduced. If the electron states were mapped one-to-one onto qubit states, then half of all qubits would contain redundant information.

Typically, electrically neutral molecules are simulated rather than ions, though the latter certainly have interesting properties, so that $\eta = \frac{N}{2}$. The initial state $|\text{init}\rangle$ is then given by

$$|\text{init}\rangle = |1\rangle^{\otimes \eta} \otimes |0\rangle^{\otimes (N-\eta)} \stackrel{\text{def}}{=} |\eta\rangle. \quad (2.37)$$

Here, the state $|\eta\rangle$ represents the initial state as a computational basis state. From this state vector, the entire Hilbert space $\mathfrak{H} = \mathbb{C}^{\otimes 2^N}$ can be probed to find a suitable Slater determinant type wavefunction to approximate the electronic ground state within the framework of Hartree-Fock.

2.2.2 The Givens rotation sequence

The principal goal of the quantum circuit is to mix the orbitals so that a Slater determinant is prepared in the new basis. A set of Givens rotations is able to achieve such mixing.

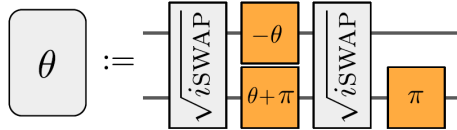


Figure 2.2: The decomposition of a Givens rotation into a series of unitary quantum gates. The orange gates θ represent a Z -rotation given by $\exp(-i\theta Z/2)$ [9].

The Givens rotation gate θ is given in figure 2.2. The matrix representation of \sqrt{iSWAP} gate is given by

$$\sqrt{iSWAP} = \begin{pmatrix} 1 & 0 & 0 & 0 \\ 0 & \frac{1}{\sqrt{2}} & \frac{i}{\sqrt{2}} & 0 \\ 0 & \frac{i}{\sqrt{2}} & \frac{1}{\sqrt{2}} & 0 \\ 0 & 0 & 0 & 1 \end{pmatrix}, \quad (2.38)$$

and the matrix representation of the $R_Z(\alpha)$ gate (orange box) is given by

$$R_Z(\alpha) = e^{-i\alpha Z/2} = \begin{pmatrix} e^{-i\alpha/2} & 0 \\ 0 & e^{i\alpha/2} \end{pmatrix}. \quad (2.39)$$

The final $\mathbb{I} \otimes R_Z(\pi)$ operation ensures that the second \sqrt{iSWAP} gate is turned into its Hermitian counterpart by the equality

$$\sqrt{iSWAP}^\dagger = \sqrt{iSWAP} (\mathbb{I} \otimes R_Z(\pi)). \quad (2.40)$$

This results in a matrix representation for the Givens rotation θ :

$$\theta = \begin{pmatrix} -1 & 0 & 0 & 0 \\ 0 & \cos \theta & \sin \theta & 0 \\ 0 & -\sin \theta & \cos \theta & 0 \\ 0 & 0 & 0 & -1 \end{pmatrix}, \quad (2.41)$$

which is different from the 'usual representation' given in literature by

$$\theta_{\text{literature}} = \begin{pmatrix} 1 & 0 & 0 & 0 \\ 0 & \cos \tilde{\theta} & -\sin \tilde{\theta} & 0 \\ 0 & \sin \tilde{\theta} & \cos \tilde{\theta} & 0 \\ 0 & 0 & 0 & 1 \end{pmatrix}. \quad (2.42)$$

The two are linked by an isomorphism $\tilde{\theta} = \pi - \theta$, however, which leaves the physics unchanged. The parameter space search algorithm for optimisation of the parameters does not care about isomorphisms either, so both representations are equivalent.

The Givens rotation decomposition follows from Thouless' theorem (2.13). This basis rotation can also be written as the unitary operator

$$U(u) = \exp \left(\sum_{pq} [\log u]_{pq} (a_p^\dagger a_q - a_q^\dagger a_p) \right). \quad (2.43)$$

This operator can be decomposed into $\frac{N(N-1)}{2} = \binom{N}{2}$ Givens rotations [42]. Because of the $SU(2)$ and $U(1)$ symmetries of the molecular Hamiltonian (2.3), this number can be reduced to $\eta(N - \eta)$ quantum gates. For an electrically neutral molecule, this has the consequence that the number of gates is reduced because the inequality $\frac{N^2}{4} < \binom{N}{2}$ holds for $N > 2$. This gate number reduction can be deduced from the fact that the set of operations that mix the orbitals contains redundant operations. Mixing between fully occupied orbitals, or between fully virtual orbitals, are examples of such redundancies, as they will only add a physically irrelevant global phase to the wavefunction.

Let $\tilde{a}_x^{(\dagger)}$ denote the creation and annihilation operators of an electron occupying orbital x in the new rotated basis, and let $a_x^{(\dagger)}$ be the creation and annihilation operators in the core orbital basis. Then a Slater determinant wavefunction is given by

$$|\psi(\kappa)\rangle = \prod_{i=1}^{\eta} \tilde{a}_i^\dagger |\text{vac}\rangle = \prod_{i=1}^{\eta} e^K a_i^\dagger e^{-K} |\text{vac}\rangle = \prod_{i=1}^{\eta} \sum_j [e^\kappa]_{ij} a_j^\dagger |\text{vac}\rangle, \quad (2.44)$$

where $|\text{vac}\rangle \stackrel{\text{def}}{=} |0\rangle$. Therefore, only the first η columns of the matrix e^κ are relevant. Let V be an arbitrary unitary operator, then it is true that

$$\prod_{i=1}^{\eta} \sum_{j=1}^{\eta} V_{ij} a_i^\dagger |\text{vac}\rangle = \det[V] \prod_{i=1}^{\eta} a_i^\dagger |\text{vac}\rangle. \quad (2.45)$$

For every unitary operator V , its determinant can be written as $e^{i\theta}$ for some $\theta \in [0, 2\pi)$, so that in (2.45), a global phase is given to the wavefunction. The structure of V can then be chosen such that Givens rotations can zero out the lower left triangle of the e^κ matrix. This is possible because Givens rotations aid in the QR-decomposition of u . Thus, the number of non-redundant two-qubit operations that remain is equal to the number of virtual orbitals multiplied by the number of occupied orbitals: $\eta(N - \eta)$.

Another property of Givens rotations is that the number of gates remains constant over many VQE optimisation steps. This is because the group of unitaries generated by the exponentiation of κ -matrices is closed and forms a homeomorphism [42]:

$$U(e^\kappa) \cdot U(e^{\kappa'}) = U(e^\kappa \cdot e^{\kappa'}). \quad (2.46)$$

Suppose that $U(e^\kappa)$ prepares a Slater determinant type wavefunction that does not correspond to the Hartree-Fock ground state $|\Psi_{HF}\rangle$. In equation form, this means that $U(e^\kappa)|\eta\rangle \neq |\Psi_{HF}\rangle$. Then, by Hessian optimisation, one can update the parameters so that a new Slater determinant is prepared that approximates the ground state better. Let $U(e^{\kappa'})$ be the unitary that performs this update. Then, $U(e^{\kappa'})U(e^\kappa)|\eta\rangle$ is a better approximation than $U(e^\kappa)|\eta\rangle$. For each iteration, a new circuit of $\eta(N - \eta)$ gates must be prepared. However, by the homeomorphism property, these circuits can be concatenated into a single circuit preparing $U(e^{\kappa'} \cdot e^\kappa)|\eta\rangle$.

2.2.3 Energy estimation

A useful quantity to describe the sampling of information about the molecular energy from this circuit are the p -marginals called the reduced density matrices. In general terms, a quantum marginal of a probability distribution is the partial trace over a subset of relevant variables so that only a small set of

p variables is considered. For a p -local Hamiltonian, it has been observed that the set of marginals of at most order p fully describe the system fully [48][49]. Their polynomial size make them an attractive candidate for reconstructing the qubit wavefunction. As a molecular Hamiltonian is 2-local, that is, it contains interaction terms between at most 2 interacting particles, only the one-particle reduced density matrix (1-RDM) and the two-particle reduced density matrix (2-RDM) are relevant. The 1-RDM \mathbf{D}^1 is given by its entries

$$[\mathbf{D}^1]_{ij} = D_{ij}^1 = \langle a_i^\dagger a_j \rangle. \quad (2.47)$$

The entries of the 2-RDM \mathbf{D}^2 are given by

$$[\mathbf{D}^2]_{pqrs} = D_{pqrs}^2 = \langle a_p^\dagger a_q^\dagger a_s a_r \rangle. \quad (2.48)$$

The energy estimation is given by the expectation value of the second quantised Hamiltonian (2.3), which by the distributive law of expectation values yields

$$E = \langle \mathcal{H} \rangle = \sum_{ij} h_{ij} \langle a_i^\dagger a_j \rangle + \sum_{pqrs} V_{pqrs} \langle a_p^\dagger a_q^\dagger a_r a_s \rangle = \sum_{ij} h_{ij} D_{ij}^1 + \sum_{pqrs} V_{pqrs} D_{pqrs}^2. \quad (2.49)$$

An interesting property of Slater determinant type wavefunctions is that their 2-RDM terms can be uniquely expressed as a function of 1-RDM terms only, as a consequence of the evaluation of each term in Wick's theorem [44]. This reduces the number of correlation functions that one must measure in order to estimate the energy from $\mathcal{O}(N^4)$ to $\mathcal{O}(N^2)$. This connection between 1-RDM and 2-RDM terms is expressed by

$$D_{pqrs}^2 = D_{pr}^1 D_{qs}^1 - D_{ps}^1 D_{qr}^1. \quad (2.50)$$

In conclusion, to estimate the energy of a molecule, one needs to

1. Sample all the 1-RDM terms to reconstruct \mathbf{D}^1 .
2. Compute, from these 1-RDM matrix entries, the 2-RDM \mathbf{D}^2 .
3. Evaluate equation (2.49).

2.2.4 Sampling the 1-RDM terms

All the necessary information that can be extracted from the quantum circuit are the entries of the 1-RDM. They can be categorised into three types: diagonal entries, one-off-diagonal entries and general off-diagonal entries. Each one requires a different protocol.

(i) Diagonal entries

First of all, using the fermionic operator basis to define measurement in is awkward. The Jordan-Wigner transformation transforms this basis into a Pauli basis, in which measurement is well-defined and well understood [19]. It is given by

$$a_j = \mathbb{I}^{\otimes j-1} \otimes \sigma^+ \otimes Z^{\otimes N-j}, \quad (2.51)$$

$$a_j^\dagger = \mathbb{I}^{\otimes j-1} \otimes \sigma^- \otimes Z^{\otimes N-j}, \quad (2.52)$$

where \mathbb{I} is the identity operator, and where the σ -matrices are given by

$$\sigma^\pm = \frac{X \pm iY}{2}. \quad (2.53)$$

As usual, the set $\{\mathbb{I}, X, Y, Z\}$ is called the non-Abelian Pauli basis P with representations

$$\mathbb{I} = \begin{pmatrix} 1 & 0 \\ 0 & 1 \end{pmatrix}, X = \begin{pmatrix} 0 & 1 \\ 1 & 0 \end{pmatrix}, Y = \begin{pmatrix} 0 & -i \\ i & 0 \end{pmatrix}, Z = \begin{pmatrix} 1 & 0 \\ 0 & -1 \end{pmatrix}. \quad (2.54)$$

These operators are unitary, Hermitian and mutually orthogonal under the Hilbert-Schmidt inner product. Throughout this thesis, they are sometimes also written as operators $\hat{\mathbb{I}}, \hat{\sigma}_x, \hat{\sigma}_y, \hat{\sigma}_z$. Henceforth, the identity operator shall be referred to as one of the Pauli operators.

A diagonal entry, with no summation over the indices implied, is given by

$$[\mathbf{D}^1]_{ii} = D_{ii}^1 = \langle a_i^\dagger a_i \rangle. \quad (2.55)$$

This is the expectation value of the number operator. This already implies that the trace of the 1-RDM is fixed according to

$$\sum_i D_{ii}^1 = \sum_i n_i = \eta. \quad (2.56)$$

If the 1-RDM is transformed to the Pauli basis under Jordan-Wigner, then the diagonal entries can be written as

$$\langle a_i^\dagger a_i \rangle = \frac{1 - \langle Z_i \rangle}{2} \stackrel{\text{def}}{=} M_i, \quad (2.57)$$

where M_i is the probability to find orbital i in an occupied state. Simply by measuring the qubit states, and averaging over many samples, one can find $\langle Z_i \rangle$ and thus also the diagonal components.

(ii) *One-off-diagonal entries*

The one-off-diagonal entries are comprised of correlation functions of the form

$$[\mathbf{D}^1]_{i,i+1} = D_{i,i+1}^1 = \langle a_i^\dagger a_{i+1} \rangle. \quad (2.58)$$

This results in awkward expressions after applying the Jordan-Wigner transform:

$$\langle a_i^\dagger a_{i+1} \rangle = \frac{1}{4} \langle (X_i - iY_i)(iY_{i+1} + X_{i+1}) \rangle. \quad (2.59)$$

In principle, it is possible to perform such measurements. There is a simpler way, however, to sample the one-off-diagonal 1-RDM terms that requires less measurements. Because of the Hermiticity of the 1-RDM, it can be concluded that

$$\langle a_i^\dagger a_{i+1} \rangle = \langle a_{i+1}^\dagger a_i \rangle^*. \quad (2.60)$$

Additionally, the 1-RDM does not contain any imaginary parts. This is because the circuit initialises qubits that have a direct one-to-one mapping to real-valued orbital functions. The circuit then performs an $SO(N)$ -type orbital rotation, so that the new superpositions are linear combinations of the old basis functions with the only phase differences between the orbitals being either 0 or π . This entails that only the real part of the sum $\langle a_i^\dagger a_{i+1} + a_{i+1}^\dagger a_i \rangle$ is measured, which corresponds to $2\Re\langle a_i^\dagger a_{i+1} \rangle$. In the Pauli basis, this corresponds to the cancellation of different terms, so that only

$$2\Re\langle a_i^\dagger a_{i+1} \rangle = \langle a_i^\dagger a_{i+1} + a_{i+1}^\dagger a_i \rangle = \frac{1}{2} (\langle X_i X_{i+1} \rangle + \langle Y_i Y_{i+1} \rangle) \quad (2.61)$$

is left, which is easier and more efficient to sample.

(iii) *General off-diagonal entries*

For general qubit architectures, it is not necessarily possible to apply two-qubit quantum gates between two random qubits, because they may not be nearest neighbours. Virtual swapping of qubits is therefore required to permute the qubit order so that their neighbours have changed. Then, the same procedure as for the one-off-diagonal terms can be applied. This repeats for all new possible permutations of the order of the qubits. Considering an arbitrary N -qubit quantum circuit, let $\{0, 1, 2, \dots, N-2, N-1\}$ be the set of fermionic modes in the abstract space \mathfrak{F} , and let (\cdot, \cdot) be the operation that swaps the respective fermionic modes according to

$$(m, n) : \mathfrak{F} \rightarrow \mathfrak{F} : \{\dots, a_m, \dots, a_n, \dots\} \mapsto \{\dots, a_n, \dots, a_m, \dots\}. \quad (2.62)$$

The numbers m, n in the swapping brackets do not refer to the values of a_m, a_n , but to their position, starting from 0 (the first entry), going to $N-1$. These fermionic swaps are generated by the F_{SWAP} operator, given by

$$F_{SWAP} = a_p^\dagger a_q + a_q^\dagger a_p - a_p^\dagger a_p - a_q^\dagger a_q. \quad (2.63)$$

The corresponding unitary is $\exp(-i\pi F_{SWAP}/2)$.

2.3 Neural networks

Interestingly, the development of VQE ties in well with the rise of artificial intelligence and machine learning. Over the past years, the advantages and utility of a fusion between quantum computing and machine learning has been debated. Especially within the fields of astrophysics, and particularly the search for dark matter, and particle physics, such a fusion is desirable. Within those fields, physicists are looking for clues of a deeper underlying theories without often knowing what those theories could look like, something for which they could benefit from machine learning algorithms. Such quantum-classical fusions have already happened for smaller algorithms, as certain classical machine learning algorithms have already been transposed into the language of quantum computing. For example, kNN has already been rewritten into a quantum algorithm called quantum- kNN that converges logarithmically faster than its classical counterpart [50], begging the question if general machine learning algorithms can be written down in the language of quantum computing. Clear analogies can be drawn between variational quantum algorithms and classical neural networks, lending those types of algorithms the name of Quantum Neural Network (QNN) at times [51].

An interesting parallel is that specifically of the VQE algorithm itself and classical neural networks, as they share a very similar structure. Classically, machine learning works by minimising some cost function that represents the accuracy of the task that the machine is supposed to perform. Quantum mechanically, there exists a cost function $L(\vec{\theta})$ that is clearly defined for VQE:

$$L(\vec{\theta}) = \langle \eta | U(\vec{\theta})^\dagger \mathcal{H} U(\vec{\theta}) | \eta \rangle, \quad (2.64)$$

where $\vec{\theta}$ is a vector of variational parameters, $|\eta\rangle$ is the initial ansatz, $U(\vec{\theta})$ the set of unitaries parameterised by $\vec{\theta}$, and \mathcal{H} is the Hamiltonian of which the ground state energy is calculated. This form can be likened to the ansatz of QNNs of N qubits, given by

$$U(\vec{\theta}) = \prod_{l=1}^N V_l \bigotimes_{j=1}^N U_j^l(\theta_j^l), \quad (2.65)$$

where V_l are parameter-independent unitaries such as those generated by multi-qubit entanglement operators and $U_j^l(\theta_j^l)$ is a unitary applied to qubit j at depth l , parameterised by $\theta_j^l \in \vec{\theta}$ [52]. This decomposition is reminiscent of some VQE implementations, where U represents the Euler rotations, and V represents the N -qubit entanglement [22]. The qubit number is tantamount to the number of neural nodes, while the circuit depth is comparable to the neural network depth. This direct comparison becomes clear from figure 2.3.

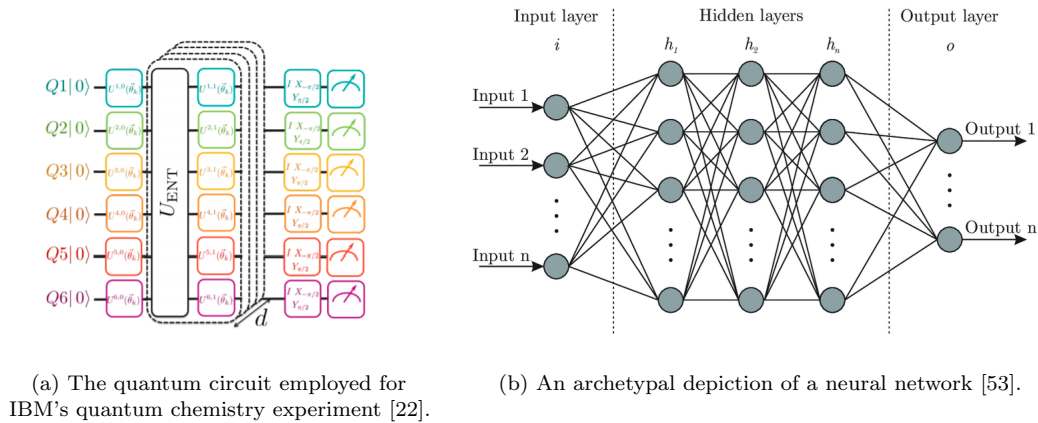


Figure 2.3: The comparison between a quantum circuit that runs the VQE algorithm and a classical neural network. Clear analogies can be drawn between qubit input \leftrightarrow input layer, entanglement \leftrightarrow node connection, depth \leftrightarrow hidden layers, and qubit read-out \leftrightarrow output layer.

Indeed, in some formulations of VQE, the quantum circuits that implement the algorithm have a very similar structure to classical neural networks. Their architecture is very alike, and so is their self-correcting nature. Where classical neural networks are able to teach themselves recognition patterns through optimising their cost function optimisation parameters through many learning iterations, so can the VQE algorithm variationally relax the parameters to find a ground state wavefunction of a quantum system after many iterations, even averaging out coherent and certain decoherent noise effects.

Writing the unitaries as exponentiations of Hermitian generators \mathbf{g} , which are expanded in the Pauli basis $P_k \in \mathcal{P}$, one obtains

$$U_j^l(\theta_j^l) = e^{-i\theta_j^l \mathbf{g}_j^l}, \quad (2.66)$$

where

$$\mathbf{g}_j^l = \sum_{k=1}^N [B_k]_j^l P_k = \sum_{k=1}^N B_{kj}^l P_k, \quad (2.67)$$

is the expansion of those generators in the Pauli basis, with relevant coefficients B_{kj}^l . This allows for the unitaries to be decomposed into a product of matrices with different dimensionalities:

$$U_j^l(\theta_j^l) = \prod_{k=1}^N \left(\cos(\theta_j^l B_{kj}^l) \mathbb{I} - i \sin(\theta_j^l B_{kj}^l) P_k \right), \quad (2.68)$$

from which gradients are easily derived [52]. Then, analytical derivatives of the cost functions follow, analogous to how classical neural networks aim to optimise their parameterisation.

Invoking machine learning in the sciences could indeed be a fruitful endeavour. This would have major implications for the development of fields like data analysis in particle physics, like it has done so outside the scope of science. Just like how chess AI engine AlphaZero could train itself to become the most powerful chess entity on the planet in a matter of hours [54], machine learning can train itself to rapidly develop the ability to predict new physics from a set of data, in such a fashion that is not immediately obvious to man [55]. Whether an extension of VQE could render variational quantum algorithms even stronger by fusing them with machine learning, remains to be seen.

3 Coherent and decoherent noise

3.1 Noise on a QPU

In the NISQ era, one of the greatest challenges that quantum computers face is the suppression of noise and the mitigation of error propagation. Because a quantum system can not be perfectly isolated from its environment, there will always be a certain amount of noise present. Usually, in real quantum computing experiments, a distinction is made between logical qubits and physical qubits. Logical qubits are theoretical qubits, whose state is perfectly known at all points in the circuit, who are either not subject to noise channels or subject to noise channels whose effects are deterministic and can be remodelled perfectly, while physical qubits are real qubits employed in experiments, and therefore subject to the imperfections of real life quantum processing units. For realistic experimental set-ups, it is common to have $\gtrsim 1000$ physical qubits for every logical qubit [56].

In VQE experiments, there is a pay-off between circuit depth and convergence rate. In principle, better entanglement will lead to more accurate results or to a faster convergence. In erroneous circuits, however, adding more depth may decrease the accuracy of the results, since errors have more time to accumulate. It is therefore important to tackle this error propagation, as naively introducing more depth and entanglement may actually decrease the VQE accuracy.

3.2 Fidelity in quantum computing

3.2.1 Mixed states and the density operator

Quantum algorithms deal theoretically with manipulating pure states to perform calculations. Environmental noise is able to pollute quantum states, turning them into mixed states. When describing erroneous quantum computing, it is necessary to go to the density operator formalism. The density operator satisfies the following mathematical properties:

1. Trace-preservation: $\text{Tr}(\rho) = 1$,
2. Hermiticity: $\rho^\dagger = \rho$,
3. Positive semi-definiteness: $\langle \psi | \rho | \psi \rangle \geq 0 \quad \forall |\psi\rangle$.

To name an example of interactions of the circuit with the environment that will cause the pure states of the qubit to transpire into mixed states, it may be useful to illustrate the necessity of using the density operator formalism with a small showcase. Consider a general qubit state $|\psi\rangle = \alpha|0\rangle + \beta e^{i\varphi}|1\rangle$. Then its density operator is given by

$$\rho = |\psi\rangle\langle\psi| = \begin{pmatrix} |\alpha|^2 & \alpha\beta^*e^{-i\varphi} \\ \alpha^*\beta e^{i\varphi} & |\beta|^2 \end{pmatrix}. \quad (3.1)$$

Suppose that by some process, such as scattering, the relative qubit phase is shifted, and suppose that this process is random, such that the relative phase difference $\delta\varphi$ is uniformly distributed on the interval $[0, 2\pi)$. Then the average density operator after many scattering processes is given by

$$\langle \rho \rangle_\varphi = \begin{pmatrix} |\alpha|^2 & \alpha\beta^* \langle e^{-i\varphi} \rangle_\varphi \\ \alpha^*\beta \langle e^{i\varphi} \rangle_\varphi & |\beta|^2 \end{pmatrix} = \begin{pmatrix} |\alpha|^2 & 0 \\ 0 & |\beta|^2 \end{pmatrix}, \quad (3.2)$$

where the latter equality holds because in the complex plane,

$$\langle e^{i\varphi} \rangle_\varphi = \lim_{N \rightarrow \infty} \frac{1}{N} \sum_{n=0}^{N-1} e^{2\pi i n \varphi / N} \rightarrow 0. \quad (3.3)$$

Clearly, there exists no pure wavefunction $|\psi\rangle$ such that it produces a density operator (3.2). Therefore, instead of using individual qubit states to quantify the effect of errors on the quantum circuit, the density operator is used. Error propagation manifests itself generally in the density matrix as the disturbance or absence of off-diagonal terms. As the Pauli operators span the space of 2×2 matrices, any density

matrix can be decomposed into the Pauli tensor basis as follows:

$$\rho = \frac{1}{2^N} \left(\mathbb{I}^{\otimes N} + \sum_{s \in S} (r_s s) \right), \quad (3.4)$$

where N is the number of qubits, S is the set of non-trivial Pauli tensor basis operators $S = \{\mathbb{I}, X, Y, Z\}^{\otimes N} \setminus \mathbb{I}^{\otimes N}$, and r_s are the components of the Bloch sphere vector $\vec{r} = \sum_{s \in S} r_s \hat{e}_s$ for each element $s \in S$, subject to the constraint $\|\vec{r}\| \leq 1$. The degree of admixture of a quantum state determines the norm of this Bloch vector. Pure states lie on the sphere and have $\|\vec{r}\| = 1$, while mixed states will lie within the sphere. In the extreme case, thus for maximally mixed states, the Bloch vector satisfies $\|\vec{r}\| \rightarrow 0$.

3.2.2 Quantum fidelity

Because quantum computers are subject to noise, real quantum simulations will deviate from their 'perfect' theoretical counterparts. Fidelity is a measure of the overlap of a certain density operator with another, and it can estimate the amount of noise that has accumulated over a certain circuit depth. The quantum fidelity F of a state $|\psi_a\rangle$, described by the density matrix ρ_a , with respect to some known state described by ρ_b , is given by [57]

$$F(\rho_a, \rho_b) = \left(\text{Tr} \left[\sqrt{\sqrt{\rho_b} \rho_a \sqrt{\rho_b}} \right] \right)^2. \quad (3.5)$$

It satisfies certain mathematical properties:

1. Symmetry: $F(\rho_a, \rho_b) = F(\rho_b, \rho_a)$.
2. Unit interval bounds: $F(\rho_a, \rho_b) \in [0, 1]$ and $F(\rho_a, \rho_b) = 1$ if and only if $\rho_a = \rho_b$.
3. Invariance under unitary transformations: $F(\rho_a, \rho_b) = F(U\rho_a U^\dagger, U\rho_b U^\dagger)$ for all unitary operations U .
4. Monotonicity: $F(\rho_a, \rho_b) \leq F(\Phi(\rho_a), \Phi(\rho_b))$ for all CPTP maps $\Phi(\cdot)$.

3.2.3 The fidelity witness

It is possible to construct a lower bound on the fidelity called the fidelity witness, nearly similar to the worst case fidelity (WCF). An observable \mathcal{W} is called a fidelity witness for a density operator ρ_t , if for $F_{\mathcal{W}}(\rho_p) \stackrel{\text{def}}{=} \text{Tr}[\mathcal{W}\rho_p]$, the following properties are satisfied:

1. $F_{\mathcal{W}}(\rho_p) = 1$ if and only if $\rho_t = \rho_p$,
2. $F > F_{\mathcal{W}}(\rho_p)$ for all states ρ_p .

On an N -qubit quantum circuit, any state ρ_t can be written as

$$\rho_t = |\psi_t\rangle \langle \psi_t| \quad (3.6)$$

where the wavefunction $|\psi_t\rangle$ is given by

$$|\psi_t\rangle = U |\boldsymbol{\omega}\rangle \quad (3.7)$$

where U is a fermionic Gaussian unitary operator and $|\boldsymbol{\omega}\rangle = (\omega_1, \dots, \omega_N)$ is an N -bit string, called the initialisation vector. This ket is a Fock-basis state vector where $\omega_j \in \{0, 1\}$ represents the excitation number of the j -th fermionic modem so that

$$n_j |\boldsymbol{\omega}\rangle = \omega_j |\boldsymbol{\omega}\rangle. \quad (3.8)$$

Then one can also introduce a total excitation number operator $n^{(\boldsymbol{\omega})}$ in a flipped basis where $|\boldsymbol{\omega}\rangle$ is the null vector:

$$n^{(\boldsymbol{\omega})} = \sum_{i=1}^N [(1 - \omega_i)n_i + \omega_i(\mathbb{I} - n_i)], \quad (3.9)$$

such that $n^{(\omega)}|\omega\rangle = 0$. Any other basis state would then be an excited state with respect to the null vector $|\omega\rangle$ and the operator $n^{(\omega)}$. With this operator at hand, it is possible to construct the observable

$$\mathcal{W} = U \left(\mathbb{I} - n^{(\omega)} \right) U^\dagger, \quad (3.10)$$

which is proven to be a fidelity witness for the state ρ_t in work conducted by Gluza et al. for non-interacting fermionic wavefunctions [58]. Knowledge of the RDM terms gives insight in this fidelity witness. Let \mathfrak{D} be the matrix of expectation values $\langle \rho, a_i^\dagger a_j \rangle$ and let $\mathbf{u} = e^\kappa$ be the generator of the circuit. Then the identity

$$\text{Tr} \left[U \rho U^\dagger a_i^\dagger a_j \right] = [\mathbf{u} \mathfrak{D} \mathbf{u}^\dagger]_{ij} \quad (3.11)$$

holds. Using this, the fidelity witness can be rewritten as

$$F_{\mathcal{W}}(\rho) = 1 - \sum_{j=1}^N \left([\mathbf{u}^\dagger \mathfrak{D} \mathbf{u}]_{jj} + \omega_j - 2\omega_j [\mathbf{u}^\dagger \mathfrak{D} \mathbf{u}]_{jj} \right). \quad (3.12)$$

3.3 Quantification of high-fidelity propagation

3.3.1 Clifford gates

Clifford gates are a set of gates belonging to the Clifford group on N qubits

$$\mathfrak{C}_N = \{U \mid U P_N U^\dagger = P_N\}, \quad (3.13)$$

formally corresponding to the normaliser of the Pauli group [59]. It is known that the Hadamard gate

$$H = \frac{1}{\sqrt{2}} \begin{pmatrix} 1 & 1 \\ 1 & -1 \end{pmatrix} \quad (3.14)$$

and the phase gate

$$S = \begin{pmatrix} 1 & 0 \\ 0 & i \end{pmatrix} \quad (3.15)$$

are elements of \mathfrak{C}_1 , while the CNOT gate is an element of \mathfrak{C}_2 . Together, they span a universal set of quantum gates, and by extension, they span $\bigcup_k \mathfrak{C}_k$. Let \mathfrak{C}^L denote a string of L single-qubit Clifford gates. Then an identity-proportional string, meaning $\mathfrak{C}^L \rightarrow \mathbb{I}$, can be employed to gauge the error propagation through an arbitrary N -qubit channel. For the single-qubit case, let an initial qubit state $|0\rangle$ be prepared, and sent through this Clifford channel. Then, the average of the 0-state projector $\langle \Pi_0 \rangle$ is given by [60]

$$\langle \Pi_0 \rangle = \left| \langle 0 | \mathfrak{C}^L | 0 \rangle \right|^2. \quad (3.16)$$

By tracking this quantity as a function of string length L , one can verify error propagation through any N -qubit channel. Therefore, it serves as an excellent benchmark for the accuracy of the RDA algorithm, introduced in section ??, as well as a good quantifier for error propagation in a certain type of quantum computer.

3.3.2 Concurrence and n -tangles

Besides having a formal measure of the preservation of a pure quantum state under noise channels, it is also valuable to have a measure of the degree of entanglement, called the concurrence. When transporting entangled states through a qubit register, both fidelity and concurrence track how preserved this delicate state is. Let the single-qubit state $|\tilde{\psi}\rangle$ be given by

$$|\tilde{\psi}\rangle = i\sigma_y |\psi\rangle^*, \quad (3.17)$$

which formally corresponds to the time-reversal operation of a spin- $\frac{1}{2}$ particle, which reverses the spin orientation [61]. Here, $|\psi\rangle^*$ is the complex conjugation of the wavefunction in the standard basis. The

factor i is convention, but the concurrence is blind to it. Then, this definition can be extended to two-qubit wavefunctions:

$$|\tilde{\psi}\rangle = -\sigma_y \otimes \sigma_y |\psi\rangle^*. \quad (3.18)$$

The two-qubit concurrence is then given by the overlap [62]

$$C(|\psi\rangle) \stackrel{\text{def}}{=} \left| \langle \psi | \tilde{\psi} \rangle \right|. \quad (3.19)$$

This quantity serves as a rigorous measure of degree of entanglement, and generates the entanglement entropy $S[C(|\psi\rangle)]$.

The common denominator between concurrence and fidelity is that they are bounded in the interval $[0, 1]$, but the critical difference between them is that fidelity measures the overlap of two quantum states, usually between a theoretical prediction and a real state that is prone to errors. Concurrence, on the other hand, measures the self-overlap of a quantum state, fine-tuned to be a useful quantity when discussing entanglement.

Generally, entanglement between qubits in a register is not restricted to nearest neighbours. Let ρ be the density operator of the whole register, and let ρ_{ij} be the density operator of the register, restricted to qubits i and j :

$$\rho_{ij} = \text{Tr}_{k \neq i, j}[\rho]. \quad (3.20)$$

Between these qubits, the concurrence is defined as

$$C_{ij} = C(\rho_{ij}) = \inf_{p_n, |\psi_n\rangle} \sum_n p_n C(|\psi_n\rangle), \quad (3.21)$$

where the classical probabilities p_n and states $|\psi_n\rangle$ are determined through the spectral decomposition

$$\rho_{ij} = \sum_n p_n |\psi_n\rangle \langle \psi_n|. \quad (3.22)$$

For three-qubit entanglement, one can define an analogy known as the three-tangle $\tau^{(3)}$, given by [63]

$$\tau_{i,j,k}^{(3)} = T_{jk}^2 - C_{ij}^2 - C_{ik}^2, \quad (3.23)$$

acting on qubits i, j and k , where

$$T_{jk} \stackrel{\text{def}}{=} \sqrt{2(1 - \text{Tr}[\rho_{jk}])}. \quad (3.24)$$

This discussion can be extended to the entanglement degree of an arbitrary number of qubits. Such a measure is called the n -tangle, though it is not defined for odd $n > 3$ [64].

3.4 Coherent noise channels

In principle, noise on a quantum computer can be divided into two types: coherent noise and decoherent noise. Errors arising from the former type, coherent errors, are systematic errors that arise in the quantum computer through insufficient or incorrect knowledge about what drives the unitary gates. This ignorance could manifest itself as an unknown part $\delta\mathcal{H}$ of a Hamiltonian that generates the evolution of the qubit states. These errors can in theory be reconstructed deterministically and then compensated for with the right measures. In general, they can be reversed by a unitary operator U .

An example of a coherent noise channel is the systematic phase error in some quantum gates. For example, Google AI reports that their $\sqrt{\text{iSWAP}}$ gate has a systematic $|11\rangle\langle 11|$ phase error of $\sim \pi/24$ [9]. Another example is the 'slow walk' of a qubit state along the Bloch sphere. Where no operation is performed (\mathbb{I}), a very slow deviation through ignorance in the control dynamics may be expected instead, of the form $U = e^{i\epsilon X}$ [65]. Arguably, these are the most common coherent error types, in the VQE formulation that has been adhered to in this thesis.

3.5 Decoherent noise channels

3.5.1 Decoherent noise

The other type of errors, decoherent errors, arise from stochastic interactions. They are probabilistic in nature, and will cause the qubit array state to become mixed over time. They can not be described by the coherent Schrödinger or von Neumann equations and must therefore be described by modified theories, such as the Lindbladian equation or Markovian dynamics. Unlike coherent errors, they are irreversible, which means that they can not be systematically removed from the system by compensation. Other measures such as RDA must be invoked then.

3.5.2 Qubit relaxation and dephasing

Qubit relaxation and dephasing are two major decoherence processes that impose a constraint on the coherence time of a quantum circuit. Relaxation refers to the process in which a qubit decays to its ground state. This depends on the physical type of qubit that has been employed and the qubit mapping that has been taken. This exponential decay is characterised by the relaxation time scale T_1 . Dephasing refers to the process in which the relative phase of a qubit can vary over time, causing pure states to transpose into mixed states. The energy difference between the $|0\rangle$ and $|1\rangle$ states are usually fixed. Small perturbations, however, can induce small variations in this energy difference, causing the two qubit basis states to evolve at different rates, manifesting itself as phase shifts. An example has already been introduced in section 3.2.1, where the phase shifts of many scattering processes can lead to mixed states. The characteristic timescale for dephasing is called T_2 . Often, in literature, a third timescale T_2^* exists, caused by the combined effects of dephasing and the inhomogeneity of applied external fields [66].

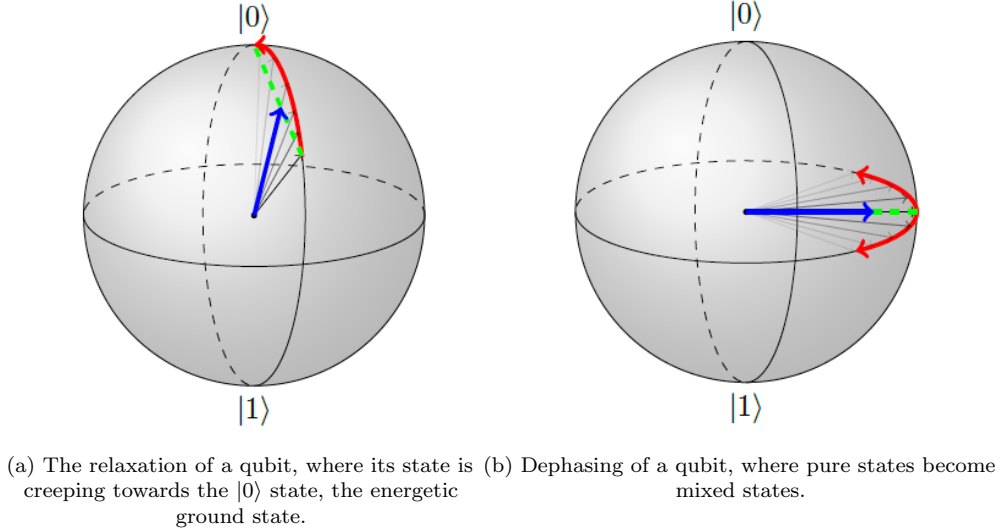


Figure 3.1: The Bloch sphere representation of qubit relaxation and dephasing processes [67]. The blue arrows represent the qubit state, while the red arrows show the trend of the state evolution. The green dashed line shows the trajectory of the qubits.

These timescales impose a crucial constraint on the quantum circuit. For calculation times $\tau \ll T_1, T_2$, the system will preserve its coherence up to small perturbations. For calculation times $\tau \gtrsim T_1, T_2$, coherence will mostly be lost, and the results will be rendered inaccurate.

3.5.3 Depolarisation channel

A depolarisation channel is a decoherent error channel that depends on a single noise parameter ξ . It can be described by a CPTP map \mathfrak{P}_ξ whose effect on a single-qubit density operator ρ_1 and a two-qubit

density operator ρ_2 is given by

$$\mathfrak{P}_\xi(\rho_1) = (1 - \xi)\rho_1 + \frac{\xi}{3} \sum_{i=1,2,3} \sigma^i \rho_1 \sigma^i \quad (3.25)$$

and

$$\mathfrak{P}_\xi(\rho_2) = (1 - \xi)\rho_2 + \frac{\xi}{15} \sum_{\substack{i,j=0,1,2,3 \\ \{i,j\} \neq \{0,0\}}} \sigma_l^j \sigma_m^i \rho_2 \sigma_m^i \sigma_l^j \quad (3.26)$$

respectively [68]. The indices $\{l, m\}$ refer to a set of nearest neighbour qubits in the given connectivity of the circuit architecture. The constants 3 and 15 are present to preserve the trace of the density operator. This depolarisation channel can be used to gauge the strength of an entanglement operator versus the strength of noise disrupting the VQE algorithm and increasing the energy estimate on average. From simulations it then follows that there exists an optimal number of entanglement operations before the VQE algorithm actually returns a higher energy estimate.

3.6 The Lindbladian

3.6.1 The von Neumann equation

In essence, the von Neumann equation is the equivalent of the time-dependent Schrödinger equation for density operators ρ instead of wavefunctions $|\psi\rangle \in \mathfrak{H}$. The latter is given by

$$i\hbar \frac{\partial |\psi\rangle}{\partial t} = \mathcal{H} |\psi\rangle, \quad (3.27)$$

where \mathcal{H} is the Hamiltonian. In the dual Hilbert space \mathfrak{H}^* , this equation reads

$$i\hbar \frac{\partial \langle\psi|}{\partial t} = \langle\psi| \mathcal{H}. \quad (3.28)$$

Then the time derivative of the density operator is given by

$$\frac{\partial \rho}{\partial t} = \frac{\partial |\psi\rangle \langle\psi|}{\partial t} = \frac{\partial |\psi\rangle}{\partial t} \langle\psi| + |\psi\rangle \frac{\partial \langle\psi|}{\partial t} = -\frac{i}{\hbar} \mathcal{H} |\psi\rangle \langle\psi| - \frac{i}{\hbar} |\psi\rangle \langle\psi| \mathcal{H}, \quad (3.29)$$

where in the last equation, the Schrödinger equations in the regular and dual Hilbert spaces were substituted. Noting that on the right hand side, $|\psi\rangle \langle\psi| = \rho$ returns the density operator, the von Neumann equation is obtained:

$$\frac{\partial \rho}{\partial t} = -\frac{i}{\hbar} [\mathcal{H}, \rho], \quad (3.30)$$

where $[\cdot, \cdot]$ denotes commutator brackets [69].

3.6.2 The Born-Markov master equation

A master equation is an equation that follows the time evolution of a system that is in a probabilistic combination of different states, where the dynamics are encoded in an intensity matrix. The qubit interactions with the environment can be described by a system-bath type of interaction, where the qubits in the quantum circuit constitute a system s with a Hamiltonian \mathcal{H}_s and the environment constitutes a bath b with a Hamiltonian \mathcal{H}_b . Then the total Hamiltonian is given by

$$\mathcal{H} = \mathcal{H}_s \otimes \mathbb{I}_b + \mathbb{I}_s \otimes \mathcal{H}_b + \epsilon \mathcal{H}_{sb}, \quad (3.31)$$

where \mathbb{I}_a denotes the identity operator on subsystem a , \mathcal{H}_{sb} represents the interaction Hamiltonian and ϵ characterises the strength of this interaction. Closely following C.A. Brasil et al. [70], it is convenient to switch over to the interaction picture, where

$$\mathcal{H}(t) = e^{i(\mathcal{H}_s + \mathcal{H}_b)t} \mathcal{H}_{sb} e^{-i(\mathcal{H}_s + \mathcal{H}_b)t} \quad (3.32)$$

and

$$\rho(t) = e^{i(\mathcal{H}_s + \mathcal{H}_b)t} \rho_{sb} e^{-i(\mathcal{H}_s + \mathcal{H}_b)t}, \quad (3.33)$$

in which case the von Neumann equation reads

$$\frac{\partial \rho(t)}{\partial t} = -\frac{i}{\hbar} \epsilon [\mathcal{H}(t), \rho(t)]. \quad (3.34)$$

One can construct an iterative expansion of the right-hand side of equation (3.34), as the equation can be integrated over, and the resulting expression of $\rho(t)$ can be plugged back into the original equation. To second order in ϵ , this yields

$$\frac{\partial \rho(t)}{\partial t} = -\frac{i}{\hbar} \epsilon [\mathcal{H}(t), \rho(0)] - \frac{1}{\hbar^2} \epsilon^2 \int_0^t [\mathcal{H}(t), [\mathcal{H}(t'), \rho(t')]] dt'. \quad (3.35)$$

Under the tensor decomposition $\rho(t) = \rho_s(t) \otimes \rho_b$, it is possible to trace the bath degrees of freedom out of equation (3.35), yielding

$$\frac{\partial \rho_s(t)}{\partial t} = -\frac{i}{\hbar} \epsilon \text{Tr}_b([\mathcal{H}(t), \rho(0)]) - \frac{1}{\hbar^2} \epsilon^2 \text{Tr}_b\left(\int_0^t [\mathcal{H}(t), [\mathcal{H}(t'), \rho(t')]] dt'\right). \quad (3.36)$$

One can define the interaction \mathcal{H}_{sb} in such a way that the first time on the right-hand side vanishes. Assuming a strong decay for timescales much greater than the characteristic correlation time in the bath ($t \gg \tau_{corr}$), the boundary of the integral may be shifted over to infinity. Lastly, the density operator inside the integral swaps variables $t' \mapsto t$ because ρ varies slowly¹. What remains is the Born-Markov master equation

$$\frac{\partial \rho_s(t)}{\partial t} = -\frac{1}{\hbar^2} \epsilon^2 \text{Tr}_b\left(\int_0^\infty [\mathcal{H}(t), [\mathcal{H}(t'), \rho(t)]] dt'\right). \quad (3.37)$$

3.6.3 The Lindblad equation

Consider an interaction between the system and the bath that is semi-separable, such that it can be written as

$$\mathcal{H}_{sb} = \hbar (SB^\dagger + S^\dagger B), \quad (3.38)$$

where S is an operator acting on the system, and B is an operator acting on the bath. If S commutes with the system Hamiltonian,

$$[S, H_s] = 0, \quad (3.39)$$

then this operator will remain time-independent in the interaction picture: $S(t) = S$. To derive the Lindblad equation, some assumptions can be made. For one, the bath Hamiltonian can be written as a bosonic bath according to

$$\mathcal{H}_b = \hbar \sum_k \omega_k a_k^\dagger a_k, \quad (3.40)$$

where ω_k are the specific angular frequencies of the bosonic modes k with momentum k and a_k^\dagger , a_k are creation and annihilation operators respectively of such modes k . A bath operator that looks like

$$B(t) = \sum_k g_k^* a_k e^{-i\omega_k t} \quad (3.41)$$

in the interaction picture represent a Jaynes-Cummings like model [71]. The initial bath density operator is in a vacuum state over all modes:

$$\rho_b = |\text{vac}\rangle \langle \text{vac}|, \quad (3.42)$$

where the vacuum state is given by

$$|\text{vac}\rangle = \bigotimes_{n=1}^N |0\rangle. \quad (3.43)$$

¹Consider a Taylor expansion of ρ like $\epsilon^2 \rho(t') \approx \epsilon^2 [\rho(t) + (t' - t) d\rho(t)/dt + \dots] = \epsilon^2 \rho(t) + \mathcal{O}(\epsilon^4)$. Then any deviation to this approximation is fourth order in the interaction parameter and may be discarded.

With further assumptions, the Born-Markov equation with the full interactions turned on ($\epsilon \rightarrow 1$) transforms into

$$\frac{\partial \rho_s(t)}{\partial t} = \gamma \left[S \rho_s(t) S^\dagger - \frac{1}{2} \{ S^\dagger S, \rho_s(t) \} \right], \quad (3.44)$$

where the small parameter γ is given by the expression

$$\gamma = 2\pi \int_0^\infty \left(\sum_l |g_l|^2 \delta(\omega - \omega_l) \right) \delta(\omega) d\omega, \quad (3.45)$$

characterising the strength of the system-bath interactions [70]. Returning back to the original picture, using

$$\rho_s = e^{-\frac{i}{\hbar} \mathcal{H}_s t} \rho_s(t) e^{\frac{i}{\hbar} \mathcal{H}_s t}, \quad (3.46)$$

equation (3.44) becomes

$$\frac{\partial \rho_s}{\partial t} = -\frac{i}{\hbar} [\mathcal{H}_s, \rho_s] + \gamma \left[S \rho_s S^\dagger - \frac{1}{2} \{ S^\dagger S, \rho_s \} \right]. \quad (3.47)$$

Most common, the right-hand side of this equation contains many such terms, a superposition of so-called Lindblad operators L_j , such that the Lindblad equation is obtained:

$$\frac{\partial \rho_s}{\partial t} = -\frac{i}{\hbar} [\mathcal{H}_s, \rho_s] + \gamma \mathcal{L}(\rho_s), \quad (3.48)$$

where the Lindbladian $\mathcal{L}(\rho_s)$ is given by [72]

$$\mathcal{L}(\rho_s) = \sum_j \left[S_j \rho_s S_j^\dagger - \frac{1}{2} \{ S_j^\dagger S_j, \rho_s \} \right]. \quad (3.49)$$

This Lindblad equation is linear in its argument, and contains a coherent part resulting from the Schrödinger equation, and a decoherent part resulting from interactions of the quantum circuit with a noisy environment. The former is called the Liouvillian and describes unitary evolution. The latter contains a term where all degrees of freedom of the bath have been traced out, and only the Jaynes-Cummings like interaction is present in the equation through the small interaction parameter γ . This partial trace is non-unitary, and therefore this term describes the non-unitary evolution of the density operator under decoherent noise.

4 Error mitigation and quantification techniques

4.1 Introduction to partial QEC

Currently, there is not yet access to a full quantum error correction code that renders quantum computer completely fault tolerant. However, major gains have been made during the past decades to come up with (theoretical) measures to mitigate errors in a quantum circuit [65]. This is a non-trivial task, for simply transposing classical ideas of error correction does not work for quantum computing. To illustrate this with a brief example, in classical computers, one of the simplest error correction codes is the binary repetition code. For instance, the bits 0 and 1 can be copied into 3-tuples, such that

$$0 \mapsto 000, \quad 1 \mapsto 111. \quad (4.1)$$

This mapping can tolerate 1 bit flip, and a majority decision decides what the original code used to be. Then, a bit string of 001 is understood to originate from 000, thus it represents the state 0. But 110, on the other hand, comes from 111, thus 1. Such a code can not be achieved in quantum computing by virtue of the no-cloning theorem, which states that there exists no operation that maps a quantum state $|\alpha\rangle$ to $|\alpha\rangle^{\otimes k}$ for arbitrary natural numbers $k \geq 2$ [73][74].

Full fault-tolerant error correction for $\gtrsim 10^5$ qubits is not yet within the range of experimental possibilities. A step towards this full QEC is partial QEC, where some form of error correction is used that mitigates some errors by at most a few orders of magnitude. The central idea to partial QEC is the following: suppose there exists some noise channel \mathcal{E} acting on a density operator, given by its spectral decomposition

$$\rho = \sum_i p_i |w_i\rangle \langle w_i|, \quad (4.2)$$

where $|w_i\rangle$ are pure states that have a classical probability $p_i \in (0, 1]$ of occurring. Then, does there also exist an error correction channel \mathcal{R} such that for an arbitrary accuracy threshold,

$$\|\mathcal{R} \circ \mathcal{E}(\rho) - \rho\| < \epsilon? \quad (4.3)$$

4.2 Post-circuit error mitigation for VQE

4.2.1 Post-selection

Each Givens rotation commutes with the number operator. This ensure that, theoretically, the entire quantum circuit as depicted in figure 2.1 must preserve the total electron number and therefore also the qubit parity. For an electrically neutral system such as an unionised molecule, it is given that $\langle Z_{tot} \rangle = 0$. Because of error propagation, there is a small probability that, for example, a bit flip occurs in one of the qubit arrays. Sampling such qubit outputs will therefore not have the correct required physical interpretation as chemically, electrons would have spontaneously been destroyed or created. Such results must therefore be discarded: this process is known as post-selection.

A small problem arises when post-rotational gates are applied to the qubits after the Givens rotations so that $\langle XX \rangle$ and $\langle YY \rangle$ can be sampled. These Pauli operators do not commute with the total number operator as they are not diagonalised, unlike the identity operator \mathbb{I} and Z . Additional quantum hardware must be invoked so that the X and Y operators can be transformed into something that allows them to be sampled, but such that they do respect electron conservation. Only then will post-selection lead to robust error mitigation.

Let the so-called T -gate be given by

$$T = R_Z(\pi/4) = \begin{pmatrix} e^{-i\pi/8} & 0 \\ 0 & e^{i\pi/8} \end{pmatrix}, \quad (4.4)$$

and let the diagonaliser V be given by

$$V = (T \otimes T^\dagger) \sqrt{iSWAP}. \quad (4.5)$$

Then, this unitary operator will diagonalise the $\frac{1}{2}(XX + YY)$ Hamiltonian according to

$$V \begin{pmatrix} 0 & 0 & 0 & 0 \\ 0 & 0 & 1 & 0 \\ 0 & 1 & 0 & 0 \\ 0 & 0 & 0 & 0 \end{pmatrix} V^\dagger = \begin{pmatrix} 0 & 0 & 0 & 0 \\ 0 & 1 & 0 & 0 \\ 0 & 0 & -1 & 0 \\ 0 & 0 & 0 & 0 \end{pmatrix}. \quad (4.6)$$

The right-hand side of equation (4.6) now commutes with the particle-number operator, while retaining some of the character of the X and Y Pauli operators. Let the Hamiltonian act on nearest neighbour qubits $i, i + 1$, then the following equality can be identified [9]:

$$\left\langle V \frac{1}{2} (X_i X_{i+1} + Y_i Y_{i+1}) V^\dagger \right\rangle = \frac{1}{2} \langle Z_i - Z_{i+1} \rangle = \frac{1}{2} (M_{i+1} - M_i). \quad (4.7)$$

By this transformation, it is still possible to check for particle conservation. Instead of measuring correlation functions, it is now sufficient to measure single-qubit states only. This method of post-selection renders the VQE algorithm more robust because outputs that do not make physically sense² can be discarded by checking for the condition

$$\langle Z_{tot} \rangle = 0. \quad (4.8)$$

4.2.2 McWeeny purification

By repeatedly sampling the correlation functions $\langle a_i^\dagger a_j \rangle$, one can reconstruct the 1-RDM matrix. Because of circuit errors, readout errors and the finite number of samples, this matrix will not replicate the true 1-RDM to infinite precision. The latter will always satisfy 3 conditions [48][75]:

1. $\text{Tr}[D] = \eta$: the trace of the 1-RDM gives the total number of electrons as implied by (2.56).
2. $D^2 = D$: the 1-RDM is idempotent as a result of idempotency of the pure ground state density matrix.
3. $D \succeq 0$: the 1-RDM is positive semi-definite.

Because of errors, the reconstructed 1-RDM will generally not satisfy these conditions. The reconstructed 1-RDM lives in the space of $N \times N$ matrices, \mathbf{M}_N . One can define a subset within this space, called the idempotency manifold³, the set of all 1-RDMs that satisfy the three conditions mentioned above, onto which the reconstructed 1-RDM can be projected. This process is known as purification. Let \tilde{D} be this projected 1-RDM in the idempotency manifold satisfying the minimization condition:

$$\min_{\text{Tr}[\tilde{D}] = \eta, \tilde{D}^2 = \tilde{D}, \tilde{D} \succeq 0} \|D - \tilde{D}\|_m, \quad (4.9)$$

where $\|\cdot\|_m$ is the matrix norm

$$\|A\|_m = \sup_{\|x\|=1} \|Ax\|_2, \quad (4.10)$$

where $\|\cdot\|_2$ is the linear algebraic 2-norm

$$\|r\|_2 = \sqrt{\sum_i |r_i|^2}. \quad (4.11)$$

There exists a systematic way of projecting the sampled 1-RDM onto the manifold of idempotency. Let $D = D_0$ be the 0-th iteration of this process, then the following iterative process,

$$D_{k+1} = 3D_k^2 - 2D_k^3, \quad (4.12)$$

called McWeeny purification, will eventually project D onto \tilde{D} within an arbitrarily small radius of convergence [76]. After each iteration, the eigenvalues will be moved closer to $\{0, 1\}$. This process is given in figure 4.1.

²This depends on the type of quantum system to be studied with VQE. For quantum chemistry, electron conservation is the condition that is referred to as making physically sense here.

³Though it is called the idempotency manifold, the 1-RDMs that comprise this manifold also satisfy properties 1 and 3.

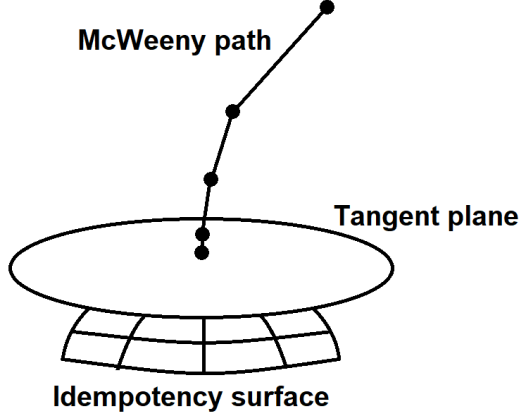


Figure 4.1: The McWeeny path through matrix space, projecting the measured 1-RDM onto the idempotency surface.

Realistically, on the order of 10^5 samples are taken to perform accurate experiments. This leads to a high number of significant numbers, and so the McWeeny purification process may not converge exactly within a small time window. A cutoff can be established to ensure 'sufficient' convergence. Typically, the algorithm is finished at step m if

$$\|D_m - \tilde{D}\| < \epsilon \quad (4.13)$$

for some small error margin ϵ . A priori, the projection \tilde{D} of the 1-RDM onto the idempotency manifold is not known, because if it were, the McWeeny purification process would be redundant. Equation (4.14) is then replaced with

$$\|D_m^2 - D_m\| < \epsilon, \quad (4.14)$$

where $\epsilon = 10^{-8}$ is chosen to be an arbitrary small bound for the GoogleAI experiment [77]. The energy estimation (2.49) then uses these new purified 1-RDM entries rather than the measured ones.

Of course, this entire McWeeny procedure relies on the fact that in Hartree-Fock theory, one is interested in a Slater determinant type wavefunction so that the 2-RDM components are uniquely determined by the 1-RDM components. Further research has been conducted to see if this work can be generalised and if a McWeeny purification procedure can also be constructed for the 2-RDM, though results are not clear on if it is achievable in a meaningful way [78].

4.2.3 Countering gate/propagation imperfections

The coherent errors caused by gate imperfections or qubit propagation errors, mentioned in section 3.4, can be countered by the following procedure. Let U denote the unitary operation to be implemented, and let $U(\mathbb{I} + \epsilon\delta U)$ be the actual erroneous unitary operation, where ϵ is a small parameter introduced for bookkeeping. Then, the unitary operator $V \stackrel{\text{def}}{=} V_0(\mathbb{I} + \epsilon\delta V)$ is meant to counter the error term δU , to second order in the error parameter ϵ . To find V , one can solve

$$U(\mathbb{I} + \epsilon\delta U)V_0(\mathbb{I} + \epsilon\delta V) = U + \mathcal{O}(\epsilon^2). \quad (4.15)$$

Separating each order of ϵ , this yields

$$UV_0 + \epsilon(U\delta UV_0 + UV_0\delta V) + \mathcal{O}(\epsilon^2) = U + \mathcal{O}(\epsilon^2). \quad (4.16)$$

This gives $V_0 = \mathbb{I}$ and $U\delta UV_0 + UV_0\delta V = U\delta U + U\delta V = 0$. So, $\delta V = -\delta U$. In conclusion, to counter a small gate imperfection or propagation imperfections, one must first find the coherent error term δU , and apply the unitary $V = \mathbb{I} - \epsilon\delta U$. Of course, for an erroneous U that is still unitary, one can reverse its effect by U^\dagger , but it is not always obvious for tiny errors ($\epsilon \ll 1$), what this Hermitian conjugate is, so that above procedure may find itself of more use.

4.3 Richardson's deferred approach to the limit

4.3.1 Richardson extrapolation

Suppose that $A(h)$ is a distribution that gives a sequence of estimates, dependent on a disturbance parameter h with the constraint that $A_\star = \lim_{h \rightarrow 0} A(h)$ is the disturbance-free limit of the distribution. Then, Richardson extrapolation accelerates the convergence rate of this sequence [79][80]. Let the Taylor expansion of this sequence around A_\star be given by

$$A(h) = A_\star + Ch^n + \mathcal{O}(h^{n+1}), \quad (4.17)$$

where n is the lowest order to which the distribution can be expanded. Then the Richardson extrapolation $R(h, t)$ improves the accuracy of the estimates, defined by

$$R(h, t) = \frac{t^n A(h/t) - A(h)}{t^n - 1}. \quad (4.18)$$

Here, t is an auxiliary parameter that introduces the splitting of disturbance scales h and h/t . An explicit calculation would reveal that (4.18) gives

$$R(h, t) = A_\star + \mathcal{O}(h^{n+1}), \quad (4.19)$$

which improves the rate of convergence. Because this works for arbitrary lowest order n , then by induction, Richardson extrapolation can remove any number of k lowest orders. This approach is called RDA: Richardson's deferred approach to the limit, and it provides a consistent way of removing lowest order corrections to a disturbed distribution.

4.3.2 The original proposal

Relating Richardson's deferred approach to the limit to improving the accuracy of quantum computational calculations, one can estimate the VQE expectation value of a quantum observable such as the energy eigenvalue of a molecular system under noise, to arbitrary precision by cancelling the noise parameter to arbitrary order in the expansion of the observable estimate. Using RDA, the density matrix of the noisy quantum circuit $\tilde{\rho}(T)$, running for a time T , allows for the reconstruction of the noise-free density matrix $\rho(T)$, rendering the solution more accurate.

Let P_α be the set of Pauli operators $\{\mathbb{I}, X, Y, Z\}^{\otimes \alpha}$ acting on N qubits. Let $\sum_\alpha P_\alpha$ represent, with slight abuse of notation, the direct sum of all these sets of Pauli operators on different Hilbert spaces \mathfrak{H}_α , so that

$$\sum_\alpha P_\alpha \stackrel{\text{def}}{=} \bigoplus_\alpha P_\alpha \quad (4.20)$$

is the complete basis set of the Hilbert space $\mathfrak{H} \stackrel{\text{def}}{=} \bigoplus_\alpha \mathfrak{H}_\alpha$. Then, a quantum circuit can be experimentally realised by a drive Hamiltonian

$$K(t) = \sum_\alpha J_{P_\alpha}(t) P_\alpha, \quad (4.21)$$

where J_{P_α} is the corresponding interaction parameter that may or may not be time-dependent.

The total evolution of the density matrix under decoherence is given by the modified Von Neumann equation

$$\frac{\partial \rho(t)}{\partial t} = -i[K(t), \rho(t)] + \lambda \mathcal{L}(\rho(t)). \quad (4.22)$$

Here, λ is a noise parameter that quantifies the noise strength, while $\mathcal{L}(\rho(t))$ is a linear function of ρ that describes the noise generation. Dependent on its nature, λ could be the interaction strength of the circuit with its environment (the bath), to name an example, in which case $\mathcal{L}(\rho(t))$ would be the Lindblad operator. Three constraints are tied to the use of this equation [81]:

1. The generator $\mathcal{L}(\rho(t))$ is invariant under time scaling, and is independent of the Hamiltonian.
2. The noise parameter $\lambda \ll 1$ is small, so that perturbation theory can be applied.

3. If $l_n = \mathcal{O}(N^n)$ is at most a function of at least order n , then $\|\mathcal{L}_{I,t_1} \circ \dots \circ \mathcal{L}_{I,t_n}\|_1 = l_n$, where $\mathcal{L}_{I,t_i} = e^{iK(t)t_i} \mathcal{L} e^{-iK(t)t_i}$ is the generator in the interaction picture, and where $\|\cdot\|_1$ is the 1-norm given by

$$\|A\|_1 = \max_i \sum_j |A_{ij}|. \quad (4.23)$$

Let $E_K(\lambda)$ be the estimate of the quantum observable A under the drive Hamiltonian $K(t)$ and noise λ , given by $\text{Tr}(A\rho_\lambda(T))$. Expanding this estimate in terms of λ gives

$$E_K(\lambda) = E_\star + \sum_{k=1}^n a_k \lambda^k + \mathcal{O}(\lambda^{n+1}), \quad (4.24)$$

where $E_\star = \text{Tr}(A\rho_0(T))$ is the noise-free energy, and where a_k are expansion parameters that depend on the noise model, typically growing like $\sim (NT)^k$ [60]. To be more precise, this expansion is around the small parameter $NT\lambda$. As noise will cause disruptions in the measurement, one is only interested in $\lim_{\lambda \rightarrow 0} E_K(\lambda) = E_\star$, but has only access to $E_K(\lambda)$, which will always have an offset of $\mathcal{O}(\lambda)$ to the true solution. By application Richardson's deferred approach to the limit, it is possible to cancel all orders of λ to arbitrary convergence. The offset can then be reduced to $\mathcal{O}(\lambda^{n+1})$.

Because of the nature of VQE, it is not possible to improve the ground state energy by averaging over all samples because VQE always overestimates the energy. In general, noise will counter the tendency of VQE to improve a wavefunction so that the energy is lowered. Therefore, a clever trick is needed that extrapolates these noise-ridden energy estimates to a lower energy, but not below the true ground state energy in the limit of $\lambda \rightarrow 0$, as is forbidden by VQE. This principle is illustrated, and compared to regular averaging, in figure 4.2.

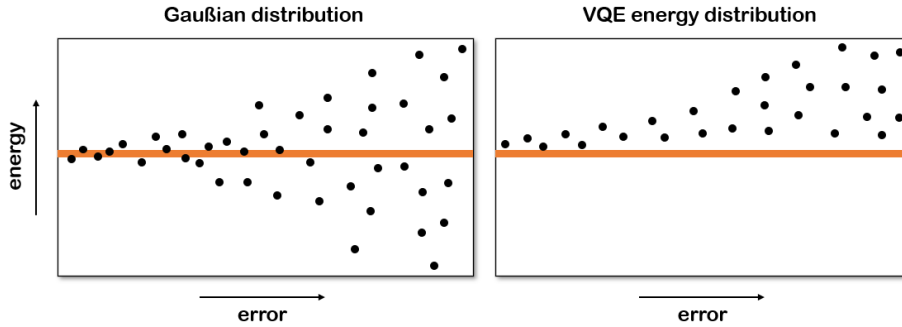


Figure 4.2: A Gaussian distribution is centered around an average, with the standard deviation determined by the error strength. Averaging over the energy estimates gives a good approximation to the average. For VQE, there is no such centering, so that averaging does not work.

Suppose that $n + 1$ different quantum circuits run the same algorithm, each circuit labeled by $j \in \{0, 1, \dots, n-1, n\}$, at different noise scales λ_j . Each noise scale can be represented as a scaled version of the original noise such that $\lambda_j = c_j \lambda$. Then there will be $n + 1$ experimental estimates

$$\hat{E}_K(\lambda_j) = E_K(\lambda_j) + \Delta_j. \quad (4.25)$$

Here, Δ_j is an error induced by the finite nature of the sampling process, as well as additional circuit errors. It then holds true that the superposition of these energies given by

$$\hat{E}_K^n(\lambda) = \sum_{j=0}^n \gamma_j \hat{E}_K(\lambda_j) \quad (4.26)$$

improves the approximation of E_\star to order $\mathcal{O}(\lambda^{n+1})$. The linear factors γ_j satisfy the linear set of equations

$$\sum_{j=0}^n \gamma_j c_j^k = \delta_{k,0} \quad \forall k \in \{0, 1, \dots, n-1, n\}. \quad (4.27)$$

The solutions of these equations are found by Gaussian elimination, yielding the compact form

$$\gamma_j = \prod_{m \neq j} \frac{c_m}{c_m - c_j}. \quad (4.28)$$

Eventually, this leads to an upper bound to the error that is quantified by the inequality

$$|\hat{E}_K^n(\lambda) - E_\star| \leq \Gamma_n \left(\max_j |\Delta_j| + \|A\| \frac{l_{n+1}(\lambda T)^{n+1}}{(n+1)!} \right), \quad (4.29)$$

where $\Gamma_n = \sum_{j=0}^n |\gamma_j| c_j^{n+1}$.

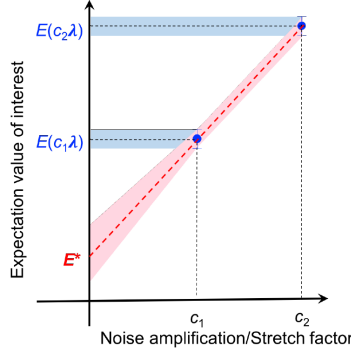


Figure 4.3: In the context of VQE, RDA imposes a band of convergence around the erroneous data and extrapolates it to the noiseless limit [82]. Unlike VQE, this energy estimation can actually go below the true ground state energy.

What this method effectively achieves, is enveloping the noise amplified energy estimations in a narrow band, as seen in figure 4.3. The result becomes more accurate if there are more data points and if the scaling factors c_j are high enough. Extrapolation to $c \rightarrow 0$ yields an estimate for E_\star within an uncertainty band of $\mathcal{O}(\lambda^{n+1})$. In stark contrast to VQE, RDA is technically able to achieve an energy estimate that lies below the true ground state energy. The higher the value of n , the stricter this uncertainty band becomes, preventing the severity of such underestimations. Indeed, in the noise limit $\rightarrow 0$, there is no underestimation.

4.3.3 Application to VQE

In experiments, one cannot control certain types of decoherent noise. It is possible to mitigate noise-induced errors, or to use technological advancements to make the system less susceptible to environmental interactions or circuit imperfections, or to counter gate imperfections, to name a few example. But it is impossible to have precise control over λ . By that argument, it is also impossible to scale the noise by an exact amount given by the scaling parameters c_j . To perform the $n+1$ experiments that are used in Richardson extrapolation, one must therefore refer to different techniques. One such mathematical trick exists: by rescaling the Hamiltonian and the total circuit time scale, the system can be effectively cheated into simulating a system where it is only the noise that is scaled.

Let $c_0 = 0$ and $c_j > 1$ be the scaling parameters. Then, the new simulation time is scaled as $T_j = c_j T$. The rescaled Hamiltonian is given by [81]

$$K_j(t) = \sum_{\alpha} J_{P_{\alpha},j}(t) P_{\alpha}, \quad (4.30)$$

where

$$J_{P_{\alpha},j}(t) = \frac{1}{c_j} J_{P_{\alpha}} \left(\frac{t}{c_j} \right). \quad (4.31)$$

This inevitably leads to a rescaled density matrix as well: $\rho_j(t) = \rho\left(\frac{t}{c_j}\right)$. As it turns out, this new density matrix that is subject to a noisy system with noise parameter λ and time scale T_j , is equivalent to the old density matrix being subject to a scaled noise $c_j\lambda$ for a time T :

$$\rho_{j,\lambda}(T_j) = \rho_{\lambda_j}(T). \quad (4.32)$$

If an experimentalist has full control over the circuit, they can modify the drive Hamiltonian to effectively scale up the noise. The time scaling can be potentially problematic, though. If a single iteration of the VQE algorithm runs for too long, beyond the relaxation and dephasing times, coherence will be lost. Such results would be too inaccurate even for RDA to recover. Therefore, the additional constraint

$$T_j \leq \max\{T_1, T_2, T_2^*\} \quad \forall j \quad (4.33)$$

must be imposed. For this reason, RDA is more beneficial for quantum computers of which qubits have long coherence times.

5 Rydberg quantum circuits

5.1 Physics of Rydberg atoms

5.1.1 Introduction

Rydberg atoms are atoms where one of the electrons is excited to a state that has a high principle quantum number n . Typically, n falls in the range $\gtrsim 20$. The presence of an electron in such a state gives the atom some extreme properties. The typical size of an atom scales like $\sim n^2$, so that Rydberg atoms are typically of the μm size. They are also very sensitive to applications of external fields: their polarisability scales like $\sim n^7$. Rydberg atoms also have strong van der Waals interactions between them whose interaction coefficient C_6 scales like $\sim n^{11}$. They also have long lifetimes τ , scaling like $\sim n^3$ [83]. Such lifetimes are given by the rate of spontaneous emission with characteristic timescale τ_{sp} , and the rate of stimulated emission over timescales τ_{st} , dependent on the temperature T [84]:

$$\frac{1}{\tau} = \frac{1}{\tau_{sp}} + \frac{1}{\tau_{st}(T)}. \quad (5.1)$$

Because of recent advancements within the field of ultracold quantum physics, Rydberg atoms have become a prominent candidate for the realisation of quantum computers because their high level of experimental control allows an experimentalist to fine tune specific interactions [85][86]. A universal set of quantum gates can be constructed from Rydberg atoms by employing their long-range interactions, but also many types of multi-qubit entanglement operations are possible. Both analog and digital quantum computing are within the realm of possibilities, as analog quantum computing with Rydberg atoms have already been shown to be able to be effectively simulated. Analog quantum computers mimic a certain quantum system of interest, or an entire family of systems, by either tuning the circuit Hamiltonian to resemble the system's or by finding an isomorphism between the two Hamiltonians. Digital quantum computers perform computations by mapping the quantum system onto qubit and qubit operators.

Rydberg energy levels are represented by the quantum numbers n , the principal quantum number, l , s and j . The latter three denote the orbital angular momentum, the spin angular momentum and the total angular momentum quantum numbers respectively. The energy of such a level is given by

$$E_{nlj} = -\frac{Ry}{(n - \delta_{lj}(n))^2}, \quad (5.2)$$

where Ry is the Rydberg constant and $\delta_{lj}(n)$ is the quantum defect: a correction to the energy that slowly varies with n and corrects for hyperfine splittings and the phase shift for low energy electron-ion scattering processes [85][87]. Ry is material-dependent, meaning it is slightly different for different atoms. For an alkali metal such as Rubidium, this Rydberg constant equals ≈ 0.4999673250 [88]. The Rydberg-Ritz formula allows for the calculation of the quantum defect according to its expansion

$$\delta_{nlj} = \sum_{k=0}^{\infty} \frac{\delta_{2k}}{(n - \delta_0)^{2k}} = \delta_0 + \frac{\delta_2}{(n - \delta_0)^2} + \frac{\delta_4}{(n - \delta_0)^4} + \dots, \quad (5.3)$$

where the coefficients $\delta_0, \delta_2, \delta_4, \dots$ are experimentally measured and tabled [89]. They depend most strongly on the azimuthal quantum number l .

The 4 quantum numbers that describe a Rydberg state are encapsulated into the state ket $|e\rangle = |n, l, j, m_j\rangle$. These are eigenstates of the single-atom Hamiltonian, but not of the two-atom Hamiltonian, as their dipolar interactions shift the eigenvectors.

5.1.2 Laser excitation

An electron can be excited to a Rydberg state through means of optical excitation. The dipole moment of the Rydberg atom couples to laser light that is tuned to a frequency corresponding to certain atomic transitions. This dipole moment $\vec{\mu}$ is given by

$$\vec{\mu} = -e\vec{r}, \quad (5.4)$$

where e is the elementary charge and \vec{r} is the position vector of the displaced electron. The matrix elements of this operator reveal whether two states are dipole coupled. That is, if the matrix element

$$\langle n, l, j, m_j | \vec{\mu} | n', l', j', m'_j \rangle \quad (5.5)$$

vanishes, then the two respective states are not dipole coupled. The conditions for when these matrix elements vanish give rise to selection rules. This is evident from the separability of the dipole matrix elements into a radial matrix element $\langle r \rangle_{nlj}^{n'l'j'}$ and a matrix element $\mathcal{A}_{ljm_j}^{l'j'm'_j}$ that takes the regular and spin angular momenta into account. They are given by [83]

$$\langle r \rangle_{nlj}^{n'l'j'} = \int_0^\infty P_{nlj}(r) r P_{n'l'j'}(r) dr \quad (5.6)$$

and

$$\mathcal{A}_{ljm_j}^{l'j'm'_j} = \langle l j m_j | (\hat{\mathbf{e}}_x + \hat{\mathbf{e}}_y + \hat{\mathbf{e}}_z) | l' j' m'_j \rangle. \quad (5.7)$$

Here, the functions $P_{nlj}(r)$ are reduced wavefunctions given by their relationship to the radial wavefunction $\psi_{nlj}(r)$ that solves the Schrödinger equation:

$$\psi_{nlj}(r) \propto \frac{P_{nlj}(r)}{r}. \quad (5.8)$$

The position vector has been explicitly decomposed into its Cartesian basis vectors. Because photons, being spin-1 bosons, drive these atomic transitions, it is more convenient to project these angular momentum matrix elements, which themselves are 3-component vectors, onto a spin-1 polarisation basis. Let this new basis $\{\mathbf{e}_i\}_{i=1,2,3}$ be given by

$$\mathbf{e}_1 = \frac{\mathbf{e}_x + i\mathbf{e}_y}{\sqrt{2}}, \quad \mathbf{e}_2 = \frac{\mathbf{e}_x - i\mathbf{e}_y}{\sqrt{2}}, \quad \mathbf{e}_3 = \mathbf{e}_z, \quad (5.9)$$

corresponding to σ^+ , σ^- and linearly polarised light respectively. The matrix elements $\mathcal{A}_{ljm_j}^{l'j'm'_j}$ can be projected onto this new basis:

$$\mathbf{e}_i \cdot \mathcal{A}_{ljm_j}^{l'j'm'_j} = (-1)^{j-m_j+s+j'+1} \sqrt{(2j+1)(2j'+1)(2l+1)(2l'+1)} \left\{ \begin{matrix} j & 1 & j' \\ l' & s & l \end{matrix} \right\} \begin{pmatrix} j & 1 & j' \\ -m_j & \mu_i & m'_j \end{pmatrix} \begin{pmatrix} l & 1 & l' \\ 0 & 0 & 0 \end{pmatrix}, \quad (5.10)$$

where $s = \frac{1}{2}$ is the electron spin, curly brackets denote Wigner-6j symbols, and curved brackets denote Wigner-3j symbols, defined in Appendix A [90]. μ_i is the polarisation of light, so that $\mu_1 = 1, \mu_2 = -1, \mu_3 = 0$. In most cases, these Wigner symbols vanish. Only for a specific combination of entries do they give non-zero contributions, leading to selection rules for the transitions. It can be calculated that the transition between the states $|nljm_j\rangle$ and $|n'l'j'm'_j\rangle$ can only be driven if the conditions

1. $l' = l \pm 1$,
2. $|j - j'| \leq 1$,
3. $m_j - m'_j = \mu_i$

are met [91]. Because of the existence of selection rules, it is impossible to dipole-couple two states with like azimuthal angular momentum quantum numbers l through a laser-driven transition.

This dipole operator couples to laser light with an angular frequency ω and electric field vector \vec{E} through the interaction potential

$$\mathcal{H}_{AL} = -\frac{\vec{\mu} \cdot \vec{E}}{\hbar}. \quad (5.11)$$

The electric dipole approximation has been employed, which assumes that the variation of the electric field amplitude over the size of the atom is negligible.

The Rabi frequencies are defined as

$$\Omega_{ge} = \langle g | \frac{\vec{\mu} \cdot \vec{E}}{\hbar} | e \rangle, \quad \Omega_{er} = \langle e | \frac{\vec{\mu} \cdot \vec{E}}{\hbar} | r \rangle. \quad (5.12)$$

In many cases, the transition from one state to another is dipole forbidden, because it does not adhere to the selection rules. In such a case, the transition from a state $|g\rangle$ to a Rydberg state $|r\rangle$ can be realised by introducing an intermediate state $|e\rangle$ to the state manifold, which can be removed by a process known as adiabatic elimination, in which the detuning δ_e of the intermediate state is made very large. Then, the intermediate state is not significantly populated, and will serve only as a fast degree of freedom in the system. The effective Rabi frequency of the transition is then given by

$$\Omega = \frac{\Omega_{ge}\Omega_{er}}{2\delta_e}, \quad (5.13)$$

while the effective detuning is given by

$$\Delta = \delta_r + \frac{\Omega_{ge}^2 - \Omega_{er}^2}{4\delta_e}, \quad (5.14)$$

where δ_r denotes the detuning of the Rydberg state [92][93].

5.2 Rydberg interactions

5.2.1 Dipolar interactions

Dipole-dipole interactions are the primary mechanism through which Rydberg atoms interact with one another. For interatomic distances of the order of millimeters, this interactions takes the classical form⁴

$$\mathcal{V}_{dd}(\vec{R}) = \frac{1}{4\pi\epsilon_0} \left(\frac{\vec{\mu}_1 \cdot \vec{\mu}_2}{R^3} - \frac{3(\vec{\mu}_1 \cdot \vec{R})(\vec{\mu}_2 \cdot \vec{R})}{R^5} \right), \quad (5.15)$$

where \vec{R} is the inter-nuclear vector connecting the two interacting atoms, with $R = |\vec{R}|$ [94].

Focusing solely on two-body systems, the new two-atom Hamiltonian \mathcal{H}_2 now contains single-body terms, as well as the operator \mathcal{V}_{dd} that dipole-couples the atoms. It is given by [95]

$$\mathcal{H}_2 = \mathcal{H}_1 \otimes \mathbb{I} + \mathbb{I} \otimes \mathcal{H}_1 + \mathcal{V}_{dd}(\vec{R}), \quad (5.16)$$

where \mathcal{H}_1 is the electronic Hamiltonian

$$\mathcal{H}_1 = -\frac{1}{2}\nabla^2 + V_{core}(r) + \frac{\alpha^2}{r^3}\vec{L} \cdot \vec{S}, \quad (5.17)$$

where $V_{core}(r)$ is the effective potential that is felt by the outer electron in a high n Rydberg state, often described by models, r is the distance from the nucleus to that electron, α is the fine structure constant, \vec{L} is the angular momentum vector and \vec{S} is the spin angular momentum vector. The last term therefore describes spin-orbit coupling.

The presence of the \mathcal{V}_{dd} term in equation (5.16) shifts the eigenstates of the original Hamiltonian \mathcal{H}_1 . Let $|\alpha\rangle$ and $|\beta\rangle$ denote eigenstates of this single-atom Hamiltonian. Then the eigenstates of the interactionless two-atom system are tensor products of these states $|\alpha\beta\rangle = |\alpha\rangle \otimes |\beta\rangle$ with an additive eigenenergy $E_{\alpha\beta} = E_\alpha + E_\beta$. When the dipole-dipole interactions are turned on, instead of pure state kets $|n, l, j, m_j\rangle$, the new eigenstates will be a superposition of so-called pair states $|n, l, j, m_j\rangle \otimes |n', l', j', m'_j\rangle$. The new eigenenergies can be obtained from perturbation theory.

5.2.2 Van der Waals interactions

From perturbation theory, the eigenenergies of (5.16) can be obtained, revealing an interaction scaling like $\sim \frac{1}{R^6}$ for large separations, known as the van der Waals interaction. This scaling law can also be retrieved from eigenenergies of the Hamiltonian of two dipole-coupled pair states at large separation distances R .

A toy model is given by the interaction between pair states $|nS\rangle \otimes |nS\rangle$ and $|n'P\rangle \otimes |n''P\rangle$. Let the energy zero point be given by the eigenenergy of the first pair state, and let the energy difference between the

⁴Henceforth, units will be adopted where $\hbar = c = 1$.

pair states be given by ΔE , called the Förster defect. Then, the Hamiltonian matrix in this basis is given by [84]

$$\mathcal{H}_{toy} = \begin{pmatrix} 0 & V_0/R^3 \\ V_0/R^3 & \Delta E \end{pmatrix}, \quad (5.18)$$

where the potential V_0 is given by [95]

$$V_0 = R^3 \langle nSnS | \mathcal{V}_{dd} | n'Pn''P \rangle. \quad (5.19)$$

The eigenvalues of \mathcal{H}_{toy} are given by

$$E_{\pm} = \frac{1}{2} \left(\Delta E \pm \sqrt{\Delta E^2 + \frac{4V_0^2}{R^6}} \right). \quad (5.20)$$

In the resonant dipole regime, characterised by strong off-diagonal interaction energies $\frac{V_0}{R^3} \gg \Delta E$, the energies follow the typical $\frac{1}{R^3}$ scaling law for dipole energies:

$$E_{\pm} \simeq \pm \frac{V_0}{R^3}. \quad (5.21)$$

In the van der Waals regime, characterised by great separation distances $\frac{V_0}{R^3} \ll \Delta E$, the two eigenenergies split as follows:

$$E_{-} \simeq -\frac{1}{\Delta E} \frac{V_0^2}{R^6}, \quad E_{+} \simeq \Delta E + \frac{1}{\Delta E} \frac{V_0^2}{R^6}, \quad (5.22)$$

where the typical $\frac{1}{R^6}$ behaviour is recovered. The van der Waals constant C_6 is defined as

$$C_6 = \frac{V_0^2}{\Delta E}, \quad (5.23)$$

which can take either positive or negative values.

5.2.3 The Rydberg blockade effect

Because of the strength of Rydberg-Rydberg interactions at close distances, it is possible that the presence of an electron in a high n -state will shift the nearby atoms out of resonance with their laser fields. This effect is called the Rydberg blockade effect. Because the van der Waals potential drops off with increasing distance, the characteristic distance below which this blockade effect works is called the Rydberg blockade radius R_b . If the characteristic coupling strength of the van der Waals interaction is denoted by C_6 , and the laser that excites a ground state to the Rydberg state has a Rabi frequency of Ω , then this blockade radius is given by [96]

$$R_b = \left(\frac{C_6}{\Omega} \right)^{1/6}. \quad (5.24)$$

This blockade effect enables Rydberg atoms to be employed for controlled quantum gate operations. A well-known example for two qubits is the CNOT gate, given by its matrix representation

$$\text{CNOT} = \begin{pmatrix} 1 & 0 & 0 & 0 \\ 0 & 1 & 0 & 0 \\ 0 & 0 & 0 & 1 \\ 0 & 0 & 1 & 0 \end{pmatrix} \quad (5.25)$$

in the computational basis. A pulse scheme that achieves this gate operation is presented in figure 5.1. Through the blockade effect, multiple qubits can be effectively made to communicate with one another, creating entanglement in general.

Consider a system consisting of two atoms are in their respective ground states, so that the collective wavefunction is given by $|\psi\rangle = |g\rangle \otimes |g\rangle$. When one of the atoms is excited to a higher energy Rydberg state $|r\rangle$, the wavefunction symmetrises to $|\psi_{+}\rangle = \frac{1}{\sqrt{2}} (|g\rangle \otimes |r\rangle + |r\rangle \otimes |g\rangle)$ because both states have degenerate eigenenergies. A resonant laser coupling with a modified Rabi frequency of

$$\Omega = \sqrt{2}\Omega_1, \quad (5.26)$$

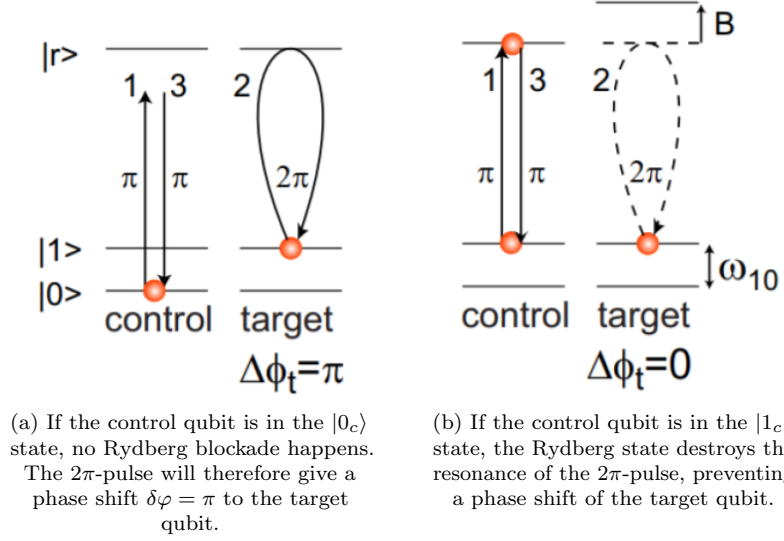


Figure 5.1: An appliance of the Rydberg blockade effect: the CNOT operation, to add a controlled qubit phase shift to a target qubit [85].

where Ω_1 is the Rabi frequency of a single-atom laser driving the $|g\rangle \leftrightarrow |r\rangle$ transition, now drives the transition of $|g\rangle \otimes |g\rangle \leftrightarrow |\psi_+\rangle$. Excitation to such a coherent superposition within the Rydberg blockade regime has been verified experimentally [97]. The coupling of the $|\psi_+\rangle$ state to the doubly excited Rydberg state $|r\rangle \otimes |r\rangle$ is now forbidden by the off-resonance of the laser, caused by the blockade effect. This transition scheme is depicted in figure 5.2. The blockade effect itself has been experimentally verified, lately with Rubidium atoms [98].

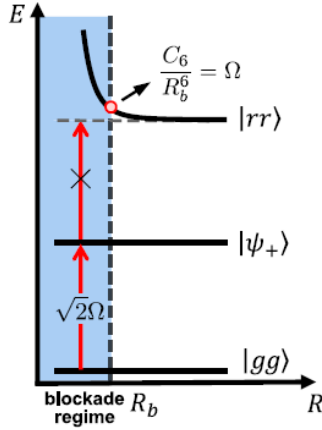


Figure 5.2: Within the blockade radius, $R < R_b$, only certain transitions are possible, with a modified Rabi frequency given by (5.26) [96].

This discussion can be extended to an ensemble of an arbitrary number of Rydberg atoms. If a volume of N particles is considered, it is possible to form the coherent superposition state

$$|W_N\rangle = \frac{1}{\sqrt{N}} \sum_{i=1}^N |g_1\rangle \otimes |g_2\rangle \otimes \cdots \otimes |r_i\rangle \otimes \cdots \otimes |g_N\rangle = \frac{1}{\sqrt{N}} \sum_{i=1}^N |g_1 g_2 \cdots r_i \cdots g_N\rangle, \quad (5.27)$$

where the latter equality introduces a shorthand notation to unclutter the tensor product notation. Such

a state shifts the single-atom Rabi frequency Ω_1 to an enhanced Rabi frequency

$$\Omega = \sqrt{\sum_{i=1}^N \Omega_1^2} = \sqrt{N} \Omega_1. \quad (5.28)$$

Sometimes also referred to as a superatomic state, these collective coherent many-body Rabi frequencies have also been observed in experiment [99][100].

5.3 Quantum gate implementation

5.3.1 Rydberg-based QPUs

The NISQ era requires high fidelities for qubit initialisation, read-out and quantum gate operations. Rydberg atoms are a very useful tool to be employed to construct a QPU that comprises the quantum mechanical part of a hybrid quantum computer, in a high fidelity fashion. The qubit states can be encoded within the state manifold $\{S\}$ of a Rydberg atom, while quantum gates can be encoded in the drive Hamiltonian and the natural strong Rydberg-Rydberg interactions. By trapping ultracold Rydberg atoms in optical traps, one can create an entire lattice Λ of qubits whose interactions can be controlled. The low temperature mitigates blackbody radiation losses as well as positional jitter that would introduce position-dependent corrections to the potential.

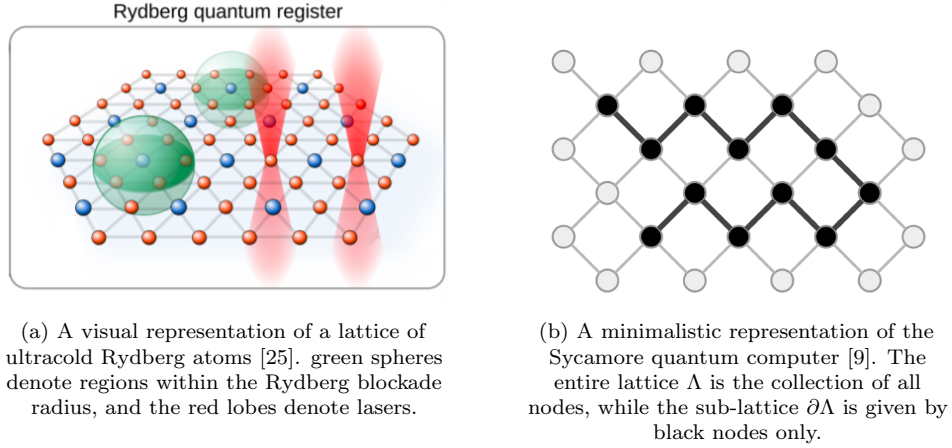


Figure 5.3: Two representations of a lattice of ultracold Rydberg atoms, on which quantum computations can be performed.

Within the lattice, a certain sub-lattice chain $\partial\Lambda$ can be chosen to represent an array of qubits. GoogleAI's Sycamore quantum computer has done the same for choosing their qubit register for performing their largest quantum chemistry experiment [9]. In principle, this allows for a few options. A linear qubit register can be chosen, so that each qubit has 2 nearest neighbours at equal distance, except for the qubits at the ends of the chain. But the register can also wrap around, as seen in figure 5.3(b), so that qubits at far ends of the chain are physically close, and therefore have stronger interactions.

5.3.2 Choice of qubits

Quantum computers based on Rydberg atoms allow for a whole range of choices for the allocation of different atomic states to the qubit states $|0\rangle$ and $|1\rangle$. Because of the flexible nature of Rydberg atoms, it is also possible to employ a different choice of qubits for quantum gates and entanglement operations. The most prominent choices are [25]:

1. *gg* qubits, where both qubit states are mapped to ground states (low n). These can either be hyperfine splittings of the electronic ground state or a combination of the electronic ground state and a metastable excited state. Their long coherence times make them an attractive option, though

their mutual interatomic interactions are weak. This can be resolved by adding an intermediate Rydberg state to the state manifold, but not to the qubit manifold.

2. *gr* qubits, where one qubit state is assigned to a ground state and the other is assigned to a Rydberg state. Typically, the *g* state is chosen to be the electronic ground state, though the metastable first excited state is a common choice as well. Their lifetime is on the order of $\sim 100\mu s$, limited by spontaneous/simulated blackbody radiation and the decay of the unstable Rydberg level. This qubit type is easily initialised, manipulated and measured, and it provides a high fidelity for entanglement operations. However, their strong interactions of the form $-\frac{C_6}{R^6} |rr\rangle \langle rr|$ are always turned on, making it difficult to perform single qubit operations without affecting nearby qubits.
3. *rr* qubits, where both qubit states are mapped to different Rydberg states $|r\rangle$ and $|r'\rangle$. For resonant states, their on-resonant dipolar interactions of the form $\frac{C_3}{R^3} (|rr'\rangle \langle r'r| + |r'r\rangle \langle rr'|)$ are always turned on. For this qubit type, it is harder to address individual qubits, and increasing the lifetime beyond the coherence time is a technical challenge.

5.3.3 Single-qubit gates

From now on, a system of *gg* qubits is considered, where the qubit states $|0\rangle$ and $|1\rangle$ are assigned to two low energy states of the outer electron. The single atom Hamiltonian for an atom $j \in \Lambda$ is given by

$$\mathcal{H}_j^{ab} = -\Delta_j |b\rangle_j \langle b|_j + \left(\frac{\Omega_j}{2} e^{i\lambda_j} |a\rangle_j \langle b|_j + h.c. \right). \quad (5.29)$$

Here, *a* and *b* refer to either the qubit states 0 and 1 or an auxiliary Rydberg state *r* that is not part of the qubit state manifold. Δ_j is the detuning of the coupling laser frequency and the atomic resonance frequency of the *b*-state, which is usually 0 for the $|1\rangle$ -state and non-zero for an $|r\rangle$ -state. Ω_j is the Rabi frequency of the transition between the $|a\rangle$ and $|b\rangle$ -states, and λ_j is the local phase generated by the polarisation of the laser.

With this Hamiltonian, a family of single-qubit gates can be generated. A general prescription from obtaining familiar gates such as the Pauli gates and the Hadamard gate can be retrieved from the general U_{xy} operator given by

$$U_{xy}(\theta, \lambda) = e^{-i\mathcal{H}_j^{01}\tau_g} = \begin{pmatrix} \cos(\theta/2) & -i \sin(\theta/2) e^{i\lambda} \\ -i \sin(\theta/2) e^{-i\lambda} & \cos(\theta/2) \end{pmatrix} \quad (5.30)$$

The angle θ is given by $\theta = \Omega\tau_g$, where τ_g is the gate time. The interpretation of this general unitary is a rotation of θ radians around an axis that lies at an angle of λ radians in the $x - y$ plane. By certain parameterisation of the experimental parameters, one can reconstruct the 3 Pauli gates and the Hadamard gate as follows:

1. From the Pauli matrix X , defined in 2.54, one can construct a rotation around the x -axis on the Bloch sphere with $R_x(\theta) = e^{-i\frac{\theta}{2}X} = U_{xy}(\theta, 0)$.
2. Likewise, a rotation around the y -axis follows from $R_y(\theta) = e^{-i\frac{\theta}{2}Y} = U_{xy}(\theta, -\pi/2)$.
3. Since the unitary U_{xy} can only perform rotations around the x and y axes, in order to create a rotation around the z -axis, 3 rotations must be applied to the Bloch sphere: $R_z(\theta) = e^{-i\frac{\theta}{2}Z} = U_{xy}(\pi/2, \pi/2)U_{xy}(\theta, 0)U_{xy}(\pi/2, -\pi/2)$.
4. The Hadamard gate H follows, up to a global phase factor, from $H = U_{xy}(\pi, 0)U_{xy}(\pi/2, -\pi/2)$.

5.3.4 Two-qubit gates

The two-atom Hamiltonian for atoms $j \in \Lambda$ and $k \in \Lambda$, in the pair state basis, is given by

$$\mathcal{H}_{jk} = \left(\frac{\mu_{ac}\mu_{bd}}{R_{jk}^3} |ab\rangle \langle cd| + h.c. \right) + \Delta_F |cd\rangle \langle cd|, \quad (5.31)$$

where $\mu_{ac} = \sqrt{4\pi\epsilon_0} \langle a | \mu | c \rangle$, and $\Delta_F = (E_d - E_b) - (E_a - E_c)$ is the Förster defect [25]. There now exist two regimes, dependent on the strength of the Förster defect, that give either rise to a dipole-dipole coupling Hamiltonian, or a van der Waals Hamiltonian. In this work, Δ_F is solely determined by the resonance of the interacting Rydberg states, though pair states can also be brought into resonance through the application of an external electric field [101].

(I) *Resonant interactions* ($\Delta_F \approx 0$)

When the Rydberg-Rydberg interactions are resonant, they will take the form of a coherent state exchange process with a characteristic scaling law $\sim \frac{1}{r^3}$. This Hamiltonian is denoted with 4 different Roman superscript letters:

$$\mathcal{H}_{jk}^{abcd} = \frac{\mu_{ac}\mu_{bd}}{R_{jk}^3} |ab\rangle \langle cd| + h.c. \quad (5.32)$$

with a potential $V_{jk} = \frac{\mu_{ac}\mu_{bd}}{R_{jk}^3}$. This Hamiltonian is naturally realised if both atoms have the same dipole-coupled states, for example $a = d = nS$ and $c = b = nP$. The system can also be brought into Förster resonance by application of an electrical field, but this will not be considered here. The flip-flop term will dominate, and the system will dominantly interact through dipole-dipole couplings.

(II) *Non-resonant interactions* ($\Delta_F \gg \frac{|\mu_{ac}\mu_{bd}|}{R_{jk}^3}$)

When the states are not directly dipole-coupled, then the dipole interaction Hamiltonian can be treated with second order perturbation theory, giving

$$\mathcal{H}_{jk}^{abab} = -\frac{C_6}{R_{jk}^6} |ab\rangle \langle ab| \quad (5.33)$$

with a potential $V_{jk} = -\frac{C_6}{R_{jk}^6}$ and a van der Waals coefficient $C_6 = \frac{|\mu_{ac}\mu_{bd}|^2}{\Delta_F}$. This Hamiltonian is a natural result for atoms that are prepared in the very same Rydberg states (for example $a = b = nS$) or atoms in different Rydberg states that are not directly dipole-coupled (for example $a = nS, b = n'S$).

Another gate that can be constructed is the controlled phase gate

$$\text{CPHASE} = \begin{pmatrix} e^{i\varphi_{00}} & 0 & 0 & 0 \\ 0 & e^{i\varphi_{01}} & 0 & 0 \\ 0 & 0 & e^{i\varphi_{10}} & 0 \\ 0 & 0 & 0 & e^{i\varphi_{11}} \end{pmatrix}, \quad (5.34)$$

which is an entanglement operator provided that $\varphi_{00} - \varphi_{01} - \varphi_{10} + \varphi_{11} \neq 2k\pi$ for integer values of k . From this general gate, more specific gates such as the CZ gate can be retrieved by specific parameterisation. The pulse scheme is given by

$$\text{CZ} = \exp \left[-iH_c^{r1} \tau_1 \right] \exp \left[-i \left(H_t^{r1} + H_{ct}^{rrrr} \right) \tau_2 \right] \exp \left[-iH_c^{r1} \tau_1 \right], \quad (5.35)$$

where $\Delta_c = \Delta_t = 0$, $\Omega_c = \Omega_t = \Omega$, $\tau_1 = \frac{\pi}{\Omega}$ and $\tau_2 = 2\tau_1$ [25].

5.3.5 Multi-qubit gates

The CNOT gate, together with the single-qubit gates, constitute a set of universal operators. This means that any quantum gate can be decomposed into these basis gates. For most gates, however, this decomposition would slow down the quantum computation speed, because of an increase in resources. Rydberg atoms allow for building a flexible quantum simulator where some gates can be directly implemented in some fashion, meaning that no decomposition has to be taken. With their strong and long-ranged dipole interactions, Rydberg atoms are a natural means of directly implementing multi-qubit entanglement gates without having to resort to a decomposition into a numerous number of single-qubit and two-qubit gates.

A few examples are given here, taken from the work by M. Morgado et al. [25]. References for the implementations of the latter two gates can be found in there.

The asymmetric blockade gate $C_k Z$

One of the most well known multi-qubit gates is the natural extension of the CZ gate to an arbitrary number of control qubits: the $C_k Z$ gate, where k is the number of control qubits. Its matrix representation is given by

$$C_k Z = \begin{pmatrix} \mathbb{I}_{f(k)} & 0 \\ 0 & Z \end{pmatrix}, \quad (5.36)$$

where $\mathbb{I}_{f(k)}$ is the $(2^{k+1} - 2) \times (2^{k+1} - 2)$ identity operator on the subspace spanned by the first k qubits. A pulse scheme that realises this gate is given by

$$C_k Z = \exp \left[-i \sum_k H_k^{r0}(\lambda_k = \pi) \tau_1 \right] \exp \left[-i \left(H_t^{r1}(\lambda_t = 0) + \sum_k H_{kt}^{rr'rr'} \right) \tau_2 \right] \exp \left[-i \sum_k H_k^{r0}(\lambda_k = 0) \tau_1 \right], \quad (5.37)$$

where $\Omega_k = \Omega_c$, $\tau_1 = \frac{\pi}{\Omega_c}$ and $\tau_2 = \frac{2\pi}{\Omega_t}$.

The multi-qubit Toffoli gate $C_k NOT$

The $C_k NOT$ gate is a generalisation of the Rydberg blockade effect, given by

$$C_k NOT = \begin{pmatrix} \mathbb{I}_{f(k)} & 0 \\ 0 & X \end{pmatrix}, \quad (5.38)$$

where $\mathbb{I}_{f(k)}$ is again given by the $(2^{k+1} - 2) \times (2^{k+1} - 2)$ identity operator.

The multi-qubit fan-out gate $CNOT^k$

$$CNOT^k = \begin{pmatrix} \mathbb{I}_{g(k)} & 0 \\ 0 & X_{g(k)} \end{pmatrix}, \quad (5.39)$$

where $\mathbb{I}_{g(k)}$ is the $2^k \times 2^k$ identity operator, and where $X_{g(k)}$ is the generalisation of the Pauli X -gate, given by the anti-diagonal 2^k -dimensional matrix with 1s on the anti-diagonal, and 0s otherwise.

6 Multi-qubit entanglement through perfect state transfer

6.1 PST in the single excitation manifold Γ_1

6.1.1 Introduction to PST

The most common quantum gates are single-qubit and two-qubit gates. It is an interesting research question whether the VQE algorithm can be sped up by employing multi-qubit gates, that entangle the states of multiple qubits at once without resorting to some decomposition into a universal set of quantum gates. It is possible to bring distant qubits physically close together through a string of SWAP operations, though this is very prone to error propagation and requires an active control [102]. It is preferable to have a multi-qubit entanglement operation that requires no active control, and an example of this that has been studied a lot is perfect state transfer (PST), where a quantum state is transferred from one qubit site to another with unit fidelity.

In future quantum computer builds, it is expected that PST can play an important role in quantum state transfer, entanglement distribution, as well as allowing communication between different QPUs and perhaps even a fundamental building block of realising a universal quantum computer, as generating large-scale entanglement is a core ingredient for scalable architectures [31].

There has been some mild criticism, however, on the utility of implementing PST in modern quantum computers as their unit fidelity is too demanding in comparison to realistic fidelities of other quantum operations. Despite this criticism, it is interesting to study PST as the theoretical results lead to some profound concepts in the context of information transportation in quantum computing. Alternative measures such as pretty good state transfer (PGST) have been proposed, where the fidelity of the state transfer can be made arbitrarily close to unity, though they will not be considered in this thesis [103].

The concept of state transfer was first researched by Bose, who used the Hamiltonian

$$\mathcal{H}_{Bose} = J \sum_{n=1}^{N-1} (X_n X_{n+1} + Y_n Y_{n+1} + Z_n Z_{n+1}), \quad (6.1)$$

defined on some one-dimensional qubit chain of length N , to study its viability [104]. Here, J is a parameter that characterises the coupling strength of the qubit interactions. His aim was to take an initial state $|\psi\rangle|0\rangle^{\otimes N-1}$, and he hoped that after some time t_* had elapsed, the system would find itself in a state $|0\rangle^{\otimes N-1}|\psi\rangle$, up to some global phase. It can be shown that PST is indeed possible on a qubit chain that undergoes Bose Hamiltonian dynamics, but only for $N = 2$ and $N = 3$. For higher N , it is proven that PST is impossible with this Hamiltonian. A sketch of this proof is given in Appendix B [31][105].

Though the Bose Hamiltonian lead to weak results, it was later discovered that the modulation of the coupling strength J into a position-dependent coupling J_n would indeed lead to PST for all chain lengths [105][106]. To be more precise, an entire family of generalised Hamiltonians was found that would allow PST dynamics, if and only if certain conditions were met. This will be discussed in the upcoming sections. This general family of Hamiltonians is given by the generalised XY -Hamiltonian

$$\mathcal{H} = \frac{1}{2} \sum_{n=1}^{N-1} J_n (X_n X_{n+1} + Y_n Y_{n+1}) - \sum_{n=1}^N B_n Z_n, \quad (6.2)$$

under the influence of a local external magnetic field B_n ⁵. When implemented using Rydberg dressed atoms, this 'magnetic field' is unavoidable, and has the interpretation of the light shift of the Rydberg atom under laser couplings that are weak relative to their detunings. The couplings J_n and B_n are real-valued parameters.

⁵Though not always a magnetic field, this name will henceforth be adopted.

6.1.2 Hilbert space decomposition analysis

The most convenient aspect about this Hamiltonian family is that the analysis of PST along qubit chains under the influence of such Hamiltonians is greatly reduced because its Hilbert space decomposes into multiple subspaces that can all be uniquely described by just a single one of them. Let henceforth the $|0\rangle$ -state be referred to as the vacuum state, and $|1\rangle$ as an exciton, or excitation. It can be observed that every Hamiltonian in the Hamiltonian family satisfies the commutation relation

$$[\mathcal{H}, S_{tot}^z] = 0, \quad (6.3)$$

where the total qubit isospin $S_{tot}^z \stackrel{\text{def}}{=} \sum_{n=1}^N Z_n$ represents the total number of excitons⁶. This means that under the action of \mathcal{H} , the total Hilbert space $\mathfrak{H} = \mathbb{C}^{2^N}$ decomposes in decoupled subspaces as follows:

$$\mathfrak{H} = \bigoplus_{k=0}^N \Gamma_k, \quad (6.4)$$

where Γ_k denote the k -exciton subspaces given by the bases

$$\Gamma_0 = \{|00 \cdots 00\rangle\}, \quad (6.5)$$

$$\Gamma_1 = \{|10 \cdots 00\rangle, |01 \cdots 00\rangle, \dots, |00 \cdots 10\rangle, |00 \cdots 01\rangle\}, \quad (6.6)$$

$$\Gamma_2 = \{|11 \cdots 00\rangle, |101 \cdots 00\rangle, \dots, |00 \cdots 11\rangle\}, \quad (6.7)$$

$$\vdots$$

$$\Gamma_N = \{|11 \cdots 11\rangle\}. \quad (6.8)$$

The dimension of each space is given by $\dim(\Gamma_k) = \binom{N}{k}$. Suppose P_{Γ_k} is the projector onto such a subspace Γ_k , then it holds true that $\text{Tr}(S_{tot}^z P_{\Gamma_k}) = k$ is the total number of excitations in said subspace [107]. It should be noted that the Hamiltonian family that is discussed in this thesis is not unique, and that other Hamiltonians that have the same Hilbert space structure can be employed successfully for PST [108][109][110], though possibly the most well-known and theory-rich PST Hamiltonian: the Krawtchouk chain [111], is part of the family discussed here.

The last term is a constant energy shift that only affects the global phase, so it may be omitted. This Hamiltonian has no local interaction terms, so that the interpretation that may be given to exciton transport along a qubit chain undergoing PST is that excitons do not 'feel' each others presence [112][?]. This will also greatly reduce the complexity of PST analysis. Every higher order k -exciton subspace Γ_k is comprised of k copies of the 1-exciton subspace Γ_1 , up to some extra phases that will be discussed in section 6.2.4. A full analysis of dynamics within Γ_1 will therefore also describe the dynamics of an arbitrary number of excitons, and thus an arbitrary number of qubits.

Lemma 6.1. *PST within Γ_1 is equivalent to transporting an exciton from one end of a one-dimensional qubit chain to the other.*

Proof. Let \hookrightarrow denote equality up to arbitrary accumulated phases, so that $e^{i\varphi_p} |p\rangle + e^{i\varphi_q} |q\rangle \hookrightarrow |p\rangle + |q\rangle$. This tool allows for some uncluttering of the notation, and relevant phases can be restored after a series of calculations is performed. Now the dynamics within Γ_1 can be analysed. Suppose the transfer $|\psi\rangle |0\rangle^{\otimes N-1} \hookrightarrow |0\rangle^{\otimes N-1} |\psi\rangle$ is to be made, where $|\psi\rangle = \alpha |0\rangle + \beta |1\rangle$. Because the N -qubit vacuum is an eigenstate of the Hamiltonian \mathcal{H} , it is preserved: $|0\rangle^{\otimes N} \xrightarrow{\text{under } \mathcal{H}} |0\rangle^{\otimes N}$. The task of PST is then reduced to realising $|1\rangle |0\rangle^{\otimes N-1} \hookrightarrow |0\rangle^{\otimes N-1} |1\rangle$ within Γ_1 . \square

⁶This is a direct result of the $\text{SU}(2)$ invariance of Heisenberg-like interactions of the form $XX + YY (+ZZ)$.

Let the state $|m\rangle$ denote the single excitation $|0\rangle^{\otimes m-1} |1\rangle |0\rangle^{N-m}$, and let $|\text{vac}\rangle \stackrel{\text{def}}{=} |0\rangle^N$. In the basis spanned by $\{|i\rangle | 1 \leq i \leq N\}$, the Hamiltonian \mathcal{H} becomes the tridiagonal matrix

$$\mathcal{H}_1 = \begin{pmatrix} B_1 & J_1 & 0 & \cdots & 0 & 0 \\ J_1 & B_2 & J_2 & \cdots & 0 & 0 \\ 0 & J_1 & B_3 & \cdots & 0 & 0 \\ \vdots & \vdots & \vdots & \ddots & \vdots & \vdots \\ 0 & 0 & 0 & \cdots & B_{N-1} & J_{N-1} \\ 0 & 0 & 0 & \cdots & J_{N-1} & B_N \end{pmatrix}. \quad (6.9)$$

6.1.3 The symmetry matching condition

Now the question arises what conditions the parameters J_n and B_n must meet in order to produce PST. The following lemma can be issued, which holds for Γ_1 , but by extension for all qubit states in H [32]:

Lemma 6.2 (Centrosymmetry). *Within the space Γ_1 , exciton transfer from $|\underline{1}\rangle$ to $|\underline{N}\rangle$ along a one-dimensional qubit chain under \mathcal{H} with open boundary conditions, occurs if the coupling parameters are centrosymmetric, that is symmetric around the center. This implies that $J_n^2 = J_{N-n}^2$ and $B_n = B_{N+1-n}$.*

Proof. Let the eigenvalues and eigenvectors of the one-exciton subspace Hamiltonian \mathcal{H}_1 be given by the eigenvalue equation

$$\mathcal{H}_1 |\lambda_n\rangle = \lambda_n |\lambda_n\rangle. \quad (6.10)$$

The qubits at the ends of the chains can then be expanded in this eigenbasis, such that

$$|\underline{1}\rangle = \sum_{n=1}^N \alpha_n |\lambda_n\rangle, \quad (6.11)$$

$$|\underline{N}\rangle = \sum_{n=1}^N \beta_n |\lambda_n\rangle. \quad (6.12)$$

Suppose that there exists a time t_{PST} after which perfect state transfer has occurred. Then it must link the $|\underline{1}\rangle$ and the $|\underline{N}\rangle$ states through unitary time evolution:

$$e^{-i\mathcal{H}_1 t_{PST}} |\underline{1}\rangle = e^{i\varphi} |\underline{N}\rangle \hookrightarrow |\underline{N}\rangle, \quad (6.13)$$

where φ is some accumulated phase. Returning to the eigenbasis and putting everything on the left-hand side yields

$$\sum_{n=1}^N \left[e^{-i\mathcal{H}_1 t_{PST}} \alpha_n - e^{i\varphi} \beta_n \right] |\lambda_n\rangle = \sum_{n=1}^N \left[e^{-i\lambda_n t_{PST}} \alpha_n - e^{i\varphi} \beta_n \right] |\lambda_n\rangle = 0. \quad (6.14)$$

Then each component must individually vanish, giving the conditions

$$e^{-i\lambda_n t_{PST}} \alpha_n = e^{i\varphi} \beta_n \quad \forall n \in \{1, \dots, N\}. \quad (6.15)$$

This says that the coefficients are related through $\alpha_n \hookrightarrow \beta_n$, or to be more precise: $|\alpha_n|^2 = |\beta_n|^2$. Since this relates the front end of the qubit chain to the back end of the chain, one can iteratively solve the equation

$$\langle \underline{1} | (\mathcal{H}_1)^k | \underline{1} \rangle = \sum_{n=1}^N \lambda_n^k |\alpha_n|^2 = \langle \underline{N} | (\mathcal{H}_1)^k | \underline{N} \rangle \quad (6.16)$$

for integer k , so that each equation produces a new equation relating J_n and B_n at the front and at the back. Let $[\mathbf{A}]_{:,j} = a_{:,j}$ denote the j -th column of the matrix A . It holds true that

$$(A^k)_{:,j} = A^{k-1}(A)_{:,j} = a_{j-1,j}(A^{k-1})_{:,j-1} + a_{j,j}(A^{k-1})_{:,j} + a_{j+1,j}(A^{k-1})_{:,j+1}, \quad (6.17)$$

proving that for tridiagonal matrices, every time the power k of the matrix increases by one, the number of diagonals increases by one [113]. Plugging in $k = 1$ gives $B_1 = B_N$. Plugging in $k = 2$ gives $B_1^2 + J_1^2 = B_N^2 + J_{N-1}^2$, which yields $J_1^2 = J_{N-1}^2$. By systematically working through higher powers, one finds that PST is possible for $J_n^2 = J_{N+1-n}^2$ and $B_n = B_{N-n}$. \square

Because of this centrosymmetry, the Hamiltonian commutes with the symmetry operator

$$\mathcal{S} = \sum_{n=1}^N |n\rangle \langle N+1-n|. \quad (6.18)$$

Under the action of \mathcal{H}_1 , the subspace Γ_1 further decomposes into a symmetric (S) and an anti-symmetric (A) subspace:

$$\Gamma_1 = \Gamma_{1,S} \oplus \Gamma_{1,A}. \quad (6.19)$$

Within their respective subspace, the eigenvectors $|\lambda_n\rangle$ can be split into symmetric eigenvectors $|\lambda_n^S\rangle$ and anti-symmetric ones $|\lambda_n^A\rangle$. The same labels S/A are attached to the eigenvalues. Then the following lemma can be proposed [32]:

Lemma 6.3 (The symmetry matching condition). *A necessary and sufficient condition for PST is that there should exist a time t_{PST} and an accumulative phase φ such that $e^{-it_{PST}\lambda_n^S} = e^{i\varphi}$ and $e^{-it_{PST}\lambda_n^A} = -e^{i\varphi}$ for all eigenvectors $|\lambda_n\rangle$.*

Proof. One can expand the $|\underline{1}\rangle$ exciton in the basis set $\{|\lambda_n\rangle\} = \{|\lambda_n^S\rangle\} \cup \{|\lambda_n^A\rangle\}$:

$$|\underline{1}\rangle = \sum_n \left(\alpha_n^S |\lambda_n^S\rangle + \alpha_n^A |\lambda_n^A\rangle \right), \quad (6.20)$$

as well as the action of the symmetry operator on it:

$$\mathcal{S} |\underline{1}\rangle = |\underline{N}\rangle = \sum_n \left(\alpha_n^S \mathcal{S} |\lambda_n^S\rangle + \alpha_n^A \mathcal{S} |\lambda_n^A\rangle \right) = \sum_n \left(\alpha_n^S |\lambda_n^S\rangle - \alpha_n^A |\lambda_n^A\rangle \right). \quad (6.21)$$

The action of \mathcal{H}_1 on the exciton reads

$$e^{-i\mathcal{H}_1 t_{PST}} |\underline{1}\rangle = \sum_n \left(e^{-i\lambda_n^S t_{PST}} \alpha_n^S |\lambda_n^S\rangle + e^{-i\lambda_n^A t_{PST}} \alpha_n^A |\lambda_n^A\rangle \right) = \sum_n \left(e^{i\varphi} \alpha_n^S |\lambda_n^S\rangle - e^{i\varphi} \alpha_n^A |\lambda_n^A\rangle \right) = e^{i\varphi} \mathcal{S} |\underline{1}\rangle, \quad (6.22)$$

which is precisely the necessary condition for PST. \square

6.1.4 The inverse eigenvalue problem

The usual procedure of studying a system is fixing the system parameters and then studying useful quantities such as eigenvectors that are solutions to the system equations. It proves itself to be useful however, to first fix the eigenvalues, and then work out what the system is supposed to look like to recreate such eigenvalues. This is known as the Inverse Eigenvalue Problem (IEP), a well studied phenomenon that appear in a lot of physical systems such as connected classical springs [114][115]. The natural question arises why it is more useful to solve PST using the IEP. A lot of quantities such as transfer speed, time uncertainty losses and the introduction of next-to-nearest couplings can all be studied by using the IEP [32][116][117].

So far, no specification has been made beyond the centrosymmetry condition of lemma 6.2. This does not always guarantee PST, however, as it is a minimal requirement. One last constraint must be added to the set of eigenvalues to uniquely constraint PST to a specific set of parameters $\{J_n\}$ and $\{B_n\}$. For PST, solving the IEP is akin to fulfilling the eigenvalue spacing requirement (ESR):

Lemma 6.4 (Eigenvalue spacing requirement). *The last condition for PST is that all eigenvalues λ_n , sorted such that $\lambda_n < \lambda_m$ for all $n < m$, are spaced by a certain amount:*

$$\lambda_n - \lambda_{n-1} = (2k_n + 1)\pi/t_{PST}, \quad (6.23)$$

where k_n is a non-negative integer that depends on n .

Proof. For $N \times N$ tridiagonal matrices with negative off-diagonals, it has been shown that the number of sign changes in the eigenvalue spectrum is equal to $N - 1$, showing that symmetric and anti-symmetric

eigenvalues are alternatively succeeding each other [114]. Because of the symmetry matching condition, the ratio $e^{-it_{PST}\lambda_n^S}/e^{-it_{PST}\lambda_n^A}$ is given by

$$e^{-it_{PST}\lambda_n^S}/e^{-it_{PST}\lambda_n^A} = -e^{i\varphi} \cdot e^{-i\varphi} = -1. \quad (6.24)$$

Because of the alternative ordering of symmetric and anti-symmetric eigenvalues, one can order the spectrum of eigenvalues such that $\lambda_n < \lambda_m$ for all $n < m$. By assigning the labels $\lambda_n^S = \lambda_n$ and $\lambda_n^A = \lambda_{n-1}$, (6.24) reads

$$e^{-i(\lambda_n - \lambda_{n-1})t_{PST}} = -1 \quad (6.25)$$

for all n . Then, because of the periodicity of the complex exponent, it must hold true that

$$\lambda_n - \lambda_{n-1} = (2k_n + 1)\pi/t_{PST} \quad (6.26)$$

for all n , giving the eigenvalue spacing requirement (ESR). This also means that the ratio of consecutive eigenvalues is always a rational number. \square

6.2 PST in higher order excitation manifolds

6.2.1 Independent fermion dynamics

As discussed before, the analysis in higher order excitation subspaces is closely related to the one made in the single exciton subspace, making it easier to perform calculations [32].

Lemma 6.5 (Free fermion dynamics). *Every Hamiltonian in the family encodes free fermion dynamics. This is now formally proven.*

Proof. This is most evident under the Jordan-Wigner transformation (2.51), (2.52). In terms of creation and annihilation operators $a_x^{(\dagger)}$ of excitons on qubit site x , \mathcal{H} now reads

$$\mathcal{H}_{JW} = \sum_{n=1}^{N-1} J_n(a_n^\dagger a_{n+1} + a_n a_{n+1}^\dagger) + \sum_{n=1}^N B_n a_n^\dagger a_n - \frac{1}{2} \sum_{n=1}^N B_n \mathbb{I}_n. \quad (6.27)$$

Another way of seeing this is by diagonalising the Hamiltonian in the complete Hilbert space basis. By introducing a basis rotation

$$b_n^{(\dagger)} = \sum_{m=1}^N \lambda_{nm} a_m^{(\dagger)}, \quad (6.28)$$

where the λ_{nm} coefficients are defined by the reverse relation

$$|\lambda_n\rangle = \sum_m \lambda_{nm} |\underline{m}\rangle. \quad (6.29)$$

By using the orthogonality relationships of these λ_{nm} 's,

$$\langle \text{vac} | a_m a_k^\dagger | \text{vac} \rangle = \sum_{n=1}^N \lambda_{nm} \lambda_{nk}^* = \delta_{mk}, \quad (6.30)$$

it is straightforward to show that $\mathcal{H}_{JW} = \sum_{n=1}^N \lambda_n b_n^\dagger b_n$, where λ_n are the single-fermion subspace eigenvalues. \square

This proves that indeed, the transfer of multiple excitons is equal to the independent uncoupled transfer of single excitons. Because they are fermions, though, they are still subject to anti-symmetrization. The best mathematical tool to automatically incorporate this behaviour is the wedge product \wedge [118]. In the following section, it is proven formally that mapping qubits onto wedge products of excitations is mathematically legal, and that indeed this exchange factor arises naturally in fermionic PST.

6.2.2 Graph vertex wedge product \wedge

The study of quantum state transfer along a qubit chain is closely related to the mathematical study of graphs, collections of vertices connected by edges. A brief introductory background to graph theory in relation to quantum walks and state transfer is given in Appendix C [119][120]. A quantum register can be thought of as a graph. Proving the validity of the wedge product is most convenient on such a graph, and through the isomorphic property of the mapping between graphs and qubit register, it can be shown that indeed fermionic exchange minus signs are to be expected throughout a PST process.

For simplicity, let the graph vertices be denoted by Roman letters. It is useful to define a wedge product $a \wedge b$ over graph vertices to directly incorporate fermionic behaviour, as the wedge product satisfies

1. *Anti-symmetry:* $a \wedge b = -b \wedge a$,
2. *Pauli exclusion principle:* $a \wedge a = 0$.

These vertices themselves form vectors that live in an abstract Hilbert space $\mathcal{H}_{\mathcal{G}}$ of the graph \mathcal{G} . Then, the subspaces Γ_k can be directly related to exterior vector spaces $\bigwedge^k(\mathcal{H}_{\mathcal{G}})$ [121]. To be more precise, they are isomorphic, shown in the following lemma [32][107]:

Lemma 6.6. *Every subspace Γ_k is isomorphic to $\bigwedge^k(\mathcal{H}_{\mathcal{G}})$.*

Proof. For $k = 0$ and $k = 1$, they are defined as $\bigwedge^0(\mathcal{H}_{\mathcal{G}}) \stackrel{\text{def}}{=} \mathbb{C}$ and $\bigwedge^1(\mathcal{H}_{\mathcal{G}}) = \mathcal{H}_{\mathcal{G}}$ respectively. For $k \geq 2$, it is defined as

$$\bigwedge^k(\mathcal{H}_{\mathcal{G}}) = \bigotimes_{m=1}^k \mathcal{H}_{\mathcal{G}} \mod \mathcal{A}_{\mathcal{G}}, \quad (6.31)$$

where $\mathcal{A}_{\mathcal{G}}$ is the vector space that is spanned by all elements of the form $|v_1, \dots, v_k\rangle$ where $v_j = v_{j'}$ for some $j \neq j'$. Here v_j denotes vertices in \mathcal{G} , while $|v_j\rangle$ denote vectors in $\mathcal{H}_{\mathcal{G}}$. In order to construct a basis for the $k + 1$ exterior vector spaces, it is necessary to invoke the wedge product \wedge , defined by

$$\wedge : \bigotimes_{m=1}^k \mathcal{H}_{\mathcal{G}} \rightarrow \bigotimes_{m=1}^k \mathcal{H}_{\mathcal{G}}, \quad (6.32)$$

and whose action on graph vertices is given by

$$|v_1 \wedge \dots \wedge v_k\rangle = \frac{1}{k!} \sum_{\pi \in S_k} \epsilon(\pi) |v_{\pi(1)}, \dots, v_{\pi(k)}\rangle. \quad (6.33)$$

Here, S_k is the permutation group of order k , and $\epsilon(\pi)$ is the sign of the permutation π . From (6.33) it also becomes evident that the dimensions of the exterior vector spaces are given by $\dim\left(\bigwedge^k(\mathcal{H}_{\mathcal{G}})\right) = \binom{N}{k}$.

A natural choice for the basis of $\bigwedge^k(\mathcal{H}_{\mathcal{G}})$ is then given by the vectors $|v_1 \wedge \dots \wedge v_N\rangle$ with $v_j \in V(\mathcal{G})$ and an ordering $v_j > v_i$ for all $j > i$. Because Γ_k and $\bigwedge^k(\mathcal{H}_{\mathcal{G}})$ are vector spaces with the same dimension, over the same field \mathbb{C} , it automatically follows that $\Gamma_k \cong \bigwedge^k(\mathcal{H}_{\mathcal{G}})$. \square

Lemma 6.7 (Legitimacy of the wedge product). *Multiple excitons of the form $|\underline{n}\rangle$ can be mapped uniquely and rigorously onto wedge products [107].*

Proof. The notion of a wedge product can now be extended to the concept of a graph wedge product. This is the wedge product defined over the entire graph, given by $\bigwedge^k \mathcal{G}$ with vertex set

$$V\left(\bigwedge^k \mathcal{G}\right) = \{(v_0, v_1, \dots, v_{k-1}) \mid v_j \in V(\mathcal{G}), v_{k-1} > v_{k-2} > \dots > v_1 > v_0\}. \quad (6.34)$$

The vertices of $\bigwedge^k \mathcal{G}$ are written as

$$v_0 \wedge v_1 \wedge \dots \wedge v_{k-1}. \quad (6.35)$$

It can be observed that the dimensions of the vectors spaces $\bigwedge^k \mathcal{G}$ and $\mathcal{H}_{\bigwedge^k \mathcal{G}}$ are identical. As they act over the same field \mathbb{C} , it follows that

$$\mathcal{H}_{\bigwedge^k \mathcal{G}} \cong \bigwedge^k (\mathcal{H}_{\mathcal{G}}). \quad (6.36)$$

By the transitive property of isomorphisms, the relation between wedge products and qubits reads

$$\mathcal{H}_{\bigwedge^k \mathcal{G}} \cong \Gamma_k. \quad (6.37)$$

This relation justifies rewriting qubit states as wedge products, because the Hilbert space of k copies of the graph vertices (representing qubits on a graph), on which a wedge product is defined, is isomorphic to the space of k excitons. \square

6.2.3 Qubit wedge product \wedge

Suppose that there exist p excitations $|a_p\rangle$ on a qubit register at sites a_p . Then this can be directly mapped through a bijection onto the state $\bigwedge_p |a_p\rangle$, as their respective spaces are isomorphic and share the same dimension. Within $\bigwedge^k (\mathcal{H}_{\mathcal{G}})$, certain calculations are easier, and the results can be mapped back to the Γ_k spaces.

To illustrate this with an example on an $N = 6$ qubit register: the state $|2\rangle$ would denote $|010000\rangle$, while $|1\rangle \wedge |4\rangle$ would denote $|100100\rangle$. Because of the anti-symmetry property of \wedge , the order of notation matters. In this thesis, the excitations are denoted from left to right. p excitations of the form $|a_p\rangle$ are therefore read as $|a_1\rangle \wedge \cdots \wedge |a_p\rangle$, where $a_i < a_j$ for all $i < j$.

The wedge product preserves normalisation, as two arbitrary states $|a\rangle = \sum_m a_m |\underline{m}\rangle$ and $|b\rangle = \sum_n b_n |\underline{n}\rangle$ give rise to a coherent excitation of the form

$$|a\rangle \wedge |b\rangle = \sum_{m < n} (a_m b_n - a_n b_m) |\underline{m}\rangle \wedge |\underline{n}\rangle, \quad (6.38)$$

with a normalisation constant [32]

$$\frac{1}{2} \sum_{m,n} |a_m b_n - a_n b_m|^2 = 1 - |\langle a|b\rangle|^2 = \begin{cases} 1 & \text{if } a \perp b \\ 0 & \text{if } a = b \end{cases} \quad (\text{PEP}). \quad (6.39)$$

With this wedge product it can be proven that the action of the \mathcal{H} Hamiltonian on multiple excitations is given by the wedge product of single-excitation evolutions under the one-particle sub-Hamiltonian \mathcal{H}_1 , so that these evolutions are decoupled. Let $\{|\lambda_n\rangle\}_n$ denote the eigenstates of \mathcal{H} with respective eigenvalues λ_n , and let two arbitrary states be given by $|a\rangle = \sum_m a_m |\lambda_m\rangle$ and $|b\rangle = \sum_n b_n |\lambda_n\rangle$. Then the total evolution is given by

$$\begin{aligned} e^{-i\mathcal{H}t} |a\rangle \wedge |b\rangle &= e^{-i\mathcal{H}t} \sum_{m,n} a_m b_n |\lambda_m\rangle \wedge |\lambda_n\rangle = \sum_{m,n} a_m b_n e^{-i(\lambda_m + \lambda_n)t} |\lambda_m\rangle \wedge |\lambda_n\rangle \\ &= \sum_{m,n} (a_m e^{-i\lambda_m t} |\lambda_m\rangle) \wedge (b_n e^{-i\lambda_n t} |\lambda_n\rangle) = (e^{-i\mathcal{H}_1 t} |a\rangle) \wedge (e^{-i\mathcal{H}_1 t} |b\rangle). \end{aligned} \quad (6.40)$$

The eigenstates of the higher exciton subspaces are then also readily found from the wedge product. In Γ_2 , they are evaluated from $|\lambda_n\rangle \wedge |\lambda_m\rangle$, in Γ_3 , they are of the form $|\lambda_n\rangle \wedge |\lambda_m\rangle \wedge |\lambda_l\rangle$, et cetera [122].

It should be noted, however, that since qubits are distinguishable entities, this fermionic exchange factor -1 is a construct in some sense. The Hamiltonian itself is blind to whether it is implemented by fermions, or bosons. Therefore, the term 'free fermion dynamics' ought to be taken lightly.

6.2.4 Local unitary corrections

Though the name suggests the perfect transfer of quantum states, just the action of the Hamiltonian \mathcal{H} alone does not lead to the perfect mirroring of a qubit register through its axis of inversion. In order to achieve this, extra unitary operations must be applied to account for phase accumulations throughout the time evolution, so far swept under the rug through the ' \leftrightarrow ' notation. These three phases are the

local magnetic phases $\sim e^{-iBt_{PST}}$, the Krawtchouk phases $\sim i^{N-1}$ and the fermionic exchange phases $\sim (-1)^{\pi(q)}$, where $\pi(q)$ denotes the parity of the qubit state.

(i) *Local magnetic phase*

In the matrix representation of \mathcal{H} , terms will appear that on the diagonal that are linear in the coefficients B_n . Let $o(q)$ of a computational basis state q denote the number of excitons, and let l denote the modified magnetic field given by

$$l = B_1 t_{PST} \frac{J}{\pi}. \quad (6.41)$$

Then the corrector to the phases, induced by the magnetic field, is given by

$$U_{corr}^{magnetic} = \text{diag} \left(e^{io(q_1)l\pi/J}, e^{io(q_2)l\pi/J}, \dots, e^{io(q_N)l\pi/J} \right). \quad (6.42)$$

(ii) *Krawtchouk phase*

A typical property of the Hamiltonian \mathcal{H} is that its unitary evolution introduces phase shifts. These Krawtchouk phases are of the form i^{N-1} and are applied to the $|1\rangle$ states. Let the family of single-qubit correctors be given by

$$C_k = \begin{pmatrix} 1 & 0 \\ 0 & i^{-k} \end{pmatrix} = \left\{ \mathbb{I} = \begin{pmatrix} 1 & 0 \\ 0 & 1 \end{pmatrix}, S^\dagger = \begin{pmatrix} 1 & 0 \\ 0 & -i \end{pmatrix}, Z = \begin{pmatrix} 1 & 0 \\ 0 & -1 \end{pmatrix}, S = \begin{pmatrix} 1 & 0 \\ 0 & i \end{pmatrix} \right\}. \quad (6.43)$$

Then, for $k = N \bmod 4$, the single-qubit correction that needs to be applied to every qubit is given by the operator C_k . The total corrector $U_{corr}^{Krawtchouk}$ is then given by

$$U_{corr}^{Krawtchouk} = \bigotimes_{n=1}^N C_k = \underbrace{C_k \otimes \dots \otimes C_k}_{N \text{ times}}. \quad (6.44)$$

(iii) *Fermionic exchange phase*

Let the parity $\pi(q)$ of a computational basis state q be defined as the number of times two excitons swap position during the PST process. If x denotes the number of $|1\rangle$ states in the state q , then this parity is given by

$$\pi(q) = \sum_{k=1}^{x-1} k = \frac{1}{2}x(x-1). \quad (6.45)$$

The unitary corrector that keeps track of all the appropriate minus signs arising from the fermionic exchange process, is then given by

$$U_{corr}^{fermionic} = \text{diag} \left((-1)^{\pi(q_1)}, (-1)^{\pi(q_2)}, \dots, (-1)^{\pi(q_N)} \right). \quad (6.46)$$

After applying all these unitaries in the form

$$U_{corr} = U_{corr}^{fermionic} U_{corr}^{Krawtchouk} U_{corr}^{magnetic}, \quad (6.47)$$

every phase is perfectly accounted for.

6.3 Examples of PST-facilitating Hamiltonians

6.3.1 The Krawtchouk chain

A well-explored Hamiltonian that enables PST is the Krawtchouk chain Hamiltonian. Its structural simplicity lends it to be possibly the easiest example, and the well-documented theory of its capabilities makes it an attractive option for implementation on a real QPU. Combined with resonant driving, it can

be used to employ cold atom qubits to form multi-qubit SWAP_N entanglement operations [111]. The Hamiltonian is given by

$$\mathcal{H}^K = -\frac{J}{4} \sum_{n=1}^{N-1} \sqrt{n(N-n)} (X_n X_{n+1} + Y_n Y_{n+1}). \quad (6.48)$$

This Hamiltonian is acquired by solving the IEP for the simplest conditions. First, no applied external fields are present. Secondly, the eigenvalue spectrum satisfies the ESR where $k_n = 0$ for all $n = 1, \dots, N$. It has been noticed that such an eigenvalue spectrum is reminiscent of that of the S_x operator of a fictitious spin- $\frac{N-1}{2}$ particle [105]. The structure of the S_x operator is known for arbitrary dimensions, so that the form of the coupling $-\frac{1}{2}J\sqrt{n(N-n)}$ can be readily read off from the matrix representation.

The Krawtchouk chain can also be employed for the generation of maximally entangled states. It is known, for instance, that the application of \mathcal{H}^K , combined with some other operations, on the $|+\rangle^{\otimes N}$ state gives the GHZ state

$$|\text{GHZ}\rangle = e^{\pm i\pi/4} \left[e^{-i\pi/4X} \right]^{\otimes N} e^{-i\pi/J\mathcal{H}^K} \frac{1}{\sqrt{2}} (|0\rangle^{\otimes N} + |1\rangle^{\otimes N}) \quad (6.49)$$

for odd N such that $N = \pm 1 \pmod{4}$ [123]. Here, $|+\rangle$ is given by $\frac{1}{\sqrt{2}}(|0\rangle + |1\rangle)$.

6.3.2 XY-Hamiltonian with magnetic field

Another example is the XY-Hamiltonian with an applied external (magnetic) field. Usually, the Krawtchouk coupling is selected for the XY-part of the Hamiltonian, while the magnetic field is subject to the centrosymmetry and eigenvalue spacing requirements for PST. This Hamiltonian is given by

$$\mathcal{H}^B = \mathcal{H}^K + \sum_{n=1}^N B_n Z_n. \quad (6.50)$$

Such an external field would have a different physical origin depending on the implementation of qubits and quantum gates. In the case of Rydberg-dressed atoms, for instance, the origin is the energy of the Rydberg level in the rotated frame, with additional light-shifts. The existence of such a term relaxes the conditions for a system to be able to facilitate PST, since many physical systems have a Hamiltonian that contains a self-interaction term proportional to $a_i^\dagger a_i$ under the Jordan-Wigner mapping, caused by self-interactions or kinetic energies, for instance.

6.4 Residual NNN couplings

The study of PST assumes that couplings between qubits can be chosen so that only nearest-neighbour interactions are turned on. In most physical systems, however, this interaction potential decays over distance, but never exactly to 0. Small residual next-to-nearest neighbour (NNN) interactions will be present, as well as higher order interactions. The presence of such couplings will not affect the Hilbert space decomposition $\mathfrak{H} = \bigoplus_{k=0}^N \Gamma_k$, rendering the discussion in this entire section relevant for this protocol as well [124].

Assume that the $N \times N$ one-exciton subspace Hamiltonian $\mathcal{H}_1(\vec{\alpha})$ depends on N parameters encapsulated into the vector $\vec{\alpha}$. Such parameters are expected to be able to be varied experimentally, such as control parameters of lasers, distance between qubits, or coupling strengths. Then the protocol, closely following Kay's approach, assures that these parameters are chosen such that they will approach the desired eigenvalues that are used to solve the IEP [124][125]. These eigenvalues are put on the diagonal of the matrix Λ . Let the Hamiltonian \mathcal{H}_1 be diagonalised by the unitary operator U_0 , if an initial guess $\vec{\alpha}^0$ is plugged in. Then one can write the Hamiltonian as

$$\mathcal{H}_1(\vec{\alpha}^0) = U_0 \Lambda (\mathbb{I}_N + \epsilon E_0) U_0^\dagger. \quad (6.51)$$

Here, E_0 is a diagonal matrix with all eigenenergy differences on the diagonal, and ϵ is a small parameter that keeps count of what terms in the perturbation expansion are sufficiently small. This ϵ tracks the parameterisation update according to

$$\vec{\alpha}^1 = \vec{\alpha}^0 + \epsilon \delta \vec{\alpha}. \quad (6.52)$$

In a similar fashion, $\mathcal{H}_1(\vec{\alpha}^1)$ is diagonalised by U_1 such that

$$\mathcal{H}_1(\vec{\alpha}^1) = U_1 \Lambda (\mathbb{I}_N + \epsilon E_1) U_1^\dagger. \quad (6.53)$$

On its own turn, U_1 can be written in terms of U_0 through the relation

$$U_1 = U_0 \cdot \frac{\mathbb{I}_N + i\epsilon Q}{\mathbb{I}_N - i\epsilon Q}, \quad (6.54)$$

where Q is a Hermitian matrix that contains information on the eigenvectors. Its exact form is unnecessary to unfold as Q will drop out to first order in perturbation theory. Substituting (6.54) into (6.53), using (6.52), one obtains to first order in perturbation theory:

$$\epsilon \sum_i \delta\alpha_i U_0^\dagger \frac{\partial \mathcal{H}}{\partial \alpha_i} \Big|_{\vec{\alpha}^0} U_0 = \epsilon (\Lambda(E_1 - E_0) + 2i [Q, \Lambda]). \quad (6.55)$$

The influence of the last term is nil for the IEP, proven in the following lemma:

Lemma 6.8. *The commutator of a Hermitian matrix and a real diagonal matrix has a zero diagonal.*

Proof. Let Q be a Hermitian matrix, and Λ a diagonal matrix with real entries. Then,

$$[Q, \Lambda]^\dagger = (Q\Lambda)^\dagger - (\Lambda Q)^\dagger = \Lambda^\dagger Q^\dagger - Q^\dagger \Lambda^\dagger = \Lambda Q - Q\Lambda = -[Q, \Lambda]. \quad (6.56)$$

Here, Hermiticity ($Q^\dagger = Q$) was used, and the identity that a real diagonal matrix must be self-adjoint as well. This proves that $[Q, \Lambda]$ is anti-Hermitian, so that it must necessarily have a zero diagonal. \square

This proves that all the information on the eigenvalues is encapsulated in the $\Lambda(E_1 - E_0)$. The objective of choosing $\delta\vec{\alpha}$ is to minimise E_1 , so this matrix can be chosen to be the null matrix. Then equation (6.56) will carry two equations implicitly: one for the diagonal terms, carrying information about the eigenvalues, and one for the off-diagonal terms, carrying information about the eigenvector shifts. The former reads

$$\mathcal{K} \cdot \delta\vec{\alpha} = \vec{e}. \quad (6.57)$$

Here, the i -th column of \mathcal{K} is given by

$$U_0^\dagger \frac{\partial \mathcal{H}}{\partial \alpha_i} \Big|_{\vec{\alpha}^0} U_0, \quad (6.58)$$

and the i -th entry of the \vec{e} vector is given by

$$-(\Lambda E_0)_{ii}, \quad (6.59)$$

with no summation over the indices implied. Such an algorithm can be efficiently performed on a classical computer.

6.5 Erroneous PST dynamics

6.5.1 Uniform coupling perturbations

One model that attempts to describe error channels in PST assumes that all relevant coupling parameters $\{J_n\}$ and $\{B_n\}$ are subject to a small disturbance

$$J_n/B_n \mapsto J_n/B_n(1 + \delta), \quad (6.60)$$

where $\delta \ll 1$ is a random small error parameter that is uniformly chosen from a predetermined interval $[-\epsilon, \epsilon]$. Such errors may arise from stochastic environmental interactions, for instance. This has been researched before for resonant coupling by C.J.M. Schoutens [111].

6.5.2 Pulse time uncertainty

The unit fidelity of PST rests on the fact that the time t_{PST} can be (experimentally) achieved to infinite precision. Of course, bringing the discussion back to laser pulses interacting with Rydberg atoms, it is to be expected that no single pulse will be exactly of length t_{PST} . Let the erroneous time t be given by

$$t = t_{PST} + \delta t, \quad (6.61)$$

where δt is a small deviation, subject to $\frac{\delta t}{t_{PST}} \ll 1$. How does the fidelity $F(t)$ rank compared to the perfect fidelity produced by PST? The propagation amplitude is given by [124]

$$f_{N1} = \langle \underline{N} | e^{-i\mathcal{H}t} | \underline{1} \rangle \hookrightarrow 1 - i\delta t \sum_n |a_n|^2 (\lambda_n - \lambda_1) - \frac{1}{2} \delta t^2 \sum_n |a_n|^2 (\lambda_n - \lambda_1)^2 + \mathcal{O}(\delta t^3). \quad (6.62)$$

The mod square reveals the fidelity to be equal to

$$F(t) = F(t_{PST} + \delta t) = 1 - \frac{1}{2} \delta t^2 \sum_n \sum_{m=1}^{n-1} |a_n|^2 |a_m|^2 (\lambda_n - \lambda_1) (\lambda_n - \lambda_m). \quad (6.63)$$

Therefore, a lower bound on the fidelity is given by

$$F(t) > 1 - \frac{1}{2} \delta t^2 \sum_n \sum_{m=1}^{n-1} |a_n|^2 (\lambda_n - \lambda_1)^2. \quad (6.64)$$

The eigenvalue spectrum that minimises this spread is the Krawtchouk Hamiltonian \mathcal{H}^K . Its spectrum is sometimes also referred to as the SMS (spectrum of minimal spread).

6.5.3 Excitation relaxation

One of the noise channels that is most detrimental to PST is the qubit relaxation channel. For analytical purposes, a model can be constructed where a spontaneous Z -operation occurs once at time $0 < \tau < t_{PST}$ with probability p . Restricting the discussion to an initial state of the form

$$|\Psi\rangle = |\psi\rangle |0\rangle^{\otimes N-1}, \quad (6.65)$$

the output density operator can be written as

$$\rho_{out} = \sum_{k=0}^N \sum_{x \in \text{basis}(\Gamma_k)} (1-p)^{N-w_x} p^{w_x} Z'_x(\tau) |\Psi\rangle \langle \Psi| Z'_x(\tau)^\dagger, \quad (6.66)$$

where $\text{basis}(\Gamma_k)$ refers to the basis set of the k -exciton space, w_x is the Hamming weight of the bit string x , and $Z'_x(\tau)$ is the application of the Z_x operator in the Heisenberg picture, incorporating the Hamiltonian dynamics with an additional qubit relaxation at time τ [32]. It is given by

$$Z'_x(\tau) = e^{-i\mathcal{H}(t_{PST}-\tau)} Z_x e^{-i\mathcal{H}\tau}. \quad (6.67)$$

This yields an average fidelity of

$$\langle F \rangle = 1 - \frac{2}{3} p(2-p) + \frac{2}{3} p(1-p) \sum_{n=1}^N |\gamma_n(t)|^4. \quad (6.68)$$

By using appropriate bounds for $|\gamma_n(t)|$, a lower and an upper bound can be found for the fidelity. This yields

$$F_{\mathcal{W}} = 1 - \frac{2}{3} p(2-p) + \frac{2}{3N} p(1-p) < \langle F \rangle < 1 - \frac{2}{3} p, \quad (6.69)$$

where $F_{\mathcal{W}}$ is a fidelity witness for the relaxation channel.

6.5.4 $XX + YY$ system-bath interactions

Another possible noise channel is the leaking of quantum information from the main chain $\partial\Lambda$ to nearby inactive qubits [126]. The results can be generalised to any Hamiltonian that has an excitation-preserving subspace structure of the form (6.4). Let the XY-Hamiltonian be referred to as the system Hamiltonian

$$\mathcal{H}_S = \frac{1}{2} \sum_{n=1}^{N-1} J_n (X_n X_{n+1} + Y_n Y_{n+1}) - \sum_{n=1}^N B_n Z_n, \quad (6.70)$$

while the bath Hamiltonian is given by

$$\mathcal{H}_B^{(n)} = \frac{1}{2} \sum_{m=1}^{M_n} g_m^{(n)} (X_n X_{(n,m)} + Y_n Y_{(n,m)}), \quad (6.71)$$

where $g_m^{(n)}$ are the system-bath couplings, and (n, m) refer to the M_n amount of nearest bath neighbours m of qubit n . The total interaction Hamiltonian would be given by

$$\mathcal{H}_{int} = \sum_{n=1}^N \mathcal{H}_B^{(n)}, \quad (6.72)$$

and the total system-bath Hamiltonian is given by

$$\mathcal{H}_{SB} = \mathcal{H}_S + \mathcal{H}_{int}, \quad (6.73)$$

acting on a larger Hilbert space \mathfrak{H} whose dimension is given by $\dim(\mathfrak{H}) = (2^N)^{1+M}$. If an excitation is present at site n , then it can leak into its own bath to generate excitations $|\uparrow\rangle$ of the form

$$|\uparrow\rangle = \frac{1}{G_n} \sum_{m=1}^{M_n} g_m^{(n)} |(\underline{n}, m)\rangle, \quad (6.74)$$

with the proper normalisation factor $G_n = \sqrt{\sum_{m=1}^{M_n} (g_m^{(n)})^2}$ [127]. It can be shown that the action of this system-bath interaction can be reduced to the action of an interaction with just a single bath-isospin within the single excitation manifold Γ_1 . Denoting this single bath-isospin as n' , this effective interaction reads

$$\mathcal{H}_B^{(n)'} = \frac{1}{2} G_n (X_n X_{n'} + Y_n Y_{n'}). \quad (6.75)$$

The eigenstates of \mathcal{H}_S are known, and given by

$$|\lambda_m\rangle = \sum_{n=1}^N \lambda_{mn} |\underline{n}\rangle. \quad (6.76)$$

This allows for a simple ansatz of the eigenstates $|\Lambda_m^k\rangle^7$ of the full interactive Hamiltonian:

$$|\Lambda_m^k\rangle = \frac{1}{2} \sum_{n=1}^N \lambda_{mn} (|\underline{n}\rangle + (-1)^k |\underline{n}'\rangle), \quad (6.77)$$

motivated by the fact that the states $\frac{1}{2} (|\underline{n}\rangle + (-1)^k |\underline{n}'\rangle)$ are eigenstates of the interactive Hamiltonian $\mathcal{H}_B^{(n)}$ with corresponding eigenenergies $\pm G$. These new eigenstates satisfy the matrix element relations

$$\mathfrak{M}_{mn}^{kl} = \langle \Lambda_m^k | \mathcal{H}_{SB} | \Lambda_n^l \rangle = \delta_{mn} \left((-1)^k G \delta^{kl} + \frac{1}{2} \lambda_n \right). \quad (6.78)$$

The structure of the matrix $[\mathfrak{M}]_{mn}^{kl}$ is block diagonal, dividing it into blocks of 2×2 that can all be diagonalised separately.

⁷This Λ has nothing to do with the symbol that denotes the lattice Λ of ultracold Rydberg atoms, or the qubit chain $\partial\Lambda$.

The system-bath coupling knows two regimes: the weakly interacting regime and the strong coupling regime, both of which generate different PST dynamics [126]:

(i) *Weakly interacting regime* $Gt_{PST} \ll 1$

In this regime, a perturbative expansion of the transfer rate can be made in the parameter Gt_{PST} (or to be more precise Gt since $t < t_{PST}$). Let $f_{nm}(t)$ denote the transfer rate between spins n and m after a time t , defined by

$$f_{nm}(t) \stackrel{\text{def}}{=} \langle \underline{n} | e^{-i\mathcal{H}_{SB}t} | \underline{m} \rangle. \quad (6.79)$$

This can be expanded as

$$f_{nm}(t) = f_{nm}^{(0)}(t) + Gt f_{nm}^{(1)}(t) + \frac{1}{2}(Gt)^2 f_{nm}^{(2)}(t) + \cdots = \sum_{k=0}^{\infty} \frac{1}{k!} (Gt)^k f_{nm}^{(k)}(t), \quad (6.80)$$

where each $f_{nm}^{(k)}(t)$ denotes a higher order expansion of the transfer rate. As it turns out, the first order contribution $f_{nm}^{(1)}(t)$ vanishes for PST, so that in the weakly interacting regime the corrections are very small: $f_{nm}(t) = f_{nm}^{(0)}(t) + \mathcal{O}(G^2)$.

(ii) *Strong coupling regime* $Gt_{PST} \gg 1$

In this regime, the transfer rate for transfer between spins n and m is given by

$$f_{nm}(t) \rightarrow \cos(Gt) f_{nm}^{(0)}\left(\frac{t}{2}\right). \quad (6.81)$$

The PST is modulated by a factor $\cos Gt$ that oscillates rapidly, while the transfer time doubles. This means that despite the strong coupling of the qubit chain to its surroundings, it is still possible to have PST. In general, unitarity of the state transfer is lost. This is to be expected as f_{nm} describes the state transfer within an open quantum system [128].

7 Engineering PST for Rydberg QPUs

7.1 Natural Rydberg $XX + YY$ interactions

7.1.1 Dipole-dipole flip-flop interactions

The Hamiltonian structure of the family \mathcal{H} , without a position-dependent interaction parameter, is naturally encapsulated in the dipole-dipole interactions of Rydberg interactions. If the Rydberg states on which the Hamiltonian acts are selected such that they are dipole coupled, the \mathcal{V}_{dd} operator can be rewritten as a reduced operator on this new smaller basis. Naturally, this interaction term will reduce to an XY -Hamiltonian.

By a change of basis from a Cartesian basis of operators $\vec{d} \stackrel{\text{def}}{=} (d_x, d_y, d_z)$ to a spherical basis, the structure of (5.15) will reveal an XY -Hamiltonian term. Let the new axis of quantization coincide with the z -axis, and let the angle between the z -axis and the \vec{R} vector be equal to θ . Then the set of spherical dipole operators is expressed in terms of Cartesian dipole operators like

$$d_o = d_z, \quad d_+ = -\frac{d_x + id_y}{\sqrt{2}}, \quad d_- = \frac{d_x - id_y}{\sqrt{2}}. \quad (7.1)$$

The magnetic quantum number m_j is conserved by the operator d_o , but is changed by ± 1 by d_{\pm} . The dipole-dipole interaction \mathcal{V}_{dd} can then be totally rewritten in terms of spherical coordinates and operators:

$$\mathcal{V}_{dd} = \frac{1}{4\pi\epsilon_0} \frac{1}{R^3} (\mathcal{V}_{\Delta m=0} + \mathcal{V}_{\Delta m=\pm 1} + \mathcal{V}_{\Delta m=\pm 2}), \quad (7.2)$$

where each index denotes the change in the total magnetic quantum number $\mathbf{m} = m_{j,1} + m_{j,2}$ of the terms that are coupled by that term [129]. They are given by

$$\mathcal{V}_{\Delta m=0} = \frac{1}{2} (1 - 3 \cos^2 \theta) (d_{1+} d_{2-} + d_{1-} d_{2+} + 2 d_{1o} d_{2o}), \quad (7.3)$$

$$\mathcal{V}_{\Delta m=\pm 1} = \frac{3}{\sqrt{2}} \sin \theta \cos \theta (d_{1+} d_{2o} - d_{1-} d_{2o} + d_{1o} d_{2+} - d_{1o} d_{2-}), \quad (7.4)$$

and

$$\mathcal{V}_{\Delta m=\pm 2} = -\frac{3}{2} \sin^2 \theta (d_{1+} d_{2+} + d_{1-} d_{2-}). \quad (7.5)$$

Now, this operator acts on spin- $\frac{1}{2}$ isospin states $|\uparrow\rangle$ and $|\downarrow\rangle$, denoting Rydberg states $|n, l, j, m_j\rangle$ and $|n', l', j', m'_j\rangle$ that are dipole coupled. In the two-atom basis $\{|\uparrow\uparrow\rangle, |\uparrow\downarrow\rangle, |\downarrow\uparrow\rangle, |\downarrow\downarrow\rangle\}$, the operator \mathcal{V}_{dd} couples 'like' states to 'like' states, $|\uparrow\uparrow\rangle$ to $|\downarrow\downarrow\rangle$, and 'unlike' states to 'unlike' states, $|\uparrow\downarrow\rangle$ to $|\downarrow\uparrow\rangle$. The former pair of states has an energy difference on the order of GHz, and its energy contribution because of flip-flops is negligible compared to the latter pair of states, which are degenerate and therefore resonant. Because the difference in the magnetic quantum number is equal to 0, only the $\mathcal{V}_{\Delta m=0}$ term in (7.2) will survive. In the isospin subspace spanned by $\{|\uparrow\downarrow\rangle, |\downarrow\uparrow\rangle\}$, the dipole-dipole interaction reads

$$\mathcal{V}_{dd} = \frac{1}{4\pi\epsilon_0} \frac{1 - 3 \cos^2 \theta}{2R^3} (d_{1+} d_{2-} + d_{1-} d_{2+} + 2 d_{1o} d_{2o}) = \frac{1}{4\pi\epsilon_0} \frac{1 - 3 \cos^2 \theta}{R^3} \begin{pmatrix} 0 & \tilde{C}_3 \\ \tilde{C}_3 & 0 \end{pmatrix}, \quad (7.6)$$

where \tilde{C}_3 is given by the matrix element

$$\tilde{C}_3 = \frac{1}{2} \langle \uparrow\downarrow | d_{1+} d_{2-} + d_{1-} d_{2+} + 2 d_{1o} d_{2o} | \downarrow\uparrow \rangle. \quad (7.7)$$

Eventually, the XY -form is obtained by rewriting isospin operators in terms of Pauli operators. Adopting the notation $\sigma_{\uparrow\downarrow} = |\uparrow\rangle \langle \downarrow|$, the dipole-dipole interaction is written as

$$\mathcal{V}_{dd} = \frac{C_3(\theta)}{R^3} \left(\sigma_{\uparrow\downarrow}^{(1)} \sigma_{\downarrow\uparrow}^{(2)} + h.c. \right). \quad (7.8)$$

Between each pair of Rydberg atoms, the dipole-dipole interaction has the form (7.8), so that the XY -part of the Hamiltonian becomes

$$\mathcal{H}_{XY} = \sum_{i \neq j} \frac{C_3(\theta)}{r_{ij}^3} (X_i X_j + Y_i Y_j). \quad (7.9)$$

However, this Hamiltonian contains beyond nearest neighbour interactions. For the implementation of \mathcal{H} , this can be partially resolved by truncating the Hamiltonian (7.10) to first order, and encapsulate all other orders into an error term $\partial\Gamma$ that is presumed to be very small compared to the first order terms. Then, one finds that

$$\mathcal{H}_{XY}^{dip} = \sum_{\langle i,j \rangle} \frac{C_3(\theta)}{R^3} (X_i X_j + Y_i Y_j) + \partial\Gamma, \quad (7.10)$$

where the error is given explicitly by

$$\partial\Gamma = \sum_{|i-j| \geq 2} \frac{C_3(\theta)}{|i-j|^3 R^3} (X_i X_j + Y_i Y_j). \quad (7.11)$$

Assuming $C_3(\theta)$ contribution that is equal for every pair of atoms on the lattice, this error term is quite big. In fact, the average contribution as a fraction of the first order term is $\sum_{n=2}^{\infty} 1/n^3 \approx 0.202$, about 20% of the total result. This contribution is therefore not insignificant, and a more rapid decay of the qubit interactions is required to mitigate beyond nearest neighbour effects.

7.1.2 Adiabatic elimination of van der Waals couplings

Instead of resonant states, one could also opt to use two non-resonant Rydberg states like $|n_1 S\rangle$ and $|n_2 S\rangle$, such that their van der Waals interactions are stronger on short scales, and weaker over longer distances. This will make the first order contribution to the XY -part of the Hamiltonian bigger, while also making the higher order contributions smaller.

$$\mathcal{H}^{(i)} = -\Delta_1 \sigma_{11}^{(i)} - \Delta_2 \sigma_{22}^{(i)} + \sum_{ab=01,02} \left(\Omega_{ab} \sigma_{ab}^{(i)} \right) \quad (7.12)$$

Starting from the lattice Hamiltonian

$$\mathcal{H}_\Lambda = \sum_{i=1}^N \mathcal{H}^{(i)} + \sum_{\substack{i=1 \\ j \neq i}} \frac{1}{|\vec{r}_i - \vec{r}_j|^6} \left(\frac{1}{2} C_6^{11} \sigma_{11}^{(i)} \sigma_{11}^{(j)} + \frac{1}{2} C_6^{22} \sigma_{22}^{(i)} \sigma_{22}^{(j)} + C_6^{12} \sigma_{11}^{(i)} \sigma_{22}^{(j)} + C_6^S \sigma_{12}^{(i)} \sigma_{21}^{(j)} \right), \quad (7.13)$$

where the constants $\{C_6^{11}, C_6^{22}, C_6^{12}, C_6^S\}$ are van der Waals constants that pertain to different types of van der Waals interactions between the two Rydberg levels. The factors of $\frac{1}{2}$ take over-counting into account, because of symmetry arguments. This Hamiltonian can be turned into an XXZ -Hamiltonian for the right set of parameters. The XY part of the Hamiltonian can then be extracted. This can be done by mapping \mathcal{H}_Λ onto a spin- $\frac{1}{2}$ isospin system of the two Rydberg states. For this, these states are first mapped to $|n_1 S\rangle \mapsto |s=1, m=1\rangle$ and $|n_2 S\rangle \mapsto |s=1, m=-1\rangle$. Then the ground state, which will be adiabatically eliminated afterwards, will be mapped to a neutral spin state $|g\rangle \mapsto |s=1, m=0\rangle$. The projector operators can be written in terms of the spin-1 operators

$$\hat{J}_x = \frac{1}{\sqrt{2}} \begin{pmatrix} 0 & 1 & 0 \\ 1 & 0 & 1 \\ 0 & 1 & 0 \end{pmatrix}, \quad \hat{J}_y = \frac{1}{\sqrt{2}} \begin{pmatrix} 0 & -i & 0 \\ i & 0 & -i \\ 0 & i & 0 \end{pmatrix}, \quad \hat{J}_z = \begin{pmatrix} 1 & 0 & 0 \\ 0 & 0 & 0 \\ 0 & 0 & -1 \end{pmatrix}, \quad (7.14)$$

and the raising and lowering operators

$$\hat{J}_\pm = \hat{J}_x \pm i \hat{J}_y. \quad (7.15)$$

Then the single-atom operator will become

$$\mathcal{H}^{(i)} = -\frac{\Delta_-}{2} \hat{J}_z^{(i)} - \frac{\Delta_+}{2} \left(\hat{J}_z^{(i)} \right)^2 + \frac{\Omega_+}{2\sqrt{2}} \hat{J}_x^{(i)} - \frac{\Omega_-}{2\sqrt{2}} \left(\hat{J}_x^{(i)} \hat{J}_z^{(i)} + \hat{J}_z^{(i)} \hat{J}_x^{(i)} \right), \quad (7.16)$$

where superscripts on the spin-1 operators denote the atom $i \in \Lambda$ on which the operator acts. The collective detunings are given by $\Delta_{\pm} = \Delta_1 \pm \Delta_2$, and the collective Rabi frequencies are given by $\Omega_{\pm} = \Omega_{01} \pm \Omega_{02}$. The last term in (7.13), denoting the Rydberg-Rydberg interactions, becomes

$$\mathcal{V}_{Ryd} = \sum_{i=1}^{N-1} \left\{ W^- \hat{J}_z^{(i)} \hat{J}_z^{(i+1)} + W^+ \left(\hat{J}_z^{(i)} \right)^2 \left(\hat{J}_z^{(i+1)} \right)^2 + D \left[\left(\hat{J}_z^{(i)} \right)^2 \hat{J}_z^{(i+1)} + \hat{J}_z^{(i)} \left(\hat{J}_z^{(i+1)} \right)^2 \right] + S \hat{J}_s^{(i)} \right\} + \partial\Gamma, \quad (7.17)$$

where the interaction coefficients are given by $W^{\pm} = \frac{C_6^{11} + C_6^{22} \pm 2C_6^{12}}{4a^6}$, $D = \frac{C_6^{11} - C_6^{22}}{4a^6}$ and $S = \frac{C_6^S}{4a^6}$ with a the lattice constant. The spin-swapping operator $\hat{J}_s^{(i)}$ is given by

$$\hat{J}_s^{(i)} = \left(\hat{J}_+^{(i)} \right)^2 \left(\hat{J}_-^{(i+1)} \right)^2 + \left(\hat{J}_-^{(i)} \right)^2 \left(\hat{J}_+^{(i+1)} \right)^2. \quad (7.18)$$

Finally, the term $\partial\Gamma$ contains boundary effects and higher order terms.

Now, when at least one of the detunings $\Delta_{1,2}$ is very large and positive, the ground state $|g\rangle$ will effectively disappear from the state manifold. Its effects on the transitions, however, will remain, as the Rydberg states are not directly dipole coupled, but they are coupled to second order in perturbation theory through the virtual state $|g\rangle$ which has now become a fast degree of freedom of the system. Reducing the spin-1 operators to spin- $\frac{1}{2}$ operators is almost straightforward. For operators that do not couple the Rydberg states to the ground state, such as \hat{J}_z , certain rows and columns can be cut from the matrix representation. Let \asymp denote equality after cutting, a process that effectively⁸ removes all rows and columns from a matrix representation that pertains to the state $|g\rangle$. Then,

$$\hat{J}_z = \begin{pmatrix} 1 & 0 & 0 \\ 0 & 0 & 0 \\ 0 & 0 & -1 \end{pmatrix} \asymp \begin{pmatrix} 1 & \emptyset & 0 \\ \emptyset & \emptyset & \emptyset \\ 0 & \emptyset & -1 \end{pmatrix} = \begin{pmatrix} 1 & 0 \\ 0 & -1 \end{pmatrix} = \hat{\sigma}_z. \quad (7.19)$$

Likewise,

$$\left(\hat{J}_z \right)^2 = \begin{pmatrix} 1 & 0 & 0 \\ 0 & 0 & 0 \\ 0 & 0 & 1 \end{pmatrix} \asymp \begin{pmatrix} 1 & \emptyset & 0 \\ \emptyset & \emptyset & \emptyset \\ 0 & \emptyset & 1 \end{pmatrix} = \begin{pmatrix} 1 & 0 \\ 0 & 1 \end{pmatrix} = \hat{\mathbb{I}}. \quad (7.20)$$

Operators that do couple the Rydberg states to the ground state are not so trivially cut. Instead, the formal process of adiabatic elimination must be invoked [92]. This results in

$$\frac{\Omega_+}{2\sqrt{2}} \hat{J}_x^{(i)} - \frac{\Omega_-}{2\sqrt{2}} \left(\hat{J}_x^{(i)} \hat{J}_z^{(i)} + \hat{J}_z^{(i)} \hat{J}_x^{(i)} \right) \asymp \frac{1}{2} \Omega_{12}^* \hat{\sigma}_x^{(i)}, \quad (7.21)$$

where Ω_{12}^* is the effective coupling between the two Rydberg states through second order transitions [83]. Finally, the spin-swapping operator, after cutting, becomes the flip-flop term

$$\hat{J}_s^{(i)} \asymp \left(\hat{\sigma}_x^{(i)} \hat{\sigma}_x^{(i+1)} + \hat{\sigma}_y^{(i)} \hat{\sigma}_y^{(i+1)} \right). \quad (7.22)$$

After eliminating the ground state from the state manifold, one obtains the Hamiltonian

$$\mathcal{H}_{\Lambda} = \frac{1}{2} \sum_{i=1}^N \left\{ [-\Delta_- + 4D] \hat{\sigma}_z^{(i)} + \Omega_{12}^* \hat{\sigma}_x^{(i)} \right\} + \sum_{i=1}^{N-1} \left\{ W^- \hat{\sigma}_z^{(i)} \hat{\sigma}_z^{(i+1)} + S \left[\hat{\sigma}_x^{(i)} \hat{\sigma}_x^{(i+1)} + \hat{\sigma}_y^{(i)} \hat{\sigma}_y^{(i+1)} \right] \right\} + \partial\Gamma', \quad (7.23)$$

where $\partial\Gamma'$ is the new boundary term after cutting, given by

$$\partial\Gamma' = -D \left(\hat{\sigma}_z^{(1)} + \hat{\sigma}_z^{(N)} \right) + \sum_{|i-j| \geq 2} \frac{1}{|i-j|^6} \left\{ W^- \hat{\sigma}_z^{(i)} \hat{\sigma}_z^{(j)} + S \left[\hat{\sigma}_x^{(i)} \hat{\sigma}_x^{(j)} + \hat{\sigma}_y^{(i)} \hat{\sigma}_y^{(j)} \right] \right\}. \quad (7.24)$$

Note that every term that is proportional to $\bigotimes_{i \in \Lambda} \hat{\mathbb{I}}_i$ has been removed from the Hamiltonian because those terms collectively lead to a constant energy shift that does not affect the dynamics of the system.

⁸The word 'effectively' refers to the effective Hamiltonian approach where a subspace Hamiltonian is crafted from a general superspace Hamiltonian.

The first term of $\partial\Gamma'$ contains boundary effects which are relatively small for big systems. The second term contains the higher order van der Waals interactions, which rapidly drop in interaction strength after distance beyond the lattice constant. Ignoring the W^- term, the resulting error arising from these higher order flip-flop effects is then roughly equal to $\sum_{n=2}^{\infty} 1/n^6 \approx 0.017$, barely 2% of the first order contribution.

By setting $\Delta_- = 4D$ and $\Omega_{12}^* \rightarrow 0$, the first term in (7.23) will disappear. By assuming negligibility of the boundary term, what remains is a XXZ -Hamiltonian. If it is possible to get W^- to zero, one obtains an XY -Hamiltonian

$$\mathcal{H}_{XY}^{vdW} = \sum_{\langle i,j \rangle} \frac{C_6^S}{4a^6} \left(\hat{\sigma}_x^{(i)} \hat{\sigma}_x^{(j)} + \hat{\sigma}_y^{(i)} \hat{\sigma}_y^{(j)} \right) + \partial\Gamma' \quad (7.25)$$

in contrast to (7.10). Such a Hamiltonian will therefore also allow $XX + YY$ dynamics, but it suffers from being heavily dependent on the fine-tuning of the system parameters, as opposed to the dipolar coupling which naturally lead to a $XX + YY$ -type interaction without fine-tuning. It begs the question whether it is experimentally viable to create a setup that allows for this specific fine-tuning to be implemented.

7.2 Rydberg-dressing for PST

7.2.1 Rydberg-dressed atoms

It is also possible to create a spin exchange interaction through qubits based on Rydberg-dressed atoms. These atoms have an outer electron in a ground state, yet allows for tiny admixture with a Rydberg states. The wavefunction of such a qubit takes the form

$$|\psi\rangle = \mathcal{N} (|g\rangle + \beta |r\rangle), \quad (7.26)$$

where \mathcal{N} is a constant that normalises the wavefunction, $|g\rangle$ is an electronic ground state of the atom, $|r\rangle$ is a Rydberg state of the atom, and β is called the degree of dressing or the dressing parameter, given by [130]

$$\beta = \frac{\Omega}{2\Delta}. \quad (7.27)$$

The term 'dressing' is derived from the fact that $|\beta| \ll 1$ so that the population of the Rydberg state is very small. As a consequence, the Rydberg decay rate γ_{Ryd} is severely damped:

$$\gamma \sim \left| \langle g | \vec{d} | \psi \rangle \right|^2 \sim \beta^2 \gamma_{Ryd}. \quad (7.28)$$

If the Rydberg coupling is off-resonant, the dressed atoms will interact through their mutual van der Waals interactions. Then, the Hamiltonian that describes their dynamics is given by

$$\mathcal{H}_{dressed} = \sum_{i \in \partial\Lambda} \frac{\Omega_i}{2} \sigma_x^i + \sum_{i \in \partial\Lambda} \Delta_i \sigma_{rr}^i + \sum_{i < j} V(\mathbf{r}_{ij}) \sigma_{rr}^i \sigma_{rr}^j \quad (7.29)$$

with the potential $V(\mathbf{r}_{ij}) = C_6/|\mathbf{r}_i - \mathbf{r}_j|^6$. From perturbation theory, it can be shown that this blockade effect creates a softcore potential of the form

$$U(\mathbf{r}_{ij}) = \frac{C_6^*}{R_c^6 + |\mathbf{r}_i - \mathbf{r}_j|^6}, \quad (7.30)$$

where $C_6^* = \beta^4 C_6$ is the shifted van der Waals coupling coefficient and $R_c = (C_6/2\Delta)^{1/6}$ is the characteristic blockade radius or critical radius [131]. The scaling law of C_6 with respect to the dressing parameter is to be expected: the admixture ratio of the doubly excited state scales like $\sim \beta^2$ [132], so that the matrix element $\langle rr | \mathcal{V}_{dd} | rr \rangle$ scales with $\sim \beta^4$ [130]. Inside the critical radius, excitation the doubly excited state $|rr\rangle$ is greatly suppressed because of induced off-resonance of the Rydberg blockade effect. The $1/r^6$ -tail of the van der Waals potential is then only valid outside of this radius, while inside the radius the potential levels off to a constant value.

7.2.2 Choice of qubit manifold

For the implementation of a PST-facilitating Hamiltonian, it is possible to opt for a different qubit manifold than the one used for the regular one-qubit and two-qubit gates. While performing those operations, one qubit system is adhered to. While performing PST, the qubit states are uniquely mapped onto a different set of qubit states, on which PST is performed. In order to minimise 'Rydberg contamination', where interactions are turned on at unwanted moments, choosing a Rydberg-dressed qubit system for PST boils down to choosing between either gg qubits or gr qubits. Both approaches have been investigated in the context of state transfer for Rydberg dressed atoms, and two of these that appeared promising yet failed to enable PST, are elaborated in section 7.3.

One system that does facilitate PST is one where both qubits are mapped to a state

$$|0/1\rangle = \mathcal{N}_{0/1} \left(|g/h\rangle + \beta_{0/1} |s/p\rangle \right), \quad (7.31)$$

where $|g/h\rangle \stackrel{\text{def}}{=} |g\rangle \vee |h\rangle$ are electronic ground states, and $|s/p\rangle \stackrel{\text{def}}{=} |s\rangle \vee |p\rangle$ are Rydberg excited states. β is again the dressing parameter and \mathcal{N} the normalisation constant. The subscript 0/1 pertains to which qubit is chosen. If $\Omega_{s/p}$ is the Rabi frequency of the laser that drives the $|g\rangle \leftrightarrow |s\rangle$ / $|h\rangle \leftrightarrow |p\rangle$, and $\Delta_{s/p}$ denotes the detuning of Rydberg state $|s/p\rangle$, then the dressing parameters read

$$\beta_{0/1} = \frac{\Omega_{s/p}}{2\Delta_{s/p}} \stackrel{\text{def}}{=} \beta + s/p. \quad (7.32)$$

In figure 7.1, the qubit system is depicted.

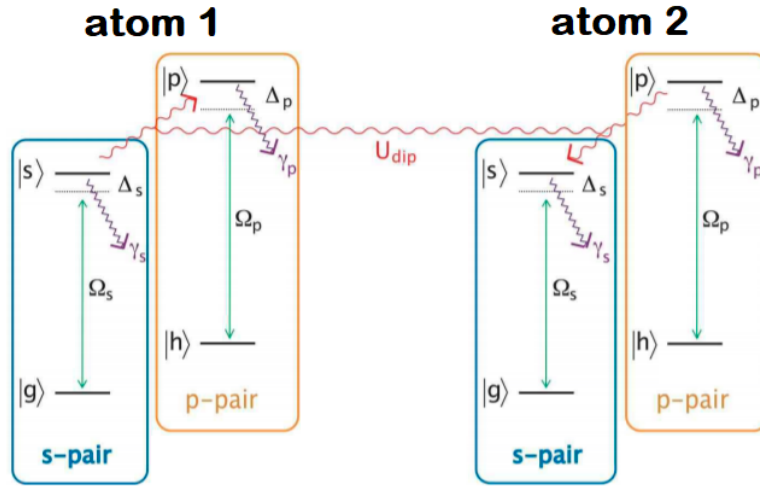


Figure 7.1: A qubit system where each qubit state is mapped to an s/p state pair containing a ground state and a Rydberg dressed state [133]. The Rydberg states are resonantly coupled by the interaction operator U_{dip} , defined in (7.34). Radiative losses are indicated by wavy photon lines with spontaneous decay rates $\gamma_{s/p}$.

In some systems, the qubit states are mapped to electronic states that are sparsely populated. Then, it is not clear how one can relate PST along a chain to such a qubit system, as every qubit state population should be accessible by an arbitrary amount. This is known as the qubit mapping problem, and it imposes serious restrictions to what systems can be employed for PST. By taking a ground state combined with its associated Rydberg state, the qubits can still communicate through their strong dipolar or van der Waals interactions, but the states $|0/1\rangle$ can still have an arbitrary population number. Therefore, by adopting such a system, a qubit mapping problem is evaded.

The system Hamiltonian is similar to (7.29), and is given by

$$\mathcal{H}_{dressed} = \sum_{i \in \partial\Lambda} \frac{\Omega_{s,i}}{2} \sigma_{x,s}^i + \sum_{i \in \partial\Lambda} \frac{\Omega_{p,i}}{2} \sigma_{x,p}^i + \sum_{i \in \partial\Lambda} \Delta_{s,i} \sigma_{ss}^i + \sum_{i \in \partial\Lambda} \Delta_{p,i} \sigma_{pp}^i + \sum_{i < j} U_{dip}(\mathbf{r}_{ij}) \sigma_{sp}^i \sigma_{ps}^j, \quad (7.33)$$

where the van der Waals interactions has made place for the dipolar interaction

$$U_{dip}(\mathbf{r}_{ij}) = -\frac{\mu^2}{|\mathbf{r}_i - \mathbf{r}_j|}, \quad (7.34)$$

where μ is the transition dipole moment [133][134]. If the axis of quantisation is taken to be orthonormal to the two-dimensional lattice Λ , then the angular dependence will drop out of the dipolar interactions, as evident from the form of (7.34). Flip-flop interactions between $|gh\rangle$ and $|hg\rangle$ states are then caused by the transition scheme

$$|gh\rangle \rightarrow |sp\rangle \rightarrow |ps\rangle \rightarrow |hg\rangle, \quad (7.35)$$

where the first and third transitions are driven by lasers, and the second transition is driven by the natural resonant dipolar interaction between the Rydberg states.

7.2.3 Van Vleck perturbation theory

In order to introduce perturbation theory, one must first wonder which systems parameters are small relative to what other parameters. For Rydberg dressed atoms, the β -parameter is very small, leading to the inequality

$$\Omega_{s/p,i} \ll |\Delta_{s/p,i}| \quad \forall i \in \partial\Lambda. \quad (7.36)$$

If the constraint of strong detuning is consistent with the Rydberg blockade effect, such that

$$\Omega_{s/p,i} \ll |\Delta_{s/p,i} + U(r_{ij})| \quad \forall (i, j) \in \partial\Lambda, \quad (7.37)$$

and if the detuning is allowed to vary slowly over the sub-lattice

$$|\Delta_{s/p,i} - \Delta_{s/p,j}| \ll |\Delta_{(s/p,i),(s/p,j)}| \quad \forall (i, j) \in \partial\Lambda, \quad (7.38)$$

then the one-exciton subspace Γ_1 contains solely elements that will have an energy that varies little.

Because the laser coupling is weak in accordance with the aforementioned inequalities, one can split $\mathcal{H}_{dressed}$ in (7.33) in an unperturbed part \mathcal{H}_0 , and an interaction part V' which weakly perturbs \mathcal{H}_0 , so that

$$\mathcal{H}_{dressed} = \mathcal{H}_0 + V'. \quad (7.39)$$

Since V' pertains to the laser coupling, it is to be understood that

$$\mathcal{H}_0 = \sum_{i \in \partial\Lambda} \Delta_{s,i} \sigma_{ss}^i + \sum_{i \in \partial\Lambda} \Delta_{p,i} \sigma_{pp}^i + \sum_{i < j} U_{dip}(\mathbf{r}_{ij}) \sigma_{sp}^i \sigma_{ps}^j \quad (7.40)$$

and

$$V' = \sum_{i \in \partial\Lambda} \frac{\Omega_{s,i}}{2} \sigma_{x,s}^i + \sum_{i \in \partial\Lambda} \frac{\Omega_{p,i}}{2} \sigma_{x,p}^i. \quad (7.41)$$

In order to rewrite the system Hamiltonian, van Vleck perturbation theory has to be invoked [135]. While initially introduced by John van Vleck, it was later modernised by I. Shavitt and L.T. Redmon [136]. This theory is concerned with perturbation theory within quasi-degenerate subspaces, i.e. subspaces whose elements have energies E with variations δE smaller than the absolute value of the energies themselves ($|\delta E/E| \ll 1$), therefore calculating the relevant couplings that replace $\{J_n\}$ and $\{B_n\}$ in the Hamiltonian family (6.2). Van Vleck perturbation theory partitions the entire Hilbert space \mathfrak{H} of states into 3 subspaces:

$$\mathfrak{H} = \text{span } P \oplus \text{span } Q \oplus \text{span } S. \quad (7.42)$$

The spaces P, Q and S refer to the ground state manifolds, the single excitation manifolds, and the doubly excited manifolds respectively, each of which is coupled through the perturbative Hamiltonian V' by

$$P \Leftrightarrow Q \Leftrightarrow S. \quad (7.43)$$

The space P contains the quasi-degenerate subspace of vectors

$$|\pi_n\rangle \stackrel{\text{def}}{=} |g_1 g_2 \cdots h_n \cdots g_N\rangle, \quad (7.44)$$

where the n -th atom finds itself in the $|h\rangle$ state. These states compromise the relevant ground state manifold in which perturbation theory applies. Without laser coupling ($V' = 0$), this would be an eigenstate of the Hamiltonian \mathcal{H}_0 . By introducing the weak coupling, however, the eigenstates shift to $|\pi_n\rangle' = |\pi_n\rangle + \mathcal{O}(\beta_{s/p}) [|\pi_n\rangle |_{g \rightarrow s} + |\pi_n\rangle |_{h \rightarrow p}]$. The states between brackets denote states like $|\pi_n\rangle$, except that one atom in the $|g\rangle$ state is now in the $|s\rangle$ state, or the $|h\rangle$ atom is now in the $|p\rangle$ state.

In a similar fashion, the Q space is made up of states like

$$|\kappa_n\rangle_p \stackrel{\text{def}}{=} |g_1 g_2 \cdots p_n \cdots g_N\rangle \quad \& \quad |\kappa_n\rangle_s \stackrel{\text{def}}{=} |h_1 h_2 \cdots s_n \cdots h_N\rangle. \quad (7.45)$$

These states make up the single excitation manifold. Within these manifolds P and Q , a full calculation within the van Vleck perturbation framework is given in the work conducted by Wüster et al. [133]. For a constant qubit separation of R , the results are calculated to be the following: within the basis set $\{|\pi_n\rangle'\}$, the matrix elements

$$\mathcal{H}_{eff,ij} = \langle \pi_i |' \mathcal{H}_{eff} | \pi_j \rangle' \quad (7.46)$$

of the effective Hamiltonian \mathcal{H}_{eff} read

$$\mathcal{H}_{eff,ij} = (L_2 + L_4)\delta_{ij} + \tilde{U}_{ij}(r), \quad (7.47)$$

where $L_{2/4}$ are coefficients called the light-shift, and appear in second and fourth order in perturbation theory respectfully, and $\tilde{U}_{ij}(r)$ is the modified potential dependent on qubit separation r . Indeed, this light shift is the origin of the magnetic field in (6.2), and is caused by the laser induced coupling between $|g/h\rangle$ and $|s/p\rangle$ states. For global detuning and Rabi frequency profiles, they are given by the expressions

$$L_2 = (N-1)\beta_s^2\Delta_s + \beta_p^2\Delta_p, \quad (7.48)$$

$$L_4 = - \left[(N-1)\beta_s^4\Delta_s + \beta_p^4\Delta_p + (N-1)\beta_s^2\beta_p^2(\Delta_s + \Delta_p) \right]. \quad (7.49)$$

The reason why s terms carry a factor of $N-1$, but not p terms, is because there are $N-1$ $|g\rangle$ states in every basis state $|\pi_n\rangle$, which are coupled to the $|s\rangle$ states, but there is only one $|h\rangle$ state. The modified potential is given by

$$\tilde{U}_{ij}(r) = \beta_s^2\beta_p^2 \left(\sum_{k \neq j} \frac{1}{1 - \bar{U}_{kj}^2} \right) (\Delta_s + \Delta_p)\delta_{ij} + \beta_s^2\beta_p^2 \frac{U_{ij}}{1 - \bar{U}_{ij}^2} (1 - \delta_{ij}), \quad (7.50)$$

where

$$\bar{U}_{ij} = \frac{U_{ij}}{\Delta_s + \Delta_p}. \quad (7.51)$$

What immediately becomes clear from the form of $\tilde{U}_{ij}(r)$, is that for large separation ($r > R, r \rightarrow \infty$), one obtains rapid decay:

$$\lim_{r \rightarrow \infty} \tilde{U}_{ij}(r) = 0. \quad (7.52)$$

This means that the nearest neighbour interactions are strong, while beyond nearest neighbour interactions become rapidly weak. While not precisely 0, which is physically not viable, this allows for the NNN protocol that has been elaborated on in section 6.4.

It is, of course, desirable to vary the detuning profile and the Rabi frequency profile, to obtain position-dependent couplings $\{J_n\}$ and $\{B_n\}$. Loosening this restriction yields a new effective Hamiltonian

$$\mathcal{H}_{eff,ij} = (L_{2,ij} + L_{4,ij}) + \tilde{U}_{ij}(r), \quad (7.53)$$

new light-shifts

$$L_{2,ij} = \left[\sum_{\substack{m \in \partial\Lambda \\ m \neq i}} \beta_{s,m}^2 \Delta_{s,m} + \beta_{p,i}^2 \Delta_{p,i} \right] \delta_{ij}, \quad (7.54)$$

$$L_{4,ij} = - \left[\sum_{\substack{m \in \partial\Lambda \\ m \neq i}} \beta_{s,m}^4 \Delta_{s,m} + \beta_{p,i}^4 \Delta_{p,i} + \sum_{\substack{m \in \partial\Lambda \\ m \neq i}} \beta_{s,m}^2 \beta_{p,i}^2 (\Delta_{s,m} + \Delta_{p,i}) \right] \delta_{ij}, \quad (7.55)$$

and a new modified potential

$$\tilde{U}_{ij}(r) = \beta_{s,i}^2 \beta_{p,i}^2 \left(\sum_{k \neq j} \frac{1}{1 - \bar{U}_{kj}^2} \right) (\Delta_{s,i} + \Delta_{p,i}) \delta_{ij} + \beta_{s,i} \beta_{p,i} \beta_{s,j} \beta_{p,j} \frac{U_{ij}}{1 - \bar{U}_{ij}^2} (1 - \delta_{ij}), \quad (7.56)$$

with the same behaviour in the limit of large separation. The extension of global detuning/Rabi frequency profiles to local ones is obtained from tracking which laser driven transitions drive which light shift.

In conclusion, this system does not suffer from the qubit mapping problem, and the coupling constants go to 0 sufficiently rapidly. Then, by solving for the Rabi frequencies and detunings, it is possible to get a PST-facilitating effective Hamiltonian, showing that PST is possible within the one-exciton state manifold comprised of states $|\pi_n\rangle'$.

7.2.4 Position-dependent coupling

The XY -Hamiltonians (7.10) and (7.25), formed from dipole-dipole interactions and van der Waals interactions respectively, have the correct operator form to replicate the Krawtchouk Hamiltonian (6.48) or the generalised XY -Hamiltonian with applied magnetic field (6.50), but their forefactors are position-independent. By opting for a Rydberg-dressed qubit system, coupling constants emerge that depend on the Rabi frequencies Ω_i , detunings Δ_i and the Rydberg-Rydberg interactions $V(r_{ij})$. The former two are experimentally controllable (within realistic ranges), while the latter is fixed for a certain qubit system. The Rabi frequency Ω that drives a certain transition is proportional to the electric field strength $|\vec{E}|$, which itself is proportional to the square root of the laser intensity \sqrt{I} . By changing the properties of the laser, giving it a position-dependent profile, one can fine-tune those coupling constants to resemble the Krawtchouk-like coupling $J_n = -\frac{1}{2}\sqrt{n(N-n)}$, and vary the magnetic field B_n so that the symmetry matching condition and the ESR are fulfilled.

7.3 Alternative Rydberg-dressed systems

7.3.1 Two-photon gr -qubit system

The viability of PST in certain alternative Rydberg-dressed systems has been researched. This section is dedicated to two examples that seemed fruitful, in their own right, but did not make the cut as they eventually turned out to be unable to support PST.

One alternative Rydberg-dressed system maps the $|0\rangle$ state to a ground state $|g\rangle$, and the $|1\rangle$ state to a Rydberg state $|r\rangle$. This qubit system is given in figure 7.2(b). Within the quasi-degenerate subspace spanned by $|\Psi_i\rangle = \{|g_1 g_2 \cdots r_i \cdots g_N\rangle\}$, the Hamiltonian (7.29) can be rewritten to second order in perturbation as [137]

$$\mathcal{H}_{eff} = \sum_i \left(\Delta_i + \frac{\Omega_i^2}{2\Delta_i} \right) \sigma_{rr}^i + \sum_{i \neq j} I_{ij} \sigma_{rr}^i \sigma_{gg}^j + J_{ij} \sigma_{rg}^i \sigma_{gr}^j, \quad (7.57)$$

where

$$I_{ij} = \frac{\Omega_j^2 V(r_{ij})}{4\Delta_j(\Delta_j + V(r_{ij}))} \quad (7.58)$$

and

$$J_{ij} = \sum_{\beta=i,j} \frac{\Omega_i \Omega_j V(r_{ij})}{8\Delta_\beta(\Delta_\beta + V(r_{ij}))}. \quad (7.59)$$

The σ_{ab} projectors are given by the usual $|a\rangle\langle b|$ operators. Such a Hamiltonian can be mapped onto creation and annihilation operators through the mapping

$$\sigma_{rg}^i \mapsto a_i^\dagger, \quad \sigma_{gr}^i \mapsto a_i, \quad (7.60)$$

giving a tight binding like Hamiltonian

$$\mathcal{H}_{eff} = \sum_i \mu_i a_i^\dagger a_i + \sum_{i<j} J_{ij} (a_i^\dagger a_j + a_j^\dagger a_i), \quad (7.61)$$

which is precisely a Hamiltonian that is able to facilitate PST. Here, $\mu_i = \Delta_i + \frac{\Omega_i^2}{2\Delta_i} + \sum_{j \neq i} I_{ij}$. The origin of this coupling J_{ij} arises from the cancellation of two Raman paths, since the transition $|gr\rangle \leftrightarrow |rg\rangle$ can happen in two ways. This process is illustrated in figure 7.2(b).

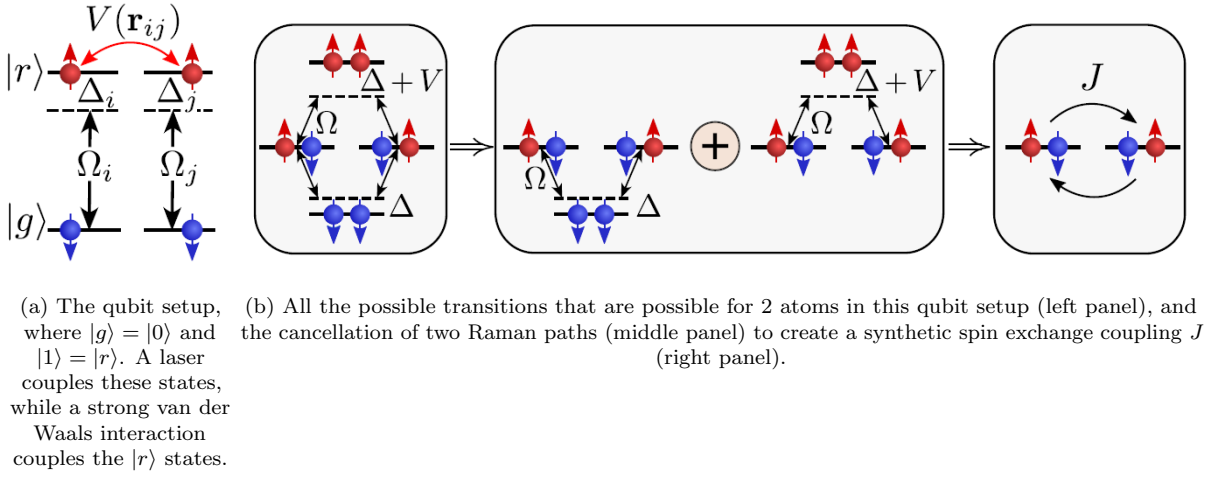


Figure 7.2: The two-photon gr qubit system that allows for the emergence of a coupling constant J to realise a Krawtchouk-like coupling [138].

Such a model naturally gives rise to a PST-facilitating Hamiltonian, but only within this one-exciton subspace, in which Van Vleck perturbation theory is valid. The qubit interpretation is then awkward: $|1\rangle$ states are mapped to Rydberg dressed states which are poorly populated. In a general qubit array, however, the 'population' of the $|1\rangle$ state should possibly take any value in the interval $[0, 1]$. This is the qubit mapping problem, and because of this severe restriction, the application possibility of this system for PST in general qubit registers is poor. Though this system is useful and straightforward for single-exciton transfer.

One last thing this system suffers from, is the over-restraining of the system parameters. If one wishes to opt for identical qubits, such that $\beta_i = \beta$, one finds that the number of equations that have to be solved to find the Rabi frequency profile/detuning profile, is equal to $N - 1$, but the number of free parameters is equal to $\frac{N}{2}$ for an even number of qubits, and $\frac{N+1}{2}$ for an odd number of qubits. Therefore, the only system sizes that allow for solutions are when $N = 2, 3$.

7.3.2 Fourth order photon process system

Several Rydberg-dressed systems have been proposed that employ fourth-order photon processes to enable flipflop interactions over large distances [139]. One such system, analysed by Van Bijnen and Pohl, maps the qubit states to ground states, defined as $|\uparrow\rangle$ and $|\downarrow\rangle$, in the Rydberg state manifold, and uses an intermediate Rydberg state $|e\rangle$ to mediate long range interactions [140]. The coupling between two-qubit

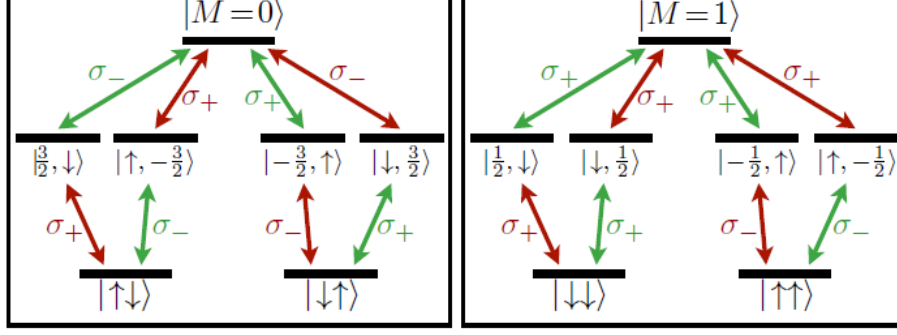


Figure 7.3: The four-photon processes that lead to two-qubit interactions, particularly the spin exchange process (left panel). The transitions are driven by σ^+ and σ^- polarised light, depending on the total angular momentum $M = 0, 1$ of the doubly excited Rydberg state $|ee\rangle$.

states is mediated through four-photon process, where circularly polarised light couples each state to 3 intermediate Rydberg states, portrayed in figure 7.3.

The matrix elements of a transition from $|p\rangle \stackrel{\text{def}}{=} |\uparrow\downarrow\rangle$ to a state $|p'\rangle \stackrel{\text{def}}{=} |\downarrow\uparrow\rangle$ is given by

$$\langle p | \mathcal{H}_{eff} | p' \rangle^{(4,D)} = - \sum_{q,q' \in Q} \sum_{\mu \in S} \frac{V_{pq'}^X V_{q'\mu}^D V_{\mu q}^D V_{qp'}^X}{E_{q'}^{(Q)} E_{\mu}^{(S)} E_q^{(Q)}}, \quad (7.62)$$

where $(4, D)$ denotes the fourth-order contribution, Q and S are the subspaces defined in section 7.2.3, V^X is the operator that couples the P to the Q space through photon interactions, V^D is the operator that couples the Q to the S space, and $E_{q/\mu}^{(Q,S)}$ is the energy of the level state q/μ in the rotated frame.

Though this system has appealing properties, such as the evasion of the qubit mapping problem by mapping the qubit states to ground states that can be significantly populated, it suffers under the fact that the associated coupling constant $J_{n,n+m}$ does not sufficiently decay as a function of m . If worked out in terms of Rabi frequencies, detunings and Rydberg-Rydberg couplings V_{ee} , the matrix element (7.62) takes the approximate form

$$\langle p | \mathcal{H}_{eff} | p' \rangle \propto \frac{\Omega^4}{\Delta^2(2\Delta - V_{ee})}. \quad (7.63)$$

In the case of distant qubit separation, $V_{ee} \rightarrow 0$, the matrix elements themselves do not vanish unlike the case in sections 7.2.3 and 7.3.1. This is evident from the identity

$$\mathcal{H}_{eff} = \sum_{p,p' \in P} |p\rangle \langle p | \mathcal{H}_{eff} | p' \rangle \langle p' | \rightarrow \sum_i \mu_i a_i^\dagger a_i + \sum_{i < j} J_{ij} (a_i^\dagger a_j + a_j^\dagger a_i), \quad (7.64)$$

giving the relationship

$$J \propto \langle p | \mathcal{H}_{eff} | p' \rangle^{(4,D)}. \quad (7.65)$$

Therefore, this system is unsuitable for implementing a Krawtchouk-like coupling $J_n = -\frac{1}{2}J\sqrt{n(N-n)}$ that explicitly requires beyond-nearest neighbour interactions to vanish, or at least decay sufficiently rapidly.

8 Simulations for PST in small qubit registers

8.1 $N = 2$ qubit register

The simplest example in which PST can be demonstrated is a register of $N = 2$ qubits. Such a register has a one-exciton Hamiltonian given by

$$\mathcal{H}_1 = \begin{pmatrix} B & -\frac{J}{2} \\ -\frac{J}{2} & B \end{pmatrix}, \quad (8.1)$$

where B and J have been defined previously in section 6, particularly equation (6.2). Though not explicit, the coupling still follows the implicit characteristic Krawtchouk square root behaviour. For $N = 2$, the magnetic field must always be global in the one-exciton subspace: no variation can exist in accordance with the symmetry matching condition. The eigenvalues of \mathcal{H}_1 readily read

$$\lambda^{(\pm)} = B \pm \frac{J}{2}. \quad (8.2)$$

The transfer time, for global magnetic field, is equal to that of the Krawtchouk chain [111], so that the PST time must be equal to $t_{PST} = \frac{\pi}{J}$. It then follows that this system automatically satisfies the ESR, as $\lambda^{(+)} - \lambda^{(-)} = (2m + 1)\frac{\pi}{t_{PST}} = J$ for all $m \in \mathbb{N} \cup \{0\}$.

Several simulations have been performed to check the validity of the PST theory that has been discussed in section 6. Most equations have been verified to be true, such as the free fermion dynamics proven in (6.40), or the existence of accumulated phases like those mentioned in section 6.2.4. Every single simulation was performed analytically, and the files can be obtained by request to the author [141]. For all simulations, the units $J = 1$ and $B = 1$ were chosen. Such simulations clearly display state transfer with unit fidelity. The probability p of the transition $|01\rangle \leftrightarrow |10\rangle$ is shown in figure 8.1. The validity and periodicity of the PST time can be observed.

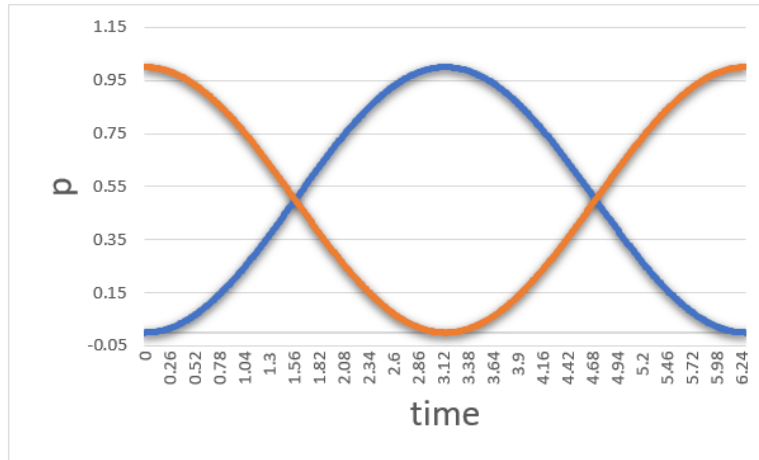


Figure 8.1: The state transfer of a qubit chain prepared in the $|01\rangle$ state (orange line) to the $|10\rangle$ state (blue line). This happens in the predicted (unitless) PST time $t_{PST} = \frac{\pi}{J}$.

A small error model that can be added to the simulations is the stochastic error given by (6.60) in section 6.5.1. For the sake of clarity of the plots, the infidelity I was chosen to be the variable of interest. Its relation to the fidelity is given by

$$I = 1 - F. \quad (8.3)$$

Where fidelity is a measure of the purity of a quantum state, infidelity is a measure of the error accumulation in a quantum state, with respect to an error-free theoretical prediction. The model can be further simplified by only varying the coupling constant J with a random stochastic error, since that is the major driver of PST compared to the magnetic field components. The results are presented in figure 8.2.

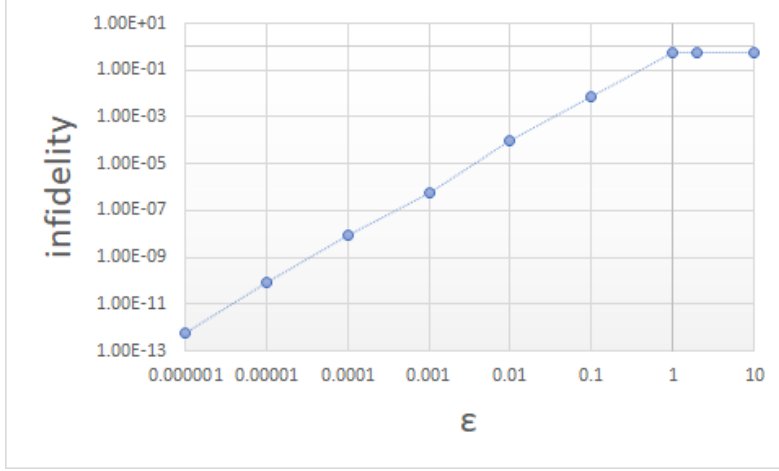


Figure 8.2: The infidelity of PST for $N = 2$ scales polynomially in the error term ϵ for $\epsilon \lesssim 1$, and is roughly constant beyond $\epsilon \gtrsim 1$. For each data point, ≈ 100 random data points were selected. The plateau has an infidelity of $I \approx 0.45$.

8.2 $N = 3$ qubit register

The first example where a varying magnetic field can still facilitate PST is for $N = 3$. The one-exciton Hamiltonian \mathcal{H}_1 is given by

$$\mathcal{H}_1 = \begin{pmatrix} b & -\frac{J}{\sqrt{2}} & 0 \\ -\frac{J}{\sqrt{2}} & B & -\frac{J}{\sqrt{2}} \\ 0 & -\frac{J}{\sqrt{2}} & b \end{pmatrix}. \quad (8.4)$$

Two options exist: either $b = B$ so that the magnetic field is global, or $b = B + 2\sqrt{\frac{\gamma}{1-\gamma}}J$, where γ is defined in Appendix D, where the entire derivation of the condition of a varying magnetic field is given. Both of these options are equally valid solutions to the IEP, and therefore facilitate PST, though the PST time for the latter case is modulated and becomes

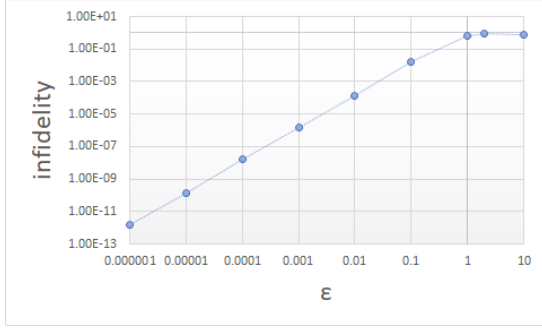
$$t_{PST} = (2m+1) \frac{\pi}{\epsilon + \sqrt{J^2 + \epsilon^2}}. \quad (8.5)$$

Plots of the infidelity against error are presented in figure 8.3 for both the global and local magnetic field scenarios. Similar curves are obtained, though the latter has a slope about twice as large as the former for the small error regime $\epsilon \lesssim 1$.

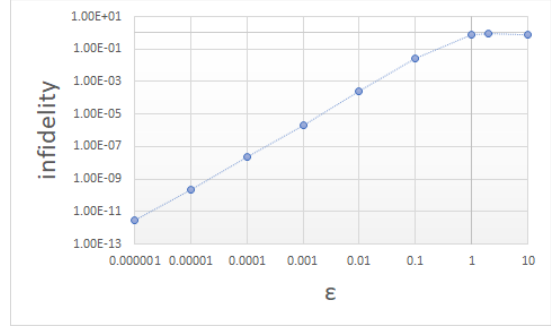
8.3 $N = 4$ qubit register

The first example that has a position-dependent coupling strength J_n is for $N = 4$ qubits. In Appendix E, the IEP is shown to have no valid solutions for a varying magnetic field. Therefore, this system is constrained to global magnetic fields only. In essence, the $N = 2$ case is quite similar to the $N = 4$ case in that regard. Though no exact solution can be extracted from the set of ESR equations, it is possible to approximate the solution to great accuracy. Such a solution would not facilitate PST, but it would facilitate PGST with great fidelity $> 99\%$. Although not perfectly equal to unity, in the NISQ era, such fidelities are still excellent and comparable to the fidelities of other gate-based operations.

The scaling of the infidelity with respect to the error is plotted in figure 8.4. Surprisingly, the maximum error that still tolerates fidelities of 90% and over is given by $\epsilon \approx 0.22$, and fidelities of 99% and over are still found up until $\epsilon \approx 0.07$. For stochastic fluctuations of that magnitude, such fidelities are high. For small qubit registers, it seems that PST is a very robust operation that tolerates high quality state transfer.



(a) PST results for a global magnetic field $B = b$.



(b) PST results for a global magnetic field

$$B = b + 2\sqrt{\frac{\gamma}{1-\gamma}}J.$$

Figure 8.3: The infidelity of PST for $N = 3$ scales polynomially in the error term ϵ for $\epsilon \lesssim 1$, and is roughly constant beyond $\epsilon \gtrsim 1$, for both scenarios. For each data point, ≈ 100 random data points were selected. Both plateaux have an infidelity of $I \approx 0.87$

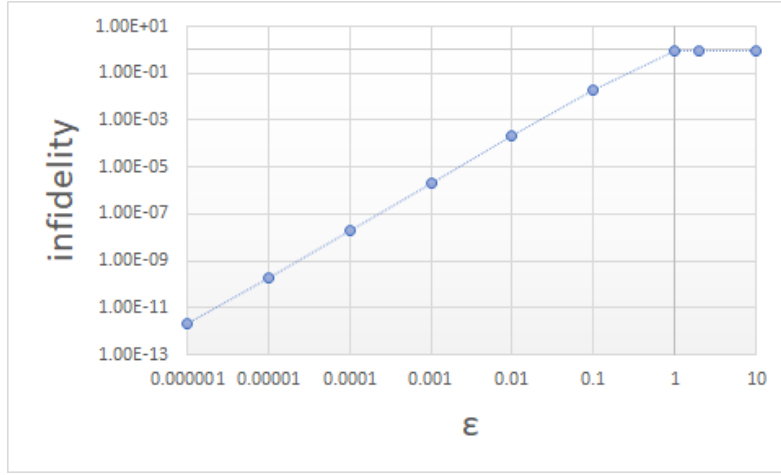


Figure 8.4: The infidelity of PST for $N = 4$ scales polynomially in the error term ϵ for $\epsilon \lesssim 1$, and is roughly constant beyond $\epsilon \gtrsim 1$. For each data point, ≈ 100 random data points were selected. The plateau has an infidelity of $I \approx 0.91$.

8.4 Beyond $N \geq 5$ qubits

It is desirable to extend the discussion in this section to qubit chains of arbitrary length. Unfortunately, as of now, no analytic model has been found to analyse qubit register of 5 or more qubits. Solving for the eigenvalues of \mathcal{H}_1 in the 5-qubit case is akin to analytically solving the roots of third degree polynomials⁹. For more qubits, this degree eventually increases. Though theoretically, solution exist for polynomials up to fourth degree, their solutions have convoluted forms, and solving the IEP for such complex eigenvalues, such that the ratios of their differences are rational, appears to be an impossible task unless some mathematical tool is devised that can find some structure in the solutions of the IEP.

While for most qubit chains, the IEP is still analytically unsolvable, the study of PST along smaller qubit chains serves as an excellent benchmark for the feasibility of mirror inversion of qubit chains in small quantum computers. Though for $N = 2$ and $N = 3$, the coupling J_n is invariant along the chain, $N = 4$ serves as the first checkpoint for non-trivial PST implementation, as this is the first qubit length after which PST demands a varying coupling constant. The experimental demonstration of PST along a qubit chain of $N = 4$ would therefore serve as the first step towards realisation of PST in real quantum

⁹In the general case, this polynomial would be of degree 5, but the symmetries of the one-exciton Hamiltonian reduce this degree to 3.

computers, despite the invariance of the magnetic field.

9 Conclusion and discussion

Quantum computing stands at a very important crossroad today. Simulators employing $\gtrsim 10$ qubits are becoming more viable for performing reliable calculations, yet taming error propagation in quantum computers is still a difficult task beyond that qubit number. The quantum advantage that is obtained for simulators with a small number of qubits, is simply lost beyond certain qubit register sizes and error scales. As of now, the scalability of most quantum computers is poor. For this reason, variational quantum algorithms operating on hybrid quantum computers seem to be a core part of quantum computing in the NISQ era. By combining the unique strengths of quantum computing and classical computing, certain algorithms can outperform classical computers without the need for a full-fledged fault tolerant quantum computer which does not yet exist. The architecture and the inner workings of a quantum circuit that runs the VQE algorithm is analogous to a classical neural network, and this machine learning like behaviour allows VQE to variationally relax the variational parameters. Through this mechanism, the system self-corrects certain errors, in some sense. Meanwhile, the classical computer efficiently runs an optimisation algorithm. This combined effort allows for quantum systems to be simulated in a way that should outperform classical calculations in the future.

Partial quantum error correction has proven itself to be of valuable use in the suppression of noise propagation in the VQE algorithm. A handful of types of error mitigation techniques that have been employed for the increase of accuracy of the Hartree-Fock solution, initiated for the VQE algorithm, have been explored. These include post-selection, so that electron number reservation was respected, McWeeny purification, so that the mathematical properties that a 1-RDM should satisfy are respected, and variational relaxation of the parameters, which is an inherent self-correcting mechanism of VQE, that counters coherent errors, and averages out some decoherent errors. The collection of these error correction techniques allow for solutions to lie within chemical accuracy, in the context of quantum chemistry. In general, the addition of these measures drops the energy estimate of the eigenenergy of molecules by about an order of magnitude: a significant amount. Though this trend breaks down beyond a certain qubit number, $x \approx 10$ for the calculation of the pseudo-molecules H_x , it shows a promising and optimistic trend that with additional error mitigation measures, one can achieve chemical accuracy for molecular problems of greater dimensions in the future as well.

Besides quantum computers based on superconducting qubits and ion trap qubits, Rydberg-based quantum computers are considered one of the main candidates for producing a relatively high fidelity hybrid quantum computer. Plenty of active control can be exerted over Rydberg atoms which give them many different choices to encode qubit states within their state manifold, and it allows them to reproduce a lot of quantum gate operations. Their strong long range interactions allows them to communicate over great distances of the order of μms , many lattice units apart, while the strong Rydberg blockade effect allows for the generation of entanglement. Many experimental setups have proven high fidelities for the qubit initialisation, read-out and propagation, particularly for gg qubits. Such a qubit system would therefore be a favourable candidate for the implementation of a Rydberg-based simulator. Another point in their favour, is that because only the Rydberg states mediate long range interactions, gg qubits have toggleable interactions.

The possibilities of quantum state transfer has also been explored. Central to this study was PST, where the fidelity of such an operation is equal to 1. With some additional unitary phase gates, PST has the capability of performing mirror inversion of an arbitrary string of qubits in arbitrary qubit states. By assuming the availability of a certain family of one-dimensional qubit chain Hamiltonians, the generalised XY -Hamiltonian with an external applied magnetic field, and parameterised by a few number of coupling constants, one can systematically deduct all necessary conditions for PST to arise along. These conditions, the symmetry matching condition and the IEP, provide a framework from which the coupling constants $\{J_n\}$ and $\{B_n\}$ can be derived. Such calculations have been performed for chains of $2 \leq N \leq 4$ qubits, and it has shown that each of them supports a unique set of parameters. The $N = 3$ chain has a constant global coupling J , but allows for the variation of the magnetic field. The $N = 4$ chain has a varying coupling J , but the magnetic field ought to be strictly constant over the entire chain length. For $N \geq 5$, chances are slim an analytic solution exists, as this is akin to solving third degree polynomials exactly and performing complex algebraic manipulations with them. Most likely, numerical solutions must be found, or a certain cohesive pattern must be found in the set of solutions.

The viability of implementing PST on a quantum qubit that is based on Rydberg-dressed qubits has been investigated. Certain systems had some attractive properties for such implementation, yet turned out to be of shortcoming. The two-photon *gr* system has been shown to allow for one-exciton transport, demonstrating the highly non-local correlated transport of states. For PST, it suffers from the qubit mapping problem and the over-restraining of the system parameters under certain conditions. The four-photon system has been shown to circumvent the qubit mapping problem by opting for *gg* qubits, where both qubit states are mapped to non-interacting electronic ground states. However, the specific transition scheme shown in figure 7.3, suffered from non-rapid decay of the coupling parameters J_n . Therefore, it is not able to support a Krawtchouk-like coupling $J_n = -\frac{1}{2}\sqrt{n(N-n)}$. A scheme that does support PST, however, is the scheme where each qubit state is mapped to the combined *gr* state, where the Rydberg state allows for small admixture with the ground state, whose excited states have a resonant dipolar interactions. The effective Hamiltonian of such a system is shown to decay sufficiently rapid, and the mapping avoids the qubit mapping problem. With such a scheme, it should be possible to experimentally verify PST of a general number of excitons.

If each qubit coupling is perturbed by some uncorrelated amount δ , chosen from a uniform distribution $[-\epsilon, \epsilon]$, PGST will occur instead with an infidelity that scales polynomially in the error, granted the error is of lower order than the actual coupling itself. Up until $N = 4$ qubits, it can be shown that fidelities of $> 99\%$ can still be achieved up to inaccuracies of $\epsilon \approx 0.07$. The most likely scenario is that the stochastic error of the coupling constants is way smaller than the absolute value of the coupling constants itself, showing that PST is robust for the case of small qubit registers. A general trend can then be obtained from extrapolation, showing that for $N \leq 5$, great fidelities (99%+) are still possible for errors up until $\epsilon \approx 0.05$.

It remains an interesting topic of research to construct a rigorous notion of entanglement power in the framework of VQE. Currently, only (numerical) simulations are available to test whether a certain multi-qubit entanglement operation is suitable for speeding up the calculation of a certain problem within VQE. Though such results may be valuable, they are not telling of how the convergence speed will scale with qubit size beyond classically computable regimes, nor is the discussion of a specific problem extendable to all problem. It is expected, namely, that certain entanglers are more tailored for certain problems, and entanglement power should reflect this notion. It is more efficient and useful to know a priori what kind of entanglement operations would provide a significant speed-up in analysing a certain quantum system using VQE.

Lots of serious steps are being made every year to elevate quantum computers to a level where they can outperform classical computers in computational complexity. Though no full quantum error correction exists yet, many efforts have been made that have clearly been demonstrated in experiments to reduce the error propagation inside the quantum simulator below set boundaries. With new theoretical work being published every day, and new high-tech experimental set-ups being constructed, the NISQ era serves as a hopeful step towards a fully fault-tolerant quantum computer in the future.

References

- [1] Gordon E. Moore. Cramming more components onto integrated circuits, reprinted from electronics, volume 38, number 8, april 19, 1965, pp.114 ff. *IEEE Solid-State Circuits Society Newsletter*, 11(3): 33–35, 2006. doi: 10.1109/N-SSC.2006.4785860.
- [2] Richard P Feynman. Simulating physics with computers. *International journal of theoretical physics*, 21(6/7):467–488, 1982.
- [3] Eric Lucero. Unveiling our new quantum ai campus, 2021. URL <https://blog.google/technology/ai/unveiling-our-new-quantum-ai-campus/>.
- [4] Robert Hackett. Ibm plans a huge leap in superfast quantum computing by 2023, 2020. URL <https://fortune.com/2020/09/15/ibm-quantum-computer-1-million-qubits-by-2030/>.
- [5] P.W. Shor. Algorithms for quantum computation: discrete logarithms and factoring. In *Proceedings 35th Annual Symposium on Foundations of Computer Science*, pages 124–134, 1994. doi: 10.1109/SFCS.1994.365700.
- [6] Lov K. Grover. A fast quantum mechanical algorithm for database search. In *Proceedings of the Twenty-Eighth Annual ACM Symposium on Theory of Computing*, STOC '96, page 212–219, New York, NY, USA, 1996. Association for Computing Machinery. ISBN 0897917855. doi: 10.1145/237814.237866. URL <https://doi.org/10.1145/237814.237866>.
- [7] Frank Arute, Kunal Arya, Ryan Babbush, Dave Bacon, Joseph C Bardin, Rami Barends, Rupak Biswas, Sergio Boixo, Fernando GSL Brandao, David A Buell, et al. Quantum supremacy using a programmable superconducting processor. *Nature*, 574(7779):505–510, 2019.
- [8] K Wright, KM Beck, S Debnath, JM Amini, Y Nam, N Grzesiak, J-S Chen, NC Pienti, M Chmielewski, C Collins, et al. Benchmarking an 11-qubit quantum computer. *Nature communications*, 10(1):1–6, 2019.
- [9] Google AI Quantum and Collaborators et al. Hartree-fock on a superconducting qubit quantum computer. *Science*, 369(6507):1084–1089, 2020. ISSN 0036-8075. doi: 10.1126/science.abb9811. URL <https://science.sciencemag.org/content/369/6507/1084>.
- [10] Nicholas Rubin. Scaling up fundamental quantum chemistry simulations on quantum hardware, 2020. URL <https://ai.googleblog.com/2020/08/scaling-up-fundamental-quantum.html>.
- [11] Daniel Gottesman. An introduction to quantum error correction and fault-tolerant quantum computation, 2009.
- [12] John Preskill. Quantum computing in the nisq era and beyond. *Quantum*, 2:79, Aug 2018. ISSN 2521-327X. doi: 10.22331/q-2018-08-06-79. URL <http://dx.doi.org/10.22331/q-2018-08-06-79>.
- [13] Antonio D. Corcoles, Abhinav Kandala, Ali Javadi-Abhari, Douglas T. McClure, Andrew W. Cross, Kristan Temme, Paul D. Nation, Matthias Steffen, and Jay M. Gambetta. Challenges and opportunities of near-term quantum computing systems. *Proceedings of the IEEE*, 108(8):1338–1352, Aug 2020. ISSN 1558-2256. doi: 10.1109/jproc.2019.2954005. URL <http://dx.doi.org/10.1109/JPROC.2019.2954005>.
- [14] Centre for Quantum Technologies. Hartree-Fock on a Superconducting Qubit Quantum Computer, 2020. URL <https://www.youtube.com/watch?v=b5z90cwRprc>.
- [15] Edward Farhi, Jeffrey Goldstone, and Sam Gutmann. A quantum approximate optimization algorithm, 2014.
- [16] Jarrod R McClean, Jonathan Romero, Ryan Babbush, and Alán Aspuru-Guzik. The theory of variational hybrid quantum-classical algorithms. *New Journal of Physics*, 18(2):023023, Feb 2016. ISSN 1367-2630. doi: 10.1088/1367-2630/18/2/023023. URL <http://dx.doi.org/10.1088/1367-2630/18/2/023023>.

- [17] Alberto Peruzzo, Jarrod McClean, Peter Shadbolt, Man-Hong Yung, Xiao-Qi Zhou, Peter J Love, Alán Aspuru-Guzik, and Jeremy L O’Brien. A variational eigenvalue solver on a photonic quantum processor. *Nature communications*, 5(1):1–7, 2014.
- [18] T Helgaker, P Jørgensen, and J Olsen. *Molecular Electronic Structure Theory*. John Wiley & Sons, LTD, Chichester, 2000.
- [19] P. Jordan and E. Wigner. Über das Paulische Äquivalenzverbot. *Zeitschrift für Physik*, 47(9-10): 631–651, September 1928. doi: 10.1007/BF01331938.
- [20] Jacob T. Seeley, Martin J. Richard, and Peter J. Love. The bravyi-kitaev transformation for quantum computation of electronic structure. *The Journal of Chemical Physics*, 137(22):224109, Dec 2012. ISSN 1089-7690. doi: 10.1063/1.4768229. URL <http://dx.doi.org/10.1063/1.4768229>.
- [21] SV Kozyrev and IV Volovich. The arrhenius formula in kinetic theory and witten’s spectral asymptotics. *Journal of Physics A: Mathematical and Theoretical*, 44(21):215202, 2011.
- [22] A. Kandala, A. Mezzacapo, K. Temme, M. Takita, M. Brink, J.M. Chow, J.M. Gambetta. Hardware-efficient variational quantum eigensolver for small molecules and quantum magnets. *Nature*, 549: 242–246, 2017. doi: <https://doi.org/10.1103/PhysRevX.8.011021>.
- [23] Parmeet Bhatia. On optimization of deep neural networks, 2020. URL <https://towardsdatascience.com/on-optimization-of-deep-neural-networks-21de9e83e1>.
- [24] J.J. Postema. The quantum computation of unitary time evolution on a $3 \otimes \bar{3} \otimes 3 \otimes \bar{3}$ ^{87}Sr spin chain. University of Amsterdam Eindhoven University of Technology, June 2020.
- [25] M. Morgado and S. Whitlock. Quantum simulation and computing with rydberg-interacting qubits. *AVS Quantum Science*, 3(2):023501, Jun 2021. ISSN 2639-0213. doi: 10.1116/5.0036562. URL <http://dx.doi.org/10.1116/5.0036562>.
- [26] R. Barends, J. Kelly, A. Megrant, A. Veitia, D. Sank, E. Jeffrey, T. C. White, J. Mutus, A. G. Fowler, B. Campbell, and et al. Superconducting quantum circuits at the surface code threshold for fault tolerance. *Nature*, 508(7497):500–503, Apr 2014. ISSN 1476-4687. doi: 10.1038/nature13171. URL <http://dx.doi.org/10.1038/nature13171>.
- [27] C.J. Ballance, T.P. Harty, N.M. Linke, M.A. Sepiol, and D.M. Lucas. High-fidelity quantum logic gates using trapped-ion hyperfine qubits. *Physical Review Letters*, 117(6), Aug 2016. ISSN 1079-7114. doi: 10.1103/physrevlett.117.060504. URL <http://dx.doi.org/10.1103/PhysRevLett.117.060504>.
- [28] Ivaylo S. Madjarov, Jacob P. Covey, Adam L. Shaw, Joonhee Choi, Anant Kale, Alexandre Cooper, Hannes Pichler, Vladimir Schkolnik, Jason R. Williams, and Manuel Endres. High-fidelity entanglement and detection of alkaline-earth rydberg atoms. *Nature Physics*, 16(8):857–861, May 2020. ISSN 1745-2481. doi: 10.1038/s41567-020-0903-z. URL <http://dx.doi.org/10.1038/s41567-020-0903-z>.
- [29] Cheng Sheng, Xiaodong He, Peng Xu, Ruijun Guo, Kumpeng Wang, Zongyuan Xiong, Min Liu, Jin Wang, and Mingsheng Zhan. High-fidelity single-qubit gates on neutral atoms in a two-dimensional magic-intensity optical dipole trap array. *Phys. Rev. Lett.*, 121:240501, Dec 2018. doi: 10.1103/PhysRevLett.121.240501. URL <https://link.aps.org/doi/10.1103/PhysRevLett.121.240501>.
- [30] T.M. Graham, M. Kwon, B. Grinkemeyer, Z. Marra, X. Jiang, M.T. Lichtman, Y. Sun, M. Ebert, and M. Saffman. Rydberg-mediated entanglement in a two-dimensional neutral atom qubit array. *Physical Review Letters*, 123(23), Dec 2019. ISSN 1079-7114. doi: 10.1103/physrevlett.123.230501. URL <http://dx.doi.org/10.1103/PhysRevLett.123.230501>.
- [31] Matthias Christandl, Nilanjana Datta, Tony C. Dorlas, Artur Ekert, Alastair Kay, and Andrew J. Landahl. Perfect transfer of arbitrary states in quantum spin networks. , 71(3):032312, March 2005. doi: 10.1103/PhysRevA.71.032312.

- [32] Alastair Kay. Perfect, efficient, state transfer and its application as a constructive tool. *International Journal of Quantum Information*, 08(04):641–676, Jun 2010. ISSN 1793-6918. doi: 10.1142/S0219749910006514. URL <http://dx.doi.org/10.1142/S0219749910006514>.
- [33] Richard Jozsa and Noah Linden. On the role of entanglement in quantum-computational speed-up. *Proceedings of the Royal Society of London. Series A: Mathematical, Physical and Engineering Sciences*, 459(2036):2011–2032, Aug 2003. ISSN 1471-2946. doi: 10.1098/rspa.2002.1097. URL <http://dx.doi.org/10.1098/rspa.2002.1097>.
- [34] R. J. P. T. de Keijzer, V. E. Colussi, B. Škorić, and S. J. J. M. F. Kokkelmans. Optimization of the variational quantum eigensolver for quantum chemistry applications, 2021.
- [35] D. R. Hartree. The wave mechanics of an atom with a non-coulomb central field. part ii. some results and discussion. *Mathematical Proceedings of the Cambridge Philosophical Society*, 24(1): 111–132, 1928. doi: 10.1017/S0305004100011920.
- [36] J. C. Slater. The Self Consistent Field and the Structure of Atoms. *Physical Review*, 32(3):339–348, September 1928. doi: 10.1103/PhysRev.32.339.
- [37] J. C. Slater. The Self Consistent Field and the Structure of Atoms. *Physical Review*, 32(3):339–348, September 1928. doi: 10.1103/PhysRev.32.339.
- [38] M. Born and R. Oppenheimer. Zur quantentheorie der molekeln. *Annalen der Physik*, 389(20): 457–484, 1927. ISSN 1521-3889. doi: 10.1002/andp.19273892002. URL <http://dx.doi.org/10.1002/andp.19273892002>. PDF of an english translation by S.M. Blinder is available.
- [39] R. Stewart. Small gaussian expansions of slater-type orbitals. *Journal of Chemical Physics*, 52: 431–438, 1970.
- [40] W. J. Hehre, R. F. Stewart, and J. A. Pople. Self-consistent molecular-orbital methods. i. use of gaussian expansions of slater-type atomic orbitals. *The Journal of Chemical Physics*, 51(6): 2657–2664, 1969. doi: 10.1063/1.1672392. URL <https://doi.org/10.1063/1.1672392>.
- [41] D.J. Thouless. Stability conditions and nuclear rotations in the Hartree-Fock theory. *Nuclear Physics*, 21:225–232, 1960. ISSN 0029-5582. doi: [https://doi.org/10.1016/0029-5582\(60\)90048-1](https://doi.org/10.1016/0029-5582(60)90048-1). URL <https://www.sciencedirect.com/science/article/pii/0029558260900481>.
- [42] Ian D Kivlichan, Jarrod McClean, Nathan Wiebe, Craig Gidney, Alán Aspuru-Guzik, Garnet Kin-Lic Chan, and Ryan Babbush. Quantum simulation of electronic structure with linear depth and connectivity. *Physical review letters*, 120(11):110501, 2018.
- [43] Attila Szabo and Neil S Ostlund. *Modern quantum chemistry: introduction to advanced electronic structure theory*. Courier Corporation, 2012.
- [44] Feiwu Chen. Wick’s theorem and reconstruction schemes for reduced density matrices. *Science in China Series B: Chemistry*, 49:402–406, 01 2006. doi: 10.1007/s11426-006-0402-9.
- [45] Werner Kutzelnigg. Generalized k-particle brillouin conditions and their use for the construction of correlated electronic wavefunctions. *Chemical Physics Letters*, 64(2):383–387, 1979.
- [46] Qiming Sun. Co-iterative augmented hessian method for orbital optimization, 2017.
- [47] Josephso Raphson. Analysis aequationum universalis seu ad aequationes algebraicas resolvendas methodus generalis, expedita, ex nova infinitarum serierum methodo, deducta ac demonstrata : cui annexum est de spatio reali, seu ente infinito conamen mathematico-metaphysicum. URL <https://www.e-rara.ch/zut/doi/10.3931/e-rara-13516>.
- [48] Nicholas C Rubin, Ryan Babbush, and Jarrod McClean. Application of fermionic marginal constraints to hybrid quantum algorithms. *New Journal of Physics*, 20(5):053020, May 2018. ISSN 1367-2630. doi: 10.1088/1367-2630/aab919. URL <http://dx.doi.org/10.1088/1367-2630/aab919>.

- [49] Maria Serna, Ronen Shaltiel, Klaus Jansen, and José Rolim. Approximation, randomization, and combinatorial optimization. algorithms and techniques. *Lecture Notes in Computer Science*, 01 2009.
- [50] Afrad Basheer, A. Afham, and Sandeep K. Goyal. Quantum k -nearest neighbors algorithm. *arXiv e-prints*, art. arXiv:2003.09187, March 2020.
- [51] Kerstin Beer, Dmytro Bondarenko, Terry Farrelly, Tobias J Osborne, Robert Salzmänn, Daniel Scheiermann, and Ramona Wolf. Training deep quantum neural networks. *Nature communications*, 11(1):1–6, 2020.
- [52] Michael Broughton, Guillaume Verdon, Trevor McCourt, Antonio J. Martinez, Jae Hyeon Yoo, Sergei V. Isakov, Philip Massey, Murphy Yuezhen Niu, Ramin Halavati, Evan Peters, Martin Leib, Andrea Skolik, Michael Streif, David Von Dollen, Jarrod R. McClean, Sergio Boixo, Dave Bacon, Alan K. Ho, Hartmut Neven, and Masoud Mohseni. Tensorflow quantum: A software framework for quantum machine learning, 2020. URL <https://arxiv.org/pdf/2003.02989.pdf>.
- [53] Facundo Bre, Juan Gimenez, and Víctor Fachinotti. Prediction of wind pressure coefficients on building surfaces using artificial neural networks. *Energy and Buildings*, 158, 11 2017. doi: 10.1016/j.enbuild.2017.11.045.
- [54] David Silver, Thomas Hubert, Julian Schrittwieser, Ioannis Antonoglou, Matthew Lai, Arthur Guez, Marc Lanctot, Laurent Sifre, Dharmashan Kumaran, Thore Graepel, Timothy Lillicrap, Karen Simonyan, and Demis Hassabis. A general reinforcement learning algorithm that masters chess, shogi, and go through self-play. *Science*, 362(6419):1140–1144, 2018. ISSN 0036-8075. doi: 10.1126/science.aar6404. URL <https://science.sciencemag.org/content/362/6419/1140>.
- [55] Sascha Caron, Jong Soo Kim, Krzysztof Rolbiecki, Roberto Ruiz de Austri, and Bob Stienen. The bsm-ai project: Susy-ai-generalizing lhc limits on supersymmetry with machine learning. *The European Physical Journal C*, 77(4), 2017. ISSN 1434-6052. doi: 10.1140/epjc/s10052-017-4814-9. URL <http://dx.doi.org/10.1140/epjc/s10052-017-4814-9>.
- [56] Earl T. Campbell, Barbara M. Terhal, and Christophe Vuillot. Roads towards fault-tolerant universal quantum computation. *Nature*, 549(7671):172–179, Sep 2017. ISSN 1476-4687. doi: 10.1038/nature23460. URL <http://dx.doi.org/10.1038/nature23460>.
- [57] Richard Jozsa. Fidelity for mixed quantum states. *Journal of modern optics*, 41(12):2315–2323, 1994.
- [58] M. Gluza, M. Kliesch, J. Eisert, and L. Aolita. Fidelity witnesses for fermionic quantum simulations. *Phys. Rev. Lett.*, 120:190501, May 2018. doi: 10.1103/PhysRevLett.120.190501. URL <https://link.aps.org/doi/10.1103/PhysRevLett.120.190501>.
- [59] Luke Schaeffer Daniel Grier. The classification of clifford gates over qubits, 2018. URL https://qutech.nl/wp-content/uploads/2018/02/t7-Luke-Schaeffer-tuesday_schaeffer.pdf.
- [60] Abhinav Kandala, Kristan Temme, Antonio D. Córcoles, Antonio Mezzacapo, Jerry M. Chow, and Jay M. Gambetta. Error mitigation extends the computational reach of a noisy quantum processor. *Nature*, 567(7749):491–495, Mar 2019. ISSN 1476-4687. doi: 10.1038/s41586-019-1040-7. URL <http://dx.doi.org/10.1038/s41586-019-1040-7>.
- [61] Michael E. Peskin and Daniel V. Schroeder. *An Introduction to quantum field theory*. Addison-Wesley, Reading, USA, 1995. ISBN 978-0-201-50397-5.
- [62] William K. Wootters. Entanglement of formation of an arbitrary state of two qubits. *Physical Review Letters*, 80(10):2245–2248, Mar 1998. ISSN 1079-7114. doi: 10.1103/physrevlett.80.2245. URL <http://dx.doi.org/10.1103/PhysRevLett.80.2245>.
- [63] Andreas J. C. Woitzik, Panagiotis Kl. Barkoutsos, Filip Wudarski, Andreas Buchleitner, and Ivano Tavernelli. Entanglement production and convergence properties of the variational quantum eigensolver. *Physical Review A*, 102(4), Oct 2020. ISSN 2469-9934. doi: 10.1103/physreva.102.042402. URL <http://dx.doi.org/10.1103/PhysRevA.102.042402>.

- [64] Alexander Wong and Nelson Christensen. Potential multiparticle entanglement measure. *Physical Review A*, 63(4), Mar 2001. ISSN 1094-1622. doi: 10.1103/physreva.63.044301. URL <http://dx.doi.org/10.1103/PhysRevA.63.044301>.
- [65] Simon J Devitt, William J Munro, and Kae Nemoto. Quantum error correction for beginners. *Reports on Progress in Physics*, 76(7):076001, Jun 2013. ISSN 1361-6633. doi: 10.1088/0034-4885/76/7/076001. URL <http://dx.doi.org/10.1088/0034-4885/76/7/076001>.
- [66] Govind Chavhan, Paul Babyn, Bejoy Thomas, Manohar Shroff, and Mark Haacke. Principles, techniques, and applications of t2*-based mr imaging and its special applications. *Radiographics : a review publication of the Radiological Society of North America, Inc*, 29:1433–49, 09 2009. doi: 10.1148/rg.295095034.
- [67] J.M.A. Peters. Variational quantum eigensolver, the effects of decoherence on quantum chemistry problems. Master’s thesis, Eindhoven University of Technology, 2020.
- [68] A. Kandala, A. Mezzacapo, K. Temme, M. Takita, M. Brink, J.M. Chow, J.M. Gambetta. Supplementary material for ‘Hardware-efficient variational quantum eigensolver for small molecules and quantum magnets’. *Nature*, 549, 2017. doi: <https://doi.org/10.1103/PhysRevX.8.011021>.
- [69] Harold J Metcalf and Peter Van der Straten. Laser cooling and trapping of neutral atoms. *The Optics Encyclopedia: Basic Foundations and Practical Applications*, 2007.
- [70] Carlos Alexandre Brasil, Felipe Fernandes Fanchini, and Reginaldo de Jesus Napolitano. A simple derivation of the Lindblad equation. *arXiv e-prints*, art. arXiv:1110.2122, October 2011.
- [71] Edwin T Jaynes and Frederick W Cummings. Comparison of quantum and semiclassical radiation theories with application to the beam maser. *Proceedings of the IEEE*, 51(1):89–109, 1963.
- [72] Daniel Manzano. A short introduction to the lindblad master equation. *AIP Advances*, 10(2): 025106, Feb 2020. ISSN 2158-3226. doi: 10.1063/1.5115323. URL <http://dx.doi.org/10.1063/1.5115323>.
- [73] William K Wootters and Wojciech H Zurek. A single quantum cannot be cloned. *Nature*, 299(5886): 802–803, 1982.
- [74] DGBJ Dieks. Communication by epr devices. *Physics Letters A*, 92(6):271–272, 1982.
- [75] Xiaojie Wu, Zhi-Hao Cui, Yu Tong, Michael Lindsey, Garnet Kin-Lic Chan, and Lin Lin. Projected density matrix embedding theory with applications to the two-dimensional hubbard model. *The Journal of Chemical Physics*, 151(6):064108, Aug 2019. ISSN 1089-7690. doi: 10.1063/1.5108818. URL <http://dx.doi.org/10.1063/1.5108818>.
- [76] R. McWeeny. Some recent advances in density matrix theory. *Rev. Mod. Phys.*, 32:335–369, Apr 1960. doi: 10.1103/RevModPhys.32.335. URL <https://link.aps.org/doi/10.1103/RevModPhys.32.335>.
- [77] ‘rmlarose’ from the Google AI team. quantumlib/recirq/recirq/hfvqe, 2020. URL <https://github.com/quantumlib/ReCirq/tree/master/recirq/hfvqe>.
- [78] Alexander J. McCaskey, Zachary P. Parks, Jacek Jakowski, Shirley V. Moore, Titus D. Morris, Travis S. Humble, and Raphael C. Pooser. Quantum chemistry as a benchmark for near-term quantum computers. *npj Quantum Information*, 5(1):99, Nov 2019. ISSN 2056-6387. doi: 10.1038/s41534-019-0209-0. URL <https://doi.org/10.1038/s41534-019-0209-0>.
- [79] L. F. Richardson. The Approximate Arithmetical Solution by Finite Differences of Physical Problems Involving Differential Equations, with an Application to the Stresses in a Masonry Dam. *Philosophical Transactions of the Royal Society of London Series A*, 210:307–357, January 1911. doi: 10.1098/rsta.1911.0009.
- [80] Lewis F. Richardson and J. Arthur Gaunt. The Deferred Approach to the Limit. Part I. Single Lattice. Part II. Interpenetrating Lattices. *Philosophical Transactions of the Royal Society of London Series A*, 226:299–361, January 1927. doi: 10.1098/rsta.1927.0008.

- [81] Kristan Temme, Sergey Bravyi, and Jay M. Gambetta. Error mitigation for short-depth quantum circuits. *Physical Review Letters*, 119(18), Nov 2017. ISSN 1079-7114. doi: 10.1103/physrevlett.119.180509. URL <http://dx.doi.org/10.1103/PhysRevLett.119.180509>.
- [82] L. F. Richardson. The Approximate Arithmetical Solution by Finite Differences of Physical Problems Involving Differential Equations, with an Application to the Stresses in a Masonry Dam. *Philosophical Transactions of the Royal Society of London Series A*, 210:307–357, January 1911. doi: 10.1098/rsta.1911.0009.
- [83] R.M.W. Bijnen, van. *Quantum engineering with ultracold atoms*. PhD thesis, Applied Physics, 2013.
- [84] Xiaoling Wu, Xinhui Liang, Yaoqi Tian, Fan Yang, Cheng Chen, Yong-Chun Liu, Meng Khoon Tey, and Li You. A concise review of rydberg atom based quantum computation and quantum simulation*. *Chinese Physics B*, 30(2):020305, Feb 2021. ISSN 1674-1056. doi: 10.1088/1674-1056/abd76f. URL <http://dx.doi.org/10.1088/1674-1056/abd76f>.
- [85] M. Saffman, T. G. Walker, and K. Mølmer. Quantum information with rydberg atoms. *Rev. Mod. Phys.*, 82:2313–2363, Aug 2010. doi: 10.1103/RevModPhys.82.2313. URL <https://link.aps.org/doi/10.1103/RevModPhys.82.2313>.
- [86] Robert Löw, Hendrik Weimer, Johannes Nipper, Jonathan B Balewski, Björn Butscher, Hans Peter Büchler, and Tilman Pfau. An experimental and theoretical guide to strongly interacting rydberg gases. *Journal of Physics B: Atomic, Molecular and Optical Physics*, 45(11):113001, May 2012. ISSN 1361-6455. doi: 10.1088/0953-4075/45/11/113001. URL <http://dx.doi.org/10.1088/0953-4075/45/11/113001>.
- [87] J. Mitroy and I. A. Ivallov. Quantum defect theory for the study of hadronic atoms. *J. Phys. G*, 27:1421–1433, 2001. doi: 10.1088/0954-3899/27/7/304.
- [88] Thijs van Putten, Ben van Linden van den Heuvell, and Richard Newell. Lifetime of rubidium rydberg atoms in a magneto-optical trap. *Bachelor thesis (Amsterdam, 2009)*.
- [89] Sebastian Weber, Christoph Tresp, Henri Menke, Alban Urvoy, Ofer Firstenberg, Hans Peter Büchler, and Sebastian Hofferberth. Calculation of rydberg interaction potentials. *Journal of Physics B: Atomic, Molecular and Optical Physics*, 50(13):133001, Jun 2017. ISSN 1361-6455. doi: 10.1088/1361-6455/aa743a. URL <http://dx.doi.org/10.1088/1361-6455/aa743a>.
- [90] E. P. Wigner. *On the Matrices Which Reduce the Kronecker Products of Representations of S. R. Groups*, pages 608–654. Springer Berlin Heidelberg, Berlin, Heidelberg, 1993. ISBN 978-3-662-02781-3. doi: 10.1007/978-3-662-02781-3_42. URL https://doi.org/10.1007/978-3-662-02781-3_42.
- [91] Keith Bonin and Thomas McIlrath. Two-photon electric-dipole selection rules. *Journal of The Optical Society of America*, 1, 03 1984. doi: 10.1364/JOSAB.1.000052.
- [92] E Brion, L H Pedersen, and K Mølmer. Adiabatic elimination in a lambda system. *Journal of Physics A: Mathematical and Theoretical*, 40(5):1033–1043, jan 2007. doi: 10.1088/1751-8113/40/5/011. URL <https://doi.org/10.1088/1751-8113/40/5/011>.
- [93] Rolf Heidemann, Ulrich Raitzsch, Vera Bendkowsky, Björn Butscher, Robert Löw, and Tilman Pfau. Rydberg excitation of bose-einstein condensates. *Phys. Rev. Lett.*, 100:033601, Jan 2008. doi: 10.1103/PhysRevLett.100.033601. URL <https://link.aps.org/doi/10.1103/PhysRevLett.100.033601>.
- [94] David J Griffiths. *Introduction to electrodynamics; 4th ed.* Pearson, Boston, MA, 2013. doi: 1108420419. URL <https://cds.cern.ch/record/1492149>. Re-published by Cambridge University Press in 2017.
- [95] J. Susanne Otto, Niels Kjærgaard, and Amita B. Deb. Strong zero-field förster resonances in k-rb rydberg systems. *Phys. Rev. Research*, 2:033474, Sep 2020. doi: 10.1103/PhysRevResearch.2.033474. URL <https://link.aps.org/doi/10.1103/PhysRevResearch.2.033474>.

- [96] Antoine Browaeys and Thierry Lahaye. Many-body physics with individually controlled rydberg atoms. *Nature Physics*, 16(2):132–142, Jan 2020. ISSN 1745-2481. doi: 10.1038/s41567-019-0733-z. URL <http://dx.doi.org/10.1038/s41567-019-0733-z>.
- [97] Alpha Gaëtan, Yevhen Miroshnychenko, Tatjana Wilk, Amodsen Chotia, Matthieu Viteau, Daniel Comparat, Pierre Pillet, Antoine Browaeys, and Philippe Grangier. Observation of collective excitation of two individual atoms in the rydberg blockade regime. *Nature Physics*, 5(2):115–118, Jan 2009. ISSN 1745-2481. doi: 10.1038/nphys1183. URL <http://dx.doi.org/10.1038/nphys1183>.
- [98] Yong Zeng, Peng Xu, Xiaodong He, Yangyang Liu, Min Liu, Jin Wang, D.J. Papoular, G.V. Shlyapnikov, and Mingsheng Zhan. Entangling two individual atoms of different isotopes via rydberg blockade. *Physical Review Letters*, 119(16), Oct 2017. ISSN 1079-7114. doi: 10.1103/PhysRevLett.119.160502. URL <http://dx.doi.org/10.1103/PhysRevLett.119.160502>.
- [99] Y. O. Dudin, L. Li, F. Bariani, and A. Kuzmich. Observation of coherent many-body rabi oscillations. *Nature Physics*, 8(11):790–794, Sep 2012. ISSN 1745-2481. doi: 10.1038/nphys2413. URL <http://dx.doi.org/10.1038/nphys2413>.
- [100] Rolf Heidemann, Ulrich Raitzsch, Vera Bendkowsky, Björn Butscher, Robert Löw, Luis Santos, and Tilman Pfau. Evidence for coherent collective rydberg excitation in the strong blockade regime. *Physical Review Letters*, 99(16), Oct 2007. ISSN 1079-7114. doi: 10.1103/PhysRevLett.99.163601. URL <http://dx.doi.org/10.1103/PhysRevLett.99.163601>.
- [101] I. I. Ryabtsev, D. B. Tretyakov, I. I. Beterov, and V. M. Entin. Observation of the stark-tuned forster resonance between two rydberg atoms. *Phys. Rev. Lett.*, 104:073003, Feb 2010. doi: 10.1103/PhysRevLett.104.073003. URL <https://link.aps.org/doi/10.1103/PhysRevLett.104.073003>.
- [102] In Ivan Djordjevic, editor, *Quantum Information Processing and Quantum Error Correction*, page iii. Academic Press, Oxford, 2012. ISBN 978-0-12-385491-9. doi: <https://doi.org/10.1016/B978-0-12-385491-9.01001-7>. URL <https://www.sciencedirect.com/science/article/pii/B9780123854919010017>.
- [103] Rúben Sousa and Yasser Omar. Pretty good state transfer of entangled states through quantum spin chains. *New Journal of Physics*, 16(12):123003, Dec 2014. ISSN 1367-2630. doi: 10.1088/1367-2630/16/12/123003. URL <http://dx.doi.org/10.1088/1367-2630/16/12/123003>.
- [104] Sougato Bose. Quantum communication through an unmodulated spin chain. *Phys. Rev. Lett.*, 91:207901, Nov 2003. doi: 10.1103/PhysRevLett.91.207901. URL <https://link.aps.org/doi/10.1103/PhysRevLett.91.207901>.
- [105] Matthias Christandl, Nilanjana Datta, Artur Ekert, and Andrew J. Landahl. Perfect state transfer in quantum spin networks. *Phys. Rev. Lett.*, 92:187902, May 2004. doi: 10.1103/PhysRevLett.92.187902. URL <https://link.aps.org/doi/10.1103/PhysRevLett.92.187902>.
- [106] Georgios M Nikolopoulos, David Petrosyan, and P Lambropoulos. Electron wavepacket propagation in a chain of coupled quantum dots. *Journal of Physics: Condensed Matter*, 16(28):4991–5002, Jul 2004. ISSN 1361-648X. doi: 10.1088/0953-8984/16/28/019. URL <http://dx.doi.org/10.1088/0953-8984/16/28/019>.
- [107] Tobias J. Osborne. Statics and dynamics of quantum XY and heisenberg systems on graphs. *Physical Review B*, 74(9), Sep 2006. ISSN 1550-235X. doi: 10.1103/PhysRevB.74.094411. URL <http://dx.doi.org/10.1103/PhysRevB.74.094411>.
- [108] C. Di Franco, M. Paternostro, and M. S. Kim. Perfect state transfer on a spin chain without state initialization. *Physical Review Letters*, 101(23), Dec 2008. ISSN 1079-7114. doi: 10.1103/PhysRevLett.101.230502. URL <http://dx.doi.org/10.1103/PhysRevLett.101.230502>.
- [109] C. Di Franco, M. Paternostro, D. I. Tsomokos, and S. F. Huelga. Control-limited perfect state transfer, quantum stochastic resonance, and many-body entangling gate in imperfect qubit registers. *Physical Review A*, 77(6), Jun 2008. ISSN 1094-1622. doi: 10.1103/PhysRevA.77.062337. URL <http://dx.doi.org/10.1103/PhysRevA.77.062337>.

- [110] Sonia L'Innocente, Cosmo Lupo, and Stefano Mancini. Quantum state transfer in aq-deformed chain. *Journal of Physics A: Mathematical and Theoretical*, 42(47):475305, nov 2009. doi: 10.1088/1751-8113/42/47/475305. URL <https://doi.org/10.1088/1751-8113/42/47/475305>.
- [111] Koen Groenland and Kareljan Schoutens. Many-body strategies for multiqubit gates: Quantum control through krawtchouk-chain dynamics. *Phys. Rev. A*, 97:042321, Apr 2018. doi: 10.1103/PhysRevA.97.042321. URL <https://link.aps.org/doi/10.1103/PhysRevA.97.042321>.
- [112] Nicolas Crampé, Rafael I Nepomechie, and Luc Vinet. Free-fermion entanglement and orthogonal polynomials. *Journal of Statistical Mechanics: Theory and Experiment*, 2019(9):093101, Sep 2019. ISSN 1742-5468. doi: 10.1088/1742-5468/ab3787. URL <http://dx.doi.org/10.1088/1742-5468/ab3787>.
- [113] Algebraic Pavel. General form for powers of tridiagonal matrices, 2015. URL <https://math.stackexchange.com/questions/1561724/general-form-for-powers-of-tridiagonal-matrices>.
- [114] Graham M. L. Gladwell. Inverse Problems in Vibration. *Applied Mechanics Reviews*, 39(7):1013–1018, 07 1986. ISSN 0003-6900. doi: 10.1115/1.3149517. URL <https://doi.org/10.1115/1.3149517>.
- [115] Graham M. L. Gladwell. *Matrix Inverse Eigenvalue Problems*, pages 1–28. Springer Vienna, Vienna, 2011. ISBN 978-3-7091-0696-9. doi: 10.1007/978-3-7091-0696-9_1. URL https://doi.org/10.1007/978-3-7091-0696-9_1.
- [116] Man-Hong Yung. Quantum speed limit for perfect state transfer in one dimension. *Phys. Rev. A*, 74:030303, Sep 2006. doi: 10.1103/PhysRevA.74.030303. URL <https://link.aps.org/doi/10.1103/PhysRevA.74.030303>.
- [117] Peter Karbach and Joachim Stolze. Spin chains as perfect quantum state mirrors. *Physical Review A*, 72(3), Sep 2005. ISSN 1094-1622. doi: 10.1103/physreva.72.030301. URL <http://dx.doi.org/10.1103/PhysRevA.72.030301>.
- [118] L.M.J. Florack. 2f800: Tensor calculus and differential geometry. URL <https://www.win.tue.nl/~lflorack/Extensions/2WAH0+2F800.html>.
- [119] V. Kendon and C. Tamon. Perfect state transfer in quantum walks on graphs. *Journal of Computational and Theoretical Nanoscience*, 8:422–433, 2011.
- [120] Siddhant Singh, Bibhas Adhikari, Supriyo Dutta, and David Zueco. Perfect state transfer on hypercubes and its implementation using superconducting qubits. *Physical Review A*, 102(6), Dec 2020. ISSN 2469-9934. doi: 10.1103/physreva.102.062609. URL <http://dx.doi.org/10.1103/PhysRevA.102.062609>.
- [121] W Fulton and J Harris. Representation theory, a first course springer-verlag. *New York*, 1991.
- [122] Claudio Albanese, Matthias Christandl, Nilanjana Datta, and Artur Ekert. Mirror inversion of quantum states in linear registers. *Physical Review Letters*, 93(23), Nov 2004. ISSN 1079-7114. doi: 10.1103/physrevlett.93.230502. URL <http://dx.doi.org/10.1103/PhysRevLett.93.230502>.
- [123] S R Clark, C Moura Alves, and D Jaksch. Efficient generation of graph states for quantum computation. *New Journal of Physics*, 7:124–124, May 2005. ISSN 1367-2630. doi: 10.1088/1367-2630/7/1/124. URL <http://dx.doi.org/10.1088/1367-2630/7/1/124>.
- [124] Alastair Kay. Perfect state transfer: Beyond nearest-neighbor couplings. *Phys. Rev. A*, 73:032306, Mar 2006. doi: 10.1103/PhysRevA.73.032306. URL <https://link.aps.org/doi/10.1103/PhysRevA.73.032306>.
- [125] AC Downing Jr and Alston S Householder. Some inverse characteristic value problems. *Journal of the ACM (JACM)*, 3(3):203–207, 1956.
- [126] Daniel Burgarth and Sougato Bose. Universal destabilization and slowing of spin-transfer functions by a bath of spins. *Phys. Rev. A*, 73:062321, Jun 2006. doi: 10.1103/PhysRevA.73.062321. URL <https://link.aps.org/doi/10.1103/PhysRevA.73.062321>.

- [127] Alastair Kay and Marie Ericsson. Geometric effects and computation in spin networks. *New Journal of Physics*, 7:143–143, jun 2005. doi: 10.1088/1367-2630/7/1/143. URL <https://doi.org/10.1088/1367-2630/7/1/143>.
- [128] Heinz-Peter Breuer and Francesco Petruccione. *The Theory of Open Quantum Systems*. 01 2006. ISBN 9780199213900. doi: 10.1093/acprof:oso/9780199213900.001.0001.
- [129] Daniel Barredo, Henning Labuhn, Sylvain Ravets, Thierry Lahaye, Antoine Browaeys, and Charles S. Adams. Coherent excitation transfer in a spin chain of three rydberg atoms. *Phys. Rev. Lett.*, 114: 113002, Mar 2015. doi: 10.1103/PhysRevLett.114.113002. URL <https://link.aps.org/doi/10.1103/PhysRevLett.114.113002>.
- [130] J. Johnson and Steven Rolston. Interactions between rydberg-dressed atoms. *Physical Review A*, 82, 06 2010. doi: 10.1103/PHYSREVA.82.033412.
- [131] N. Henkel, R. Nath, and T. Pohl. Three-Dimensional Roton Excitations and Supersolid Formation in Rydberg-Excited Bose-Einstein Condensates. , 104(19):195302, May 2010. doi: 10.1103/PhysRevLett.104.195302.
- [132] Jens Honer, Hendrik Weimer, Tilman Pfau, and Hans Peter Büchler. Collective many-body interaction in rydberg dressed atoms. *Physical Review Letters*, 105(16), Oct 2010. ISSN 1079-7114. doi: 10.1103/physrevlett.105.160404. URL <http://dx.doi.org/10.1103/PhysRevLett.105.160404>.
- [133] S Wüster, C Ates, A Eisfeld, and J M Rost. Excitation transport through rydberg dressing. *New Journal of Physics*, 13(7):073044, Jul 2011. ISSN 1367-2630. doi: 10.1088/1367-2630/13/7/073044. URL <http://dx.doi.org/10.1088/1367-2630/13/7/073044>.
- [134] M Genkin, S Wüster, S Möbius, A Eisfeld, and J M Rost. Dipole-dipole induced global motion of rydberg-dressed atom clouds. *Journal of Physics B: Atomic, Molecular and Optical Physics*, 47(9):095003, Apr 2014. ISSN 1361-6455. doi: 10.1088/0953-4075/47/9/095003. URL <http://dx.doi.org/10.1088/0953-4075/47/9/095003>.
- [135] J. H. Van Vleck. On σ -type doubling and electron spin in the spectra of diatomic molecules. *Phys. Rev.*, 33:467–506, Apr 1929. doi: 10.1103/PhysRev.33.467. URL <https://link.aps.org/doi/10.1103/PhysRev.33.467>.
- [136] Isaiah Shavitt and Lynn T. Redmon. Quasidegenerate perturbation theories. a canonical van vleck formalism and its relationship to other approaches. *The Journal of Chemical Physics*, 73(11): 5711–5717, 1980. doi: 10.1063/1.440050. URL <https://doi.org/10.1063/1.440050>.
- [137] Fan Yang, Shuo Yang, and Li You. Quantum transport of rydberg excitons with synthetic spin-exchange interactions. *Physical Review Letters*, 123(6), Aug 2019. ISSN 1079-7114. doi: 10.1103/physrevlett.123.063001. URL <http://dx.doi.org/10.1103/PhysRevLett.123.063001>.
- [138] Harry Levine, Alexander Keesling, Ahmed Omran, Hannes Bernien, Sylvain Schwartz, Alexander S. Zibrov, Manuel Endres, Markus Greiner, Vladan Vuletić, and Mikhail D. Lukin. High-fidelity control and entanglement of rydberg-atom qubits. *Physical Review Letters*, 121(12), Sep 2018. ISSN 1079-7114. doi: 10.1103/physrevlett.121.123603. URL <http://dx.doi.org/10.1103/PhysRevLett.121.123603>.
- [139] Alexander W. Glaetzle, Marcello Dalmonte, Rejish Nath, Christian Gross, Immanuel Bloch, and Peter Zoller. Designing frustrated quantum magnets with laser-dressed rydberg atoms. *Physical Review Letters*, 114(17), Apr 2015. ISSN 1079-7114. doi: 10.1103/physrevlett.114.173002. URL <http://dx.doi.org/10.1103/PhysRevLett.114.173002>.
- [140] R. M. W. van Bijnen and T. Pohl. Quantum magnetism and topological ordering via rydberg dressing near förster resonances. *Phys. Rev. Lett.*, 114:243002, Jun 2015. doi: 10.1103/PhysRevLett.114.243002. URL <https://link.aps.org/doi/10.1103/PhysRevLett.114.243002>.
- [141] jasperjpostema@gmail.com Postema, J.J.

Appendix A: Addition of angular momentum

The quantum mechanical representation of the angular momentum pseudovector is given by

$$\hat{\mathbf{L}} = -i\hbar(\mathbf{r} \times \nabla), \quad (\text{A.1})$$

where \mathbf{r} is the position vector. The square of the angular momentum is equal to

$$\hat{\mathbf{L}}^2 = -\hbar^2 \left(r^2 \nabla^2 - (\mathbf{r} \cdot \nabla)(\nabla \cdot \mathbf{r}) \right). \quad (\text{A.2})$$

Then, the Laplacian is equal to

$$\nabla^2 = \frac{1}{r^2} \frac{\partial}{\partial r} \left(r^2 \frac{\partial}{\partial r} \right) - \frac{\hat{\mathbf{L}}^2}{\hbar^2 r^2}, \quad (\text{A.3})$$

where the latter term will now represent the centrifugal barrier in the Schrödinger equation. $\hat{\mathbf{L}}$ can be decomposed into its Cartesian components

$$\hat{\mathbf{L}} = \begin{pmatrix} \hat{L}_x \\ \hat{L}_y \\ \hat{L}_z \end{pmatrix}, \quad (\text{A.4})$$

all of which satisfy, for $\{\alpha, \beta, \gamma\} \in \{x, y, z\}$, the commutation relationships

$$[\hat{L}_\alpha, \hat{L}_\beta] = i\hbar \epsilon_{\alpha\beta\gamma} \hat{L}_\gamma \quad (\text{A.5})$$

and

$$[\hat{\mathbf{L}}^2, \hat{L}_\alpha] = 0. \quad (\text{A.6})$$

This implies that a common set of eigenstates of the operators $\hat{\mathbf{L}}^2$ and \hat{L}_z exists. In spherical coordinates $\{r, \theta, \varphi\}$, they are given by

$$\hat{\mathbf{L}}^2 = -\hbar^2 r^2 \nabla^2 + \hbar^2 \frac{\partial}{\partial r} \left(r^2 \frac{\partial}{\partial r} \right), \quad (\text{A.7})$$

$$\hat{L}_z = -i\hbar \frac{\partial}{\partial \varphi}. \quad (\text{A.8})$$

Their eigenfunctions are the complex-valued spherical harmonics $Y_l^m(\theta, \varphi)$, of degree l and order m , where $-l \leq m \leq l$, given by

$$Y_l^m(\theta, \varphi) = (-1)^m \sqrt{\frac{2l+1}{4\pi} \frac{(l-m)!}{(l+m)!}} P_l^m(\cos \theta) e^{im\varphi}, \quad (\text{A.9})$$

where $P_l^m(\cos \theta)$ are the phaseless associated Legendre polynomials. These spherical harmonics satisfy the eigenvalue equations

$$\hat{\mathbf{L}}^2 Y_l^m(\theta, \varphi) = \hbar^2 l(l+1) Y_l^m(\theta, \varphi), \quad (\text{A.10})$$

$$\hat{L}_z Y_l^m(\theta, \varphi) = \hbar m Y_l^m(\theta, \varphi). \quad (\text{A.11})$$

The Wigner 3j-symbol is defined as

$$\begin{pmatrix} j_1 & j_2 & j_3 \\ m_1 & m_2 & m_3 \end{pmatrix} = \frac{(-1)^{j_1-j_2-m_3}}{\sqrt{2j_3+1}} \langle j_1 m_1 j_2 m_2 | j(-m) \rangle, \quad (\text{A.12})$$

while the 6j-symbol is defined as

$$\begin{Bmatrix} j_1 & j_2 & j_3 \\ j_4 & j_5 & j_6 \end{Bmatrix} = \sum_{m_1, \dots, m_6} (-1)^{\sum_k j_k - m_k} \begin{pmatrix} j_1 & j_2 & j_3 \\ -m_1 & -m_2 & -m_3 \end{pmatrix} \cdot \begin{pmatrix} j_1 & j_5 & j_6 \\ m_1 & -m_5 & m_6 \end{pmatrix} \cdot \begin{pmatrix} j_4 & j_2 & j_6 \\ m_4 & m_2 & -m_6 \end{pmatrix} \cdot \begin{pmatrix} j_4 & j_5 & j_3 \\ -m_4 & m_5 & m_3 \end{pmatrix}. \quad (\text{A.13})$$

Appendix B: PST under Bose Hamiltonian dynamics

Recalling the Bose Hamiltonian as given in the main text,

$$\mathcal{H}_{Bose} = J \sum_{i=1}^{N-1} (X_i X_{i+1} + Y_i Y_{i+1} + Z_i Z_{i+1}), \quad (\text{B.14})$$

one can readily calculate the set of eigenstates $\{|\tilde{k}\rangle\}$, ordered from lowest eigenenergy E_k to highest, in the basis of the single excitation manifold $\{|\underline{n}\rangle\} = \{|1000\dots\rangle, |0100\dots\rangle, |0010\dots\rangle, \dots\}$ as

$$|\tilde{k}\rangle = \sqrt{\frac{2}{N+1}} \sum_{n=1}^N \sin \frac{\pi k n}{N+1} |n\rangle \quad (\text{B.15})$$

with corresponding eigenenergies

$$E_k = -2 \cos \frac{k\pi}{N+1}. \quad (\text{B.16})$$

Using the formal definition of state transfer fidelity,

$$F(t) = \langle \underline{1} | e^{-i\mathcal{H}_{Bose}t} | \underline{N} \rangle, \quad (\text{B.17})$$

one can find that for the Bose Hamiltonian the fidelity is equal to

$$F(t) = \frac{2}{N+1} \sum_{k=1}^N \sin \frac{\pi k}{N+1} \sin \frac{\pi k N}{N+1} e^{-iE_k t}. \quad (\text{B.18})$$

For $N = 2$, the fidelity is

$$F(t)_{N=2} = \frac{2}{3} \left[\sin \frac{\pi}{3} \sin \frac{2\pi}{3} e^{it} + \sin \frac{2\pi}{3} \sin \frac{4\pi}{3} e^{-it} \right] = -i \sin t, \quad (\text{B.19})$$

while for $N = 3$, the fidelity reads

$$F(t)_{N=3} = \frac{1}{2} \left[\sin \frac{\pi}{4} \sin \frac{3\pi}{4} e^{i\sqrt{2}t} + 0 + \sin \frac{3\pi}{4} \sin \frac{6\pi}{4} e^{-i\sqrt{2}t} \right] = - \left[\sin \frac{t}{\sqrt{2}} \right]^2. \quad (\text{B.20})$$

There exist times $t = t_{PST}$ for which $F(t_{PST}) = 1$, so that PST occurs. For $N \geq 4$, there do not exist such times because the phase that is generated by the eigenenergies E_k can only cause constructive interference to achieve unit fidelities, if there are only two terms present in the summation. This is trivial for $N = 2$. For $N = 3$, the second term in the sum vanishes because $\sin \frac{4\pi}{4} = 0$. For $N \geq 4$, this does not happen any more, and there are always at least 4 terms present in the summation that always destructively interfere at all times, causing $F(t) < 1$ for all t .

Appendix C: Graph theory and quantum walks

Let the N -qubit register \mathcal{Q} be represented by a graph \mathcal{G} with the set of vertices $V(\mathcal{G})$ representing the qubits and the set of edges $E(\mathcal{G})$ representing pairs of qubits that mutually interact. It must be noted that the degrees of freedom defined on a graph \mathcal{G} are not enough so that the graph itself is isomorphic to the full Hilbert space $\mathfrak{H}_{\mathcal{Q}} = \mathbb{C}^{2^N}$. For this, copies of the graph must be made, and a special product must be constructed to allow for isomorphism to be proven. This is the wedge product discussed in section 6.2.2.

On such a graph, the adjacency matrix is defined as the matrix of edges. Let the Roman indices i, j denote vertices in the graph, then this adjacency matrix is given by

$$\mathcal{A}_{ij} = \begin{cases} 1 & \text{if } (i, j) \in E(\mathcal{G}) \\ 0 & \text{otherwise.} \end{cases} \quad (\text{C.21})$$

A time-continuous quantum walk on such a graph is given by the Schrödinger equation, where the Hamiltonian has been replaced with this adjacency matrix, in the associated Hilbert space $\mathbb{C}^{\text{card}(V)}$, where $\text{card}(V)$ is the cardinality of the vertex set. That is to say, a quantum state $|\psi(0)\rangle$ evolves in time through

$$|\psi(t)\rangle = e^{-it\mathcal{A}_{\mathcal{G}}} |\psi(0)\rangle. \quad (\text{C.22})$$

The Hilbert space $\mathfrak{H}_{\mathcal{G}}$ is defined as the vector space over \mathbb{C} generated by the vertices $v(\mathcal{G}) \in V(\mathcal{G})$ with the inner product $(v|w) \equiv v \cdot w \stackrel{\text{def}}{=} \delta_{vw}$.

Appendix D: Eigenvalues of the $N = 3$ XY -Hamiltonian

In the main text, the $N = 3$ one-exciton Hamiltonian, with a local magnetic field, was given by

$$\mathcal{H}_1 = \begin{pmatrix} b & -\frac{J}{\sqrt{2}} & 0 \\ -\frac{J}{\sqrt{2}} & B & -\frac{J}{\sqrt{2}} \\ 0 & -\frac{J}{\sqrt{2}} & b \end{pmatrix}. \quad (\text{D.23})$$

Solving for $|\mathcal{H}_1 - \lambda_n \mathbb{I}_3| = 0$, the characteristic polynomial reads

$$(b - \lambda_n)^2(B - \lambda_n) - (b - \lambda_n)J^2 = 0. \quad (\text{D.24})$$

This gives the 3 eigenvalues

$$\lambda_n = b, \quad (\text{D.25})$$

$$\lambda_n = \frac{1}{2}(b + B) \pm \sqrt{J^2 + \left(\frac{b - B}{2}\right)^2}, \quad (\text{D.26})$$

In order to order these eigenvalues, the magnetic fields can be related to each other through

$$B \stackrel{\text{def}}{=} b + \delta \stackrel{\text{def}}{=} b + 2\epsilon. \quad (\text{D.27})$$

Then the eigenvalues read

$$\lambda_n = b, \quad (\text{D.28})$$

$$\lambda_n = b + \frac{1}{2}\delta \pm \sqrt{J^2 + \frac{1}{4}\delta^2} = b + \epsilon \pm \sqrt{J^2 + \epsilon^2}. \quad (\text{D.29})$$

Since for all $J > 0$, it holds true that $\sqrt{J^2 + \epsilon^2} > \epsilon$, so that the eigenvalues can be ordered as follows:

$$\lambda^{(+)} = b + \epsilon + \sqrt{J^2 + \epsilon^2}, \quad (\text{D.30})$$

$$\lambda^{(\circ)} = b, \quad (\text{D.31})$$

$$\lambda^{(-)} = b + \epsilon - \sqrt{J^2 + \epsilon^2}, \quad (\text{D.32})$$

where $\lambda^{(+)} > \lambda^{(\circ)} > \lambda^{(-)}$. The ratio of differences between consecutive eigenvalues must be a ratio of odd numbers, so

$$\frac{\lambda^{(+)} - \lambda^{(\circ)}}{\lambda^{(\circ)} - \lambda^{(-)}} = \frac{2m + 1}{2n + 1} \quad (\text{D.33})$$

for $m, n \in \mathbb{N} \cup \{0\}$. Rewriting $\frac{2m+1}{2n+1} \stackrel{\text{def}}{=} r$, this gives

$$\frac{\epsilon + \sqrt{J^2 + \epsilon^2}}{-\epsilon + \sqrt{J^2 + \epsilon^2}} = r. \quad (\text{D.34})$$

Solving for ϵ gives

$$\epsilon = \sqrt{\frac{\gamma}{1 - \gamma}} J, \quad (\text{D.35})$$

where

$$\gamma = \left(\frac{r - 1}{r + 1}\right)^2. \quad (\text{D.36})$$

In conclusion, PST will happen if and only if $B = b + \frac{2\gamma}{1-\gamma}J$, in a modulated time of

$$t_{PST} = (2m + 1) \frac{\pi}{\epsilon + \sqrt{J^2 + \epsilon^2}}. \quad (\text{D.37})$$

In the limit of $\epsilon \rightarrow 0$, this gives the regular periodic PST time

$$t_{PST} = (2m + 1) \frac{\pi}{J}. \quad (\text{D.38})$$

Appendix E: Eigenvalues of the $N = 4$ XY-Hamiltonian

In the main text, the $N = 4$ one-exciton Hamiltonian, with a local magnetic field, was given by

$$\mathcal{H}_1 = \begin{pmatrix} b & -\frac{J\sqrt{3}}{2} & 0 & 0 \\ -\frac{J\sqrt{3}}{2} & B & -J & 0 \\ 0 & -J & B & -\frac{J\sqrt{3}}{2} \\ 0 & 0 & -\frac{J\sqrt{3}}{2} & b \end{pmatrix} \stackrel{\text{def}}{=} \begin{pmatrix} b & -j & 0 & 0 \\ -j & B & -J & 0 \\ 0 & -J & B & -j \\ 0 & 0 & -j & b \end{pmatrix}. \quad (\text{E.39})$$

Solving for $|\mathcal{H}_1 - \lambda_n \mathbb{I}_4| = 0$, the characteristic polynomial reads

$$(j^2 - (b - \lambda_n)(B + J - \lambda_n))(j^2 + (b - \lambda_n)(-B + J + \lambda_n)) = 0. \quad (\text{E.40})$$

Then using (D.27), the eigenvalues read

$$\lambda^{(+,\pm)} = b + \epsilon + \frac{1}{2}J \pm \sqrt{J^2 + \epsilon^2 + \epsilon J}, \quad (\text{E.41})$$

$$\lambda^{(-,\pm)} = b + \epsilon - \frac{1}{2}J \pm \sqrt{J^2 + \epsilon^2 - \epsilon J}, \quad (\text{E.42})$$

ordered such that for all $J > 0$, one finds that $\lambda^{(+,+)} > \lambda^{(-,+)} > \lambda^{(+,-)} > \lambda^{(-,-)}$. The first and third inequality are trivial. The second inequality stems from the fact that

$$\lambda^{(-,+)} - \lambda^{(+,-)} = -J + \sqrt{J^2 + \epsilon^2 + \epsilon J} + \sqrt{J^2 + \epsilon^2 - \epsilon J} > 0, \quad (\text{E.43})$$

as $-J + \sqrt{J^2 + \epsilon^2 + \epsilon J} > 0$ and $\sqrt{J^2 + \epsilon^2 - \epsilon J} > 0$ for all $J > 0$. From the ESR, it follows that

$$\frac{\lambda^{(+,+)} - \lambda^{(-,+)}}{\lambda^{(-,+)} - \lambda^{(+,-)}} = \frac{2m+1}{2n+1} \stackrel{\text{def}}{=} r \quad (\text{E.44})$$

and

$$\frac{\lambda^{(-,+)} - \lambda^{(+,-)}}{\lambda^{(+,-)} - \lambda^{(-,-)}} = \frac{2n+1}{2k+1} \stackrel{\text{def}}{=} R \quad (\text{E.45})$$

for some natural numbers m, n and k . Combined, this gives a new equation that is easier to solve:

$$\frac{\lambda^{(+,+)} - \lambda^{(-,+)}}{\lambda^{(+,-)} - \lambda^{(-,-)}} = \frac{\lambda^{(+,+)} - \lambda^{(-,+)}}{\lambda^{(-,+)} - \lambda^{(+,-)}} \cdot \frac{\lambda^{(-,+)} - \lambda^{(+,-)}}{\lambda^{(+,-)} - \lambda^{(-,-)}} = \frac{2m+1}{2n+1} \cdot \frac{2n+1}{2k+1} = \frac{2m+1}{2k+1}. \quad (\text{E.46})$$

As these equations only depend on the ratio $\frac{\epsilon}{J}$, it is convenient to perform a substitution $\frac{\epsilon}{J} \stackrel{\text{def}}{=} \mu$. Additionally, let the following shorthand notation be adopted:

$$S \stackrel{\text{def}}{=} \sqrt{1 + \mu^2 + \mu} - \sqrt{1 + \mu^2 - \mu}. \quad (\text{E.47})$$

Then, equation (E.46) can be rewritten as

$$\frac{1+S}{1-S} = r \cdot R \stackrel{\text{def}}{=} \rho. \quad (\text{E.48})$$

Defining $\gamma = \left(\frac{\rho-1}{\rho+1}\right)^2$, the solution can be verified to be equal to

$$\mu = \sqrt{\frac{\gamma - \frac{\gamma^2}{4}}{\gamma - 1}} \quad (\text{E.49})$$

This is not the solution to the IEP, however, as μ must also satisfy either (E.44) or (E.45). Choosing (E.44), this equation reads after some restructuring:

$$\frac{\rho}{-1 + (\rho+1)\sqrt{1 + \mu^2 - \mu}} = \frac{2m+1}{2n+1} \stackrel{\text{def}}{=} r, \quad (\text{E.50})$$

where the identity $S = \frac{\rho-1}{\rho+1}$ was used, following from (E.48). Keeping in mind that $\rho = r \cdot R$, one obtains

$$\sqrt{1 + \mu^2 - \mu} = \frac{R + 1}{\rho + 1} \stackrel{\text{def}}{=} T. \quad (\text{E.51})$$

The solutions to this equation are given by

$$\mu = \frac{1}{2} \pm \sqrt{T^2 - \frac{3}{4}}. \quad (\text{E.52})$$

Linking the two solutions for μ , this yields the equation

$$\frac{1}{2} \pm \sqrt{T^2 - \frac{3}{4}} = \sqrt{\frac{\gamma - \frac{\gamma^2}{4}}{\gamma - 1}}, \quad (\text{E.53})$$

giving the solution $R(\rho)$:

$$R(\rho) = -1 \pm \frac{1}{4} \sqrt{12 - \frac{3}{\rho} - 4s(\rho) + \rho \left(46 - 8s(\rho) + \rho (12 - 3\rho - 4s(\rho)) \right)}, \quad (\text{E.54})$$

where

$$s(\rho) = \sqrt{-\frac{(\rho - 1)^2(3 + \rho)(1 + 3\rho)}{\rho(1 + \rho)^2}}. \quad (\text{E.55})$$

R has to be real, but the only solution that returns a real R is $\rho = 1$, for which $\mu = 0$. Another option is to set the forefactor of $s(\rho)$ under the squareroot in (E.54) equal to 0, yielding

$$-4 - 8\rho - 4\rho^2 = 0, \quad (\text{E.56})$$

though this gives $\rho = -1$ which is forbidden under the ESR. Thus only the trivial solution seems to support PST. The underlying assumption that had been made to arrive to this solution is that r and R must be necessarily perfect fractions. Approximate solutions can be found, however, within certain specified accuracy intervals, that support PGST to great fidelities (99%+). By relaxing the need for perfect fractional solutions one can approximate μ at the cost of neglecting the ESR.